Title: Preparation, properties and structure of hard carbon materials for medical applications

Author: Karolina Jurkiewicz

Citation style: Jurkiewicz Karolina. (2017). Preparation, properties and structure of hard carbon materials for medical applications. Praca doktorska. Katowice : Uniwersytet Śląski

Institute of Physics

Department of Biophysics and Molecular Physics

Faculty of Mathematics, Physics and Chemistry

University of Silesia

Karolina Jurkiewicz

Ph.D. Thesis

Preparation, properties and structure of hard carbon materials for medical applications

Doctoral supervisor:

Prof. dr hab. Andrzej Burian

Chorzów, 2017

Acknowledgements

I wish to express my most sincere gratitude to prof. dr hab. Andrzej Burian for supervision of this thesis. I am very thankful for his scientific guidance, patience and encouragement throughout my doctoral studies and research work. Thank you for supporting me during these past four years.

I am grateful to dr hab. Stanisław Duber for his guidance in 'carbon world', sharing his knowledge and expertise with me, and all support.

I would like to acknowledge dr Henry Fischer for his supervision during my internship and experiment at the Institute Laue-Langevin in France.

I would also like to appreciate the help and collaboration with other scientists: dr Mirosława Pawlyta, dr hab. Dariusz Chrobak, mgr Dorota Zygadło, dr hab. Roman Wrzalik, prof. dr hab. Alicja Ratuszna.

I am grateful to SGL Carbon Polska S. A. company for help in preparing of carbon materials.

I thank all colleagues and co-workers from Institute of Physics for help and great time I spent with them at university.

Abstract

Glass-like carbons represent a wide family of non-graphitizing carbons, which cannot be converted into graphite, even under a high temperature treatment up to 3000 ^{o}C. They are hard carbon materials synthesized by pyrolysis of some polymeric precursors. Due to their relative ease of production and a diverse range of properties, such as high thermal resistance, extreme chemical stability, low density and great hardness compared with other carbons, gases impermeability and high electrical conductivity, these materials have been applied in industry since decades. Moreover, glassy carbons exhibit excellent biological compatibility with blood and living tissues, and therefore they have a high potential for the use in medicine. Nowadays, there is an increasing interest in interfacing glassy carbon microelectrodes with tissues for applications ranging from neural signal sensing and stimulation of brain. Furthermore, recent advances in additive manufacturing have led to the creation of ultrastrong glassy carbon microlattices which can be used as medical implants. Although glassy carbons are highly desirable for many applications and are extensively investigated, their properties such as mechanical or electronic performance as a function of the internal structure and processing are still not fully understood and cannot be predicted. The atomic structure of glass-like carbons is complex and strongly depends on the pyrolysis conditions. The most recent studies have suggested that the structure of glassy carbons consists of fullerene-related building blocks, but up to now there are no commonly adopted model of their nucleation and transformation during the carbonization process.

The main aim of this work is to establish preparation-structure-properties correlations of a series of glass-like carbons produced by pyrolysis of polyfurfuryl alcohol at different temperatures and go beyond the previous state of the art. Given the complexity of their structure, that can be regarded as intermediate between crystalline and amorphous, and its sensitivity to the synthesis temperature the detailed characterization of the prepared glass-like carbons requires applications of many experimental techniques and interpretation methods. They are: wide-angle X-ray and neutron scattering, Raman spectroscopy, high-resolution transmission electron microscopy, electron energy loss spectroscopy, nanoindentaion as well as computer simulations of the atomic structure. The fundamental part of these studies was the analysis of the diffraction results in both, real and reciprocal spaces, in form of the structure factors and the pair distribution functions. Theoretical models of the atomic structure were first described in the frame of the paracrystalline structure, and then classical molecular dynamics simulations were performed for energy optimization of the atomic systems

containing topological point defects. The model compatibility with the experimental data was verified by a direct comparison of the model-based calculations and the experimental diffraction data. The use of additional techniques, such as high resolution electron microscopy, Raman spectroscopy, electron energy loss spectroscopy and nanoindentation allowed obtaining detailed information about the local structure, chemical bonding between carbon atoms, and mechanical properties of the investigated materials. It has been demonstrated that the structure of the glass-like carbons at different stages of the carbonization process resembles the curvature observed in fragments of nanotubes, fullerenes or nanoonions. This curvature is responsible for hardness and mechanical strength of the glass-like carbons as well for the formation of porosity. It has been established that the constituent carbon atoms are connected mainly by the sp^2 type bonds.

Streszczenie

Węgle szklistopodobne reprezentują rodzinę niegrafityzujących materiałów węglowych, które nie mogę być przekształcone w grafit, nawet po wysokotemperaturowej obróbce do 3000 ^{o}C. Są one twardymi materiałami węglowymi otrzymywanymi w procesie pirolizy niektórych polimerów. Materiały te są znane i stosowane w przemyśle od dziesięcioleci, z uwagi na łatwość produkcji oraz szeroki zakres właściwości, takich jak wysoka wytrzymałość termiczna, duża stabilność chemiczna, niska gęstość i duża twardość w porównaniu do innych materiałów węglowych, nieprzepuszczalność gazów, dobra przewodność elektryczna. Ponadto, węgle szkliste wykazują biozgodność w kontakcie z krwią i tkankami, dlatego mają duży potencjał do zastosowań w medycynie. Obecnie zwiększone jest zainteresowanie wykorzystaniem mikroelektrod z węgla szklistego do badania sygnałów nerwowych i stymulacji mózgu. Co więcej, ostatnie postępy w rozwoju techniki tzw. additive manufacturing pozwajają na wytwarzanie utrawytrzymałych mikrosieci z węgla szklistego, które mogą być zastosowane jako implanty medyczne. Pomimo dużego zainteresowania aplikacyjnego węglem szklistym oraz wielu badań, pochodzenie właściwości węgla szklistego, oraz ich związki z warunkami syntezy oraz strukturą nadal nie są w pełni zrozumiałe i właściwości te nie mogą być przewidywane. Struktura atomowa węgli szklistych jest złożona i silnie zależy od warunków pirolizy. Ostatnie badania pokazują, że w pewnym stopniu przypomina ona strukturę fulerenów. Jednakże aż do dzisiaj brakuje modelu wyjaśniającego formowanie się fulereno-podobnych elementów struktury oraz ich transformację w procesie pirolizy węgli niegrafityzujących.

Głównym celem niniejszej pracy było ustalenie związków pomiędzy warunkami syntezy, strukturą, a właściwościami dla serii węgli szklistych wytworzonych metodą pirolizy polimeru alkoholu furfurylowego w różnych temperaturach. Biorąc pod uwagę złożoność struktury atomowej badanych węgli, która może być traktowana jako pośrednia między krystaliczną a amorficzną, oraz jej zależność od warunków syntezy, do szczegółowej charakterystyki przygotowanych węgli szklistych niezędne jest zastosowanie wielu technik eksperymentalnych i metod interpretacji. W pracy wykorzystano: szerokokątowe rozpraszanie promieniowania X i neutronów, spektroskopię Ramana, wysokorozdzielczą transmisyjną mikroskopię elektronową, spektroskopię strat energii elektronów, nanoindentację, a także komputerowe symulacje struktury. Główna część pracy dotyczy analizy danych dyfrakcyjnych w przestrzeni odwrotnej i rzeczywistej, w postaci czynników struktury oraz funkcji rozkładu par atomów. Teoretyczne modele struktury zostały w pierwszej kolejności

opisane za pomocą formalizmu struktury parakrystalicznej, a następnie wykorzystano symulacje metodą klasycznej dynamiki molekularnej do optymalizacji energii układów atomów zawierających topologiczne defekt punktowe. Poprawność modeli była weryfikowana poprzez porównanie obliczonych na ich podstawie danych dyfrakcyjnych z wynikami doświadczalnymi. Wykorzystanie dodatkowych technik, takich jak spektroskopia Ramana, wysokorozdzielcza transmisyjna mikroskopia elektronowa, spektroskopia strat energii elektronów oraz nanoindentacja, pozwoliło na uzyskanie dodatkowych informacji o lokalnej strukturze, wiązaniach chemicznych pomiędzy atomami węgla oraz właściwościach mechanicznych badanych węgli. Pokazano, że struktura węgli szklistych na różnych etapach procesu karbonizacji wykazuje krzywiznę jak we fragmentach nanorurek, fulerenów czy nanocebulek. Krzywizna struktury jest odpowiedzialna za twardość i wytrzymałość mecaniczną tego typu węgli, a także za tworzenie się porowatości. Ustalono także, że atomy węgla w badanych materiałach są połączone głównie wiązaniami typu sp^2.

This doctoral dissertation "Preparation, properties and structure of hard carbon materials for medical applications" has been prepared in the form of a guidebook on the collection of the following scientific papers:

P1: Jurkiewicz, K., Duber, S., & Burian, A. (2016). Paracrystalline structure of glass-like carbons.
International Journal of Applied Glass Science, *7*(3), 355-363,
DOI: 10.1111/ijag.12186.

P2: Jurkiewicz, K., Duber, S., Fischer, H. E., & Burian, A. (2017). Modelling of glass-like carbon structure and its experimental verification by neutron and X-ray diffraction.
Journal of Applied Crystallography, *50*(1), 36-48,
DOI: 10.1107/S1600576716017660.

P3: Jurkiewicz, K., Pawlyta, M., Zygadlo, D., Chrobak, D., Duber, S., Wrzalik, R., Ratuszna, A. & Burian, A. Evolution of glassy carbon under heat treatment: correlation structure-mechanical properties.
Journal of Materials Science,
DOI: 10.1007/s10853-017-1753-7.

Guidebook

Table of content

1. Introduction – motivation and scope

The disordered, non-graphitizing glass-like carbons, also called glassy carbons, are of significant interest within many industrial applications, particularly as electrode materials in electrochemistry, high-temperature crucibles, in vacuum technology, and for a mechanical reinforcement of constructional products [1-3]. This is due to their specific properties such as isotropy, high thermal resistance, extreme chemical stability, low density and great hardness compared with other carbons, gases impermeability, and high electrical conductivity [3-5]. In addition, glassy carbons exhibit excellent biological compatibility with blood and tissues, and therefore they have a high potential for use in medicine [6]. The glass-like carbons are typically synthesized by pyrolysis of polymeric precursors like phenolic resins or polyfurfuryl alcohol, which crosslink at elevated temperatures [4,5,7,8]. Due to their relative ease of production and a diverse range of physical properties these carbons have been extensively manufactured and investigated since decades.

The most recent studies have suggested that glass-like carbons have a fullerene-related structure. Such model of glassy carbon structure proposed by Harris [5,9-11] consists of broken and imperfect fullerene fragments - curved sp^2-bonded graphene-like planes, which can be multilayered and which often surround closed pores. The presence of curvature has been attributed to the topological defects in form of non-hexagonal carbon rings such as pentagons and heptagons that were directly observed by the high-resolution transmission electron microscopy [12]. The fullerene-related model of the glassy carbons atomic structure is more compatible with their properties than competing models assuming that the glassy carbons consist of narrow and twisted fibrils of graphitic carbon [7,13,14]. When glassy carbons are exposed to the temperature up to 3000 °C the building structural blocks start ordering in directions parallel and perpendicular to graphene-like layers [5,9-11,15,16]. This process is called 'graphitization' [15]. The stacks of graphene-like sheets form nano-sized domains extended to about 50-100 Å for glassy carbons heat treated above 2500 °C, depending on the time of annealing or starting precursor [5,17]. However, even after heat treatment at temperatures of 3000 °C and above the glass-like carbons cannot be transformed into crystalline graphite [10,15] and they preserve the general type of atomic disorder. The complex fullerene-like structure that is thermally stable even at very high annealing temperatures is believed to be the reason of the extreme resistance of glassy carbons against three-dimensional ordering [5].

Since the structure is a key parameter determining glass-like carbon porosity, mechanical and electronic properties, the possibility to control the temperature-induced structural transformation is critically important for the fabrication of the glassy carbon products with desired functional features. It is essential to note that novel glassy carbon applications, such as micro-electro-mechanical systems [18,19], that can be used for medical prostheses [20,21], require comprehensive characterization of the properties-structure relationships at the both, bulk and nanoscale level. Although many systematic investigations by different experimental techniques and model calculations [5,7,9-17,22-25] have been carried out on particular types of the glassy carbons, the formation of their atomic structure and its transformation during heat treatment is not fully elucidated. Particularly, there are no commonly adopted model of the nucleation and growth of curved structures in pyrolyzed carbons. Some works show that curved carbon surfaces can be formed due to the abundance of five-membered and other non-hexagonal carbon rings [26-28]. However, the mechanism of creation and healing of these defects is not known in details. In addition, until these days the nature of glassy carbon crystallites (in terms of the parallel-layer groups) growth and their barrier to graphitization is still not well understood.

The fundamental aim of this work was the characterization of the atomic structure of a series of glass-like carbons prepared by pyrolysis of polyfurfuryl alcohol at different temperatures from the range 600-2700 °C. The main approach selected for this task is based on the wide-angle X-ray and neutron scattering (WAXS and WANS, respectively) techniques combined with computer simulations. In order to describe the glass-like carbons using the diffraction method one has to go beyond the Bragg formalism and crystallographic analysis. The studied materials have disordered structure and in such a case it is advantageous to perform the analysis of diffraction results in both, reciprocal and real spaces. Therefore, the collected WAXS and WANS data normalized to the structure factors were converted to a real space representation of diffraction in the form of the pair distribution (or pair correlation) functions. In order to interpret the structure factors and the pair distribution functions computer simulations using paracrystalline theory of structural disorder were performed. In the next step, realistic models of the atomic structure were prepared by implementation of the theoretical paracrystalline disorder in the form of topological point defects. The models containing structural defects were relaxed using classical molecular dynamic simulations.

The principal difficulty to solving problem of structure of disorder material is that, in general, any one technique does not contain sufficient information to constrain a unique structural solution. A coherent strategy is required for combining input from multiple

experimental methods and theory in a self-consistent global optimization scheme. Only such an approach based on the different methods can make the proposed structural model reliable. Therefore, high-resolution transmission electron microscopy (HRTEM), Raman spectroscopy (RS), electron energy loss spectroscopy (EELS) and nanoindentation measurements were performed to shed more light on the evolution of the glassy carbon structure and properties during the heat treatment. HRTEM is undoubtedly one of the most powerful methods for probing the atomic arrangement and enables direct images of the structure to be recorded. In the present work, HRTEM was used to examine glass-like carbons for a better understanding of the changes in their multiscale organization, depending on the thermal history of the synthesis process. RS, on the other hand, is an indirect probe of structure but it is known to be extremely sensitive to local structural details. It seems reasonable, that RS can be used as a verification of the fullerene-related structure of glassy carbon, since the curved, defective carbon fragments should contribute in a significant way to the Raman scattering. Fullerenes and nanotubes give a fingerprint for their curved carbon network in the low-frequency region 50-1000 cm^{-1} of Raman spectra [29-31]. The occurrence of Raman peaks in this region provides evidence for the presence of fullerene- and nanotube-like elements in the investigated glassy carbons. Moreover, comparative studies of the first- and second-order Raman spectra [32-34] for the series of prepared samples were performed to reveal differences in their structural ordering and correlate them with snapshots of structure taken by HRTEM. The purpose of applying the EELS technique was to identify the bonding character of carbon atoms in these materials at different stages of carbonization process and verify the fullerene-like model of the glassy carbon atomic structure. The aim of nanoindentation experiment was to continuously follow the development of the mechanical response of the material during the carbonization process. Finally, based on the obtained results relationships between the structure affected by the carbonization conditions and mechanical properties of these glassy carbons were established.

1.1. *State of the art on the structure of glass-like carbons*

The first concept of the structure of graphitizing and non-graphitizing carbons, including glass-like carbons, was put forward by Franklin in 1951 [15]. She proposed that the structure of non-graphitizing carbons is composed of nanometer-sized randomly oriented stacks of graphite-like layers. The stacks are held apart by strong cross-linking which results in a hard bulk structure with fine pores, and which may resist long-range reorganization into

crystalline graphite even when heated as high as 3000 °C. In the case of graphitizing carbons the structural units consisting of small graphitic crystals are approximately parallel to each other and they convert to graphite during high temperature treatment. The Franklin's representation of graphitizing and non-graphitizing is shown in Fig. 1.
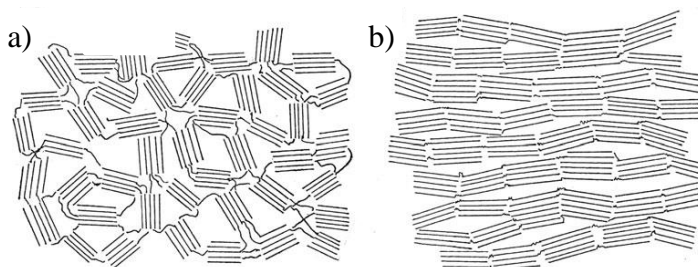

Fig. 1 Models of the structure of graphitizing (a) and non-graphitizing carbons (b) proposed by Franklin [15].

These structural units are connected by cross-links and rearrange as a whole during the heat treatment. The idea of the cross-links proposed by Franklin was deeply investigated and discussed. However, up to now the nature of these cross-links between graphitic fragments is not specified, so the difference in behavior of soft graphitizing and hard non-graphitizing carbons is not fully explained. The presence in the structure of diamond-like sp^3-bonded atoms would explain the high hardness and resistance to graphitization of glassy carbons and in the past an idea appeared that the sp^3-bonded carbons may act as the potential cross-linking [35]. However, sp^3 bonds are unstable at high temperatures. Diamond is converted into the more thermodynamically favored sp^2-hybrydized graphite at about 1700 °C, whereas the sp^3-bonded carbon atoms in amorphous films are unstable even just above 600 °C. At nanometer scale the structure of nanodiamonds at 1700 °C transforms completely into concentrically stacked spherical fullerene structures called nanoonions, in which carbon atoms are linked by the sp^2 bonds [36-37]. Therefore, it is unlikely that diamond-type structures could be responsible for the glassy carbon properties at higher temperatures. However, the presence of small amounts of sp^3 bonded carbon atoms cannot be completely ruled out.

Two of the most frequently used models of the glass-like carbon structure are the models proposed by Jenkins and Kawamura [8] and Oberlin [38]. According to the first one, glassy carbons are composed of randomly twisted ribbons of graphitic carbon. This model, however, is inconsistent with the glassy carbon impermeability to gases and low chemical reactivity. In contrast, the second model consists of crumpled graphite-like sheets. However, this model also does not explain glassy carbon properties and experimental data obtained up to now. More recently, Pesin and Baitinger have proposed a model for glassy carbon which

incorporates carbyne-like chains [14]. This model was based on a consideration of the electronic properties of glassy carbon, but there is no direct experimental support for the carbyne-like structure. The discoveries of nanoscale, non-planar carbon structures, such as fullerenes, nanotubes or nanohorns, proved that carbons containing non-six-membered rings, among the hexagonal sp^2 carbon network, can be highly stable. This prompted an idea that structure of non-graphitizing carbons can resemble the structure of fullerenes. The precursor of this idea is Harris who found evidence for this fullerene-related model in high-resolution transmission electron images [5,9-11]. He proposed that glassy carbon structure consists of fullerene fragments in the form of curved sp^2-bonded graphene-like planes. They are much larger for high-temperature glassy carbons and can be multilayered and surround closed pores. The presence of curvature has been attributed to the topological defects in form of non-hexagonal carbon rings, such as pentagons and heptagons, which were directly observed by the HRTEM [12]. Models for the structure of low temperature (a) and high temperature glassy carbon (b) proposed by Harris are shown in Fig. 2.
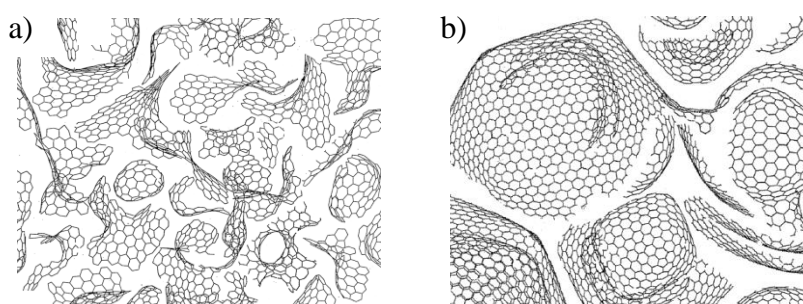

Fig. 2 Models for the structure of low temperature (a) and high temperature glass-like carbon proposed by Harris [5].

Despite the progress which is being made in understanding the structure of glassy carbons, there remain many unanswered questions. Many approaches were used to elucidate the pyrolysis process, the structure and the related properties of different carbon materials. However, many issues remain still not fully described, namely:

- influence of the structure and chemical composition of starting polymer on the structure and properties of resulting synthesized material;
- role of topological defects in the graphitization process and their influence on properties;
- effect of the presence in the structure of curved graphene-like layers on properties;
- differences in behavior of various types of carbons against heat treatment;
- mechanism of pore formation in porous carbons;

▪ origin of high hardness and closed porosity of glassy carbons.

In particular, it would be of great interest to know more about the mechanism whereby glassy carbon carbonized at lower temperature is transferred into the high-temperature structure upon heat treatment.

1.2. *Medical applications of glass-like carbons*

Glass-like carbons have a long history of use for medical applications due to their compatibility with blood and tissues, good strength and hardness, high erosion resistance and chemical inertness. Isotropic glassy carbons in pyrolytic form meet these criteria and are used in biomedical devices such as heart valves and dental implants [39-41]. However, glassy carbons produced conventionally by the carbonization of polyfurfuryl alcohol or phenolic resins are usually very brittle. Despite the fact that various biomedical applications for these glassy carbons were studied many years ago [42], potential medical applications were not successful due to their high fragility. Fracture characteristics of the glassy carbons are compared with those of float glass and graphite [43]. This was a strong limitation to the widening of glassy carbon applications. However, modern techniques in carbon materials manufacturing offer an opportunity of preparation of glassy carbon-based products which are mechanically demanding.

Recently, glassy carbon foams have been tested in vitro and in vivo for compatibility with primary cell adhesion and tissue repair [44]. It was demonstrated that this type of carbon materials is an attractive candidate for tissue engineering and regenerative medical applications. Moreover, recent advances in additive manufacturing have led to the creation of ultrastrong and lightweight glassy carbon microlattices [19]. They represent a significant step forward in the field of lightweight mechanical metamaterials and can exert a great impact for medical applications. Due to glassy carbon's good mechanical properties, electrical conductivity and biocompatibility, this material is interesting for microimplants in the line of microstents, microscaffolds for bone regeneration, and microelectrodes. It was showed that lithography patterned glassy carbon electrodes offer a new and compelling material for neural recording and stimulation [21]. The pyrolysis conditions (i.e., maximum temperature, duration, and ramp rate) during fabrications of the glassy carbon products enable a tailorability of their functionalities. Namely, the pyrolysis parameters can be varied to enable useful properties such as mechanical stiffness and hardness for stiffness-matching with

15

soft tissues, electrical impedance for impedance-matching with tissues, and electrochemical properties useful for optimized stimulation and recording.

The determination of the preparation-structure-properties relationships is essential for the design and the analysis of performance and reliability of the glass-like carbon products. The incomplete knowledge about the mechanism of structural changes in glass-like carbons prevents the improvement of their production and processing. The developed here quantitative relationships between the structure and mechanical properties may benefit the further design of novel glassy carbon systems. Therefore, it is mandatory to well characterize the material and understand the preparation-structure-properties correlations.

2. Results and discussion

The glass-like carbons being the subject of this research were prepared by pyrolysis of polyfurfuryl alcohol at different temperatures from the range 600 °C - 2700 °C. All details concerning their preparation were described in papers **P1**, **P2**, and **P3**. The materials are labeled in the text of this thesis according to the maximum heat treatment temperature. For instance, the glass-like carbon pyrolyzed at 600 °C is called GC600, and the glass-like carbon pyrolyzed at 2500 °C is GC2500, respectively.

2.1. Interpretation of diffraction data in reciprocal and real spaces

2.1.1. Paracrystalline structure modeling

The experimental wide-angle X-ray scattering data in form of the structure factors $S(Q)$ and the pair distribution functions $PDF(r)$ presented in paper **P1** confirmed that the glass-like carbons investigated here have disordered structure, intermediate between crystalline and amorphous. The $S(Q)$ functions resemble those of typical turbostratic carbons [45] and contain only the (*00 2l*) and (*hk0*) graphite-type reflections. With increasing the synthesis temperature sharpening and rise of the $S(Q)$ and $PDF(r)$ peaks can be observed, that can be explained by ordering of the atomic structure. As the carbonization process proceeds, the graphene-like planes continued to grow and rearranged to more ordered graphite-like domains. However, it was demonstrated that the models based on the graphite

structure, disordered only by the thermal vibrations of atoms and the turbostatic displacement of graphitic layers cannot reproduce all features of the experimental diffraction data and explain the real structure of these carbons.
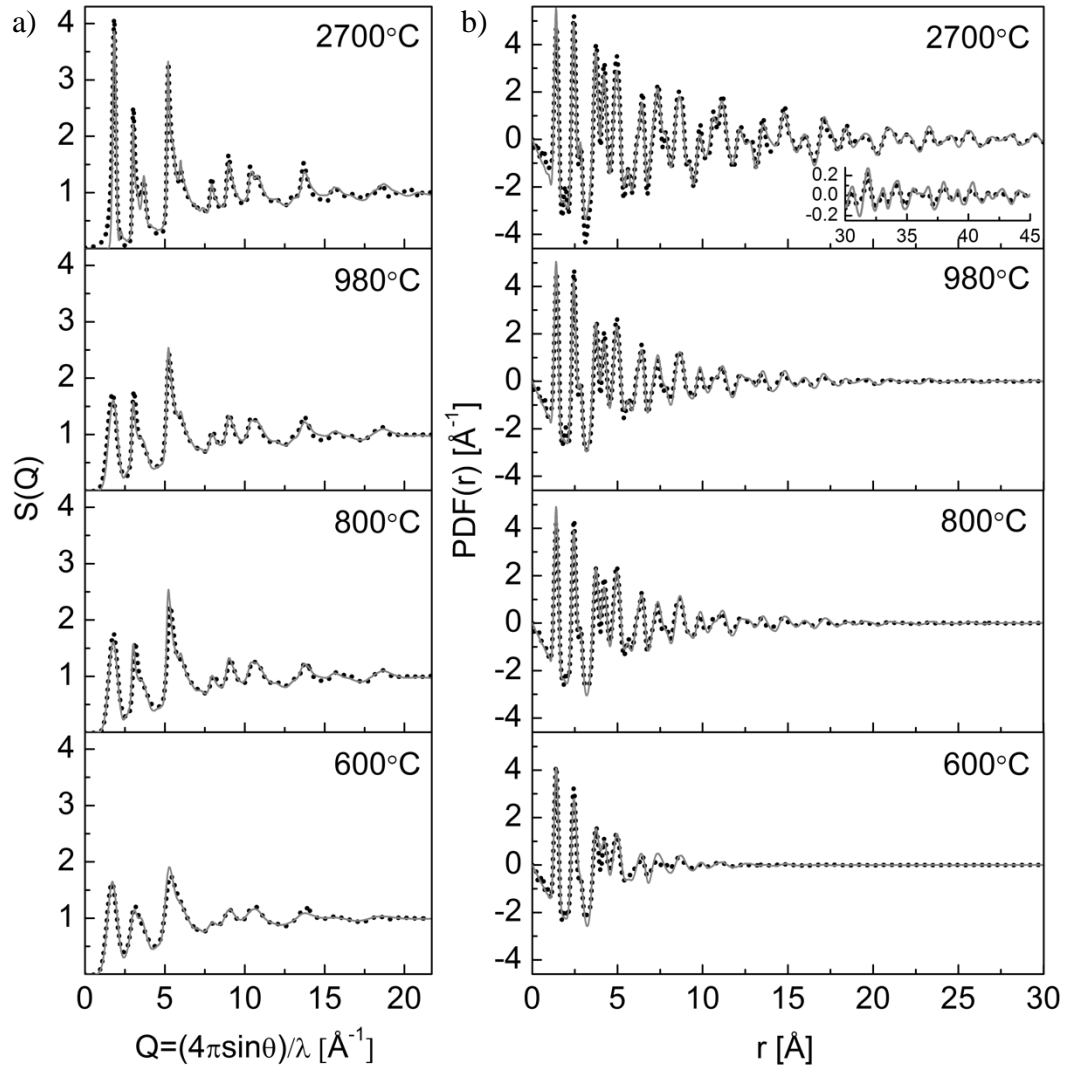

Fig. 3 Comparison of the experimental (dotted line) structure factors (a) and the pair distribution functions (b) for the glass-like carbons carbonized at different temperatures with the simulated functions (solid line) for paracrystalline models [**P1**].

Afterwards, an attempt has been made to analyze the WAXS data by introducing paracrystalline distortion of the atomic network into the models. The paracrystalline disorder assumes that the nearest-neighbour atom-atom distances fluctuate randomly without spatial correlations, leading to a network distortion which propagates proportionally to the square root of the interatomic distance [46,47]. The numbers of graphitic layers for each model, the lattice constants and the values of interlayer spacing were adjusted previously by simulations

of the turbostratic structures. Moreover, the translation of neighboring layers in the stack was kept for describing the features of experimental data related to the turbostratic structure. The paracrystalline disorder was introduced by means of the generalized Debye-Waller factor with adjustable parameters in form of standard deviations of interatomic distances. Paracrystalline stacking of layers was generated assuming Gaussian distribution of the interlayer spacing with adjustable standard deviation. The fitted model parameters are listed in Table II of paper **P1**.

The comparison of the model-based and experimental diffraction data is presented in Fig. 3. As can be seen from this comparison, the peak positions, widths, and amplitudes for the experimental and model functions in the reciprocal and real spaces are in good agreement. The paracrystalline models explain also the broadening of the pair distribution peaks with increasing the interatomic distance that can be observed for experimental functions. There is a closed correspondence between the expected changes in the structure of investigated carbons as a function of pyrolysis temperature and the parameters of paracrystalline models. In general, the values of parameters that characterize disorder decrease with increasing synthesis temperature.

2.1.2. Optimization of the atomic structure models using molecular dynamic

The most challenging task of the research intended in this thesis was the creation of realistic models of the atomic structure for the glass-like carbons pyrolyzed at different temperatures which would comply with all the diffraction data and other experimental results simultaneously. Neutron diffraction provides data for which scattering cross-section does not depend on the scattering vector Q. While in the case of X-ray diffraction the measured intensity is strongly diminishing with Q and for carbon samples the intensity in a higher Q range is dominated by the Compton scattering that may cause normalization problems. In Fig. 4, published in paper **P2,** the comparison of the neutron wide-angle scattering data measured on the D4 instrument (Disordered Materials Diffractometer) at the Institute Laue-Langevin, Grenoble and X-ray wide-angle scattering results recorded with laboratory diffractometer is shown. It is demonstrated that the carefully performed correction and normalization procedures for the X-ray measurements allowed getting reliable data that can be Fourier converted to the form of the pair distribution function with comparable quality as for the neutron measurements.
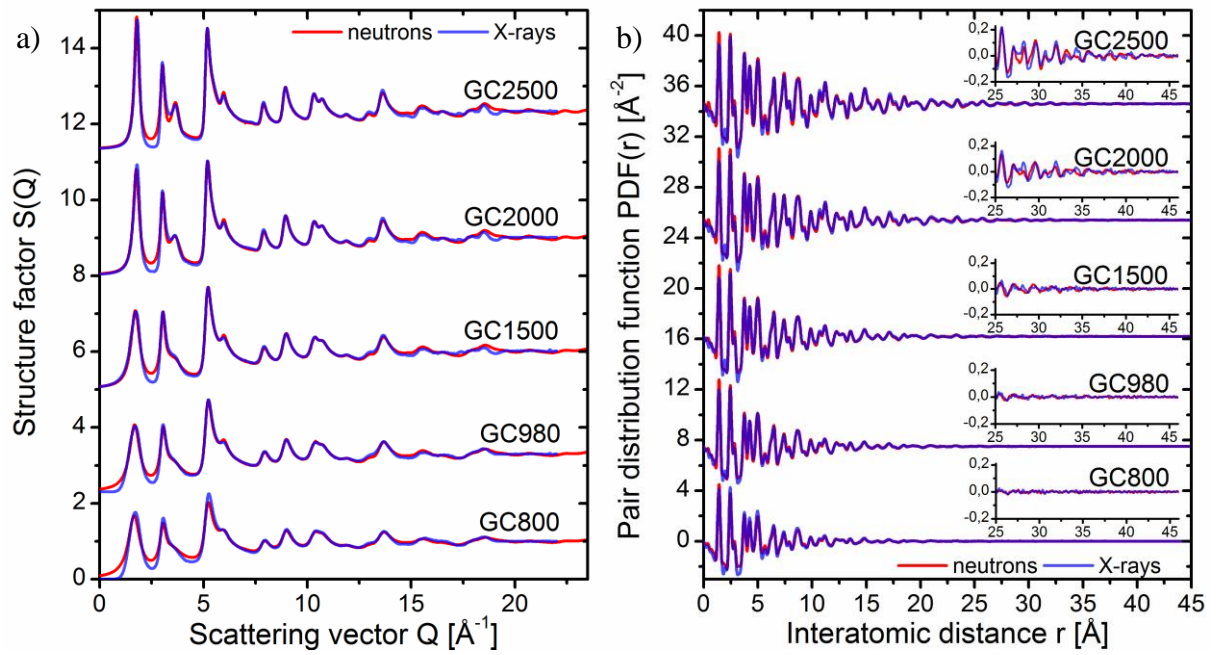
Fig. 4 Comparison of the structure factors (a) and the pair distribution functions (b) from the neutron and X-ray diffraction experiments for the glass-like carbons [**P2**].
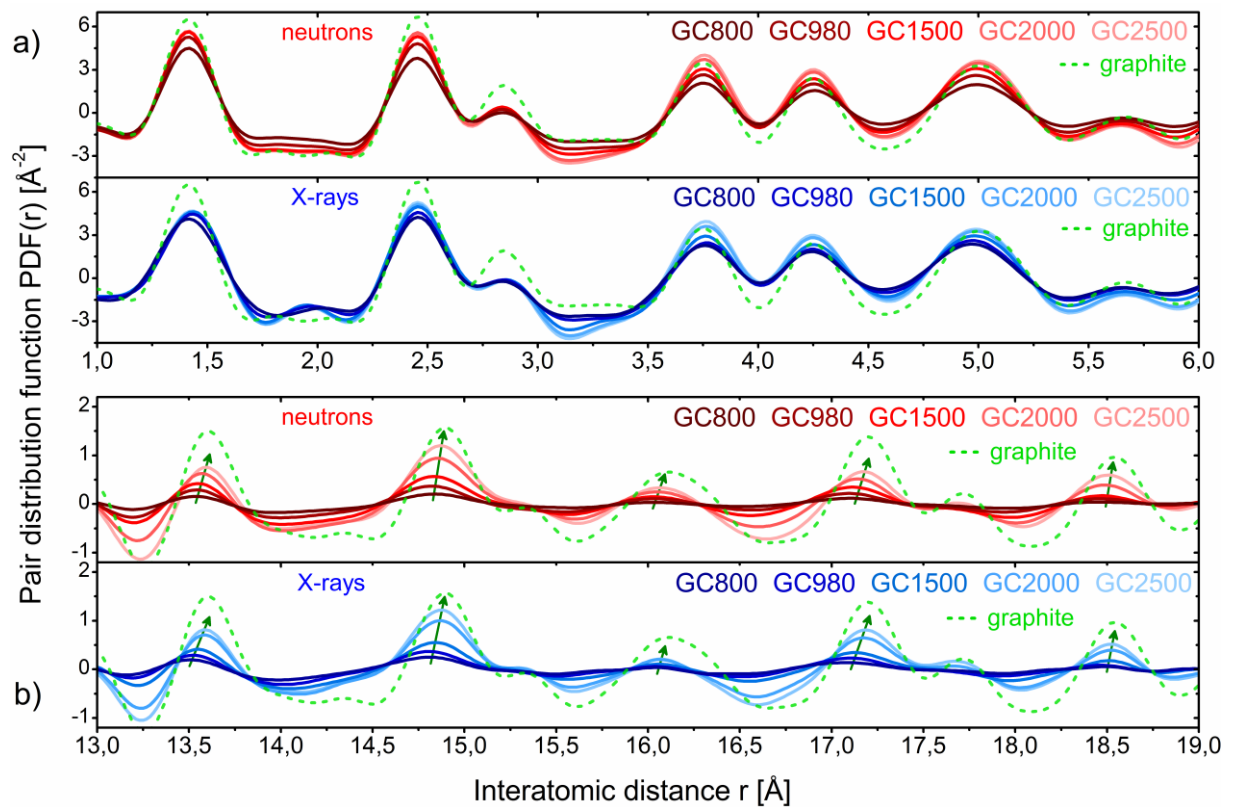

Fig. 5 Comparison of the interatomic distances of the experimental pair distribution functions for the glass-like carbons with the function calculated for a single unstrained graphite layer in the short range order (a) and in the intermediate range order (b) [**P2**].

Fig. 5 shows comparison of the experimental neutron and X-ray $PDFs(r)$ for the glassy carbon samples carbonized at different temperatures from the range of 800-2500°C with the function calculated for an unstrained single graphitic layer. As can be noticed the peak positions of the $PDF(r)$ appearing in the range of 1-6 Å are practically the same as those for the perfect hexagonal layer, but the peaks for higher r-values shift towards longer interatomic distances characteristic for the intra-layer structure with increasing heat treatment temperature. This finding can be directly related with the curvature of the atomic structure and its gradual flattening under the influence of the heat treatment.

In order to specify the degree of the curvature manifesting itself in the diffraction data and optimize structural models matching to the experimental results the classical molecular dynamic was used. The diffraction data provide averaged structural information about the coherently scattering domains. Therefore, in the first step, the models with sizes of these domains (called here 'small models') have been computer generated. It was assumed that the coherently scattering domains are arranged without spatial correlations. Then, in order to account for possible cross-correlations between such domains, larger models (called here 'big models') were constructed. Starting positions of carbon atoms were obtained from the ideal graphite structure. The successive graphene layers were randomly translated in direction perpendicular to their stacking, bringing turbostratic kind of disorder into the models. The physical implementation of paracrystalline perturbation in the structure, postulated in paper **P1** and described in the previous section, was realized by taking into account the presence of different types of topological defects in form of vacancies and Stone-Thrower-Wales defects (STW) [48]. In order to obtain stable atomic configurations and minimize the energy of the models, they were relaxed using suitable C-C potential interaction. The reactive empirical bond order potential [49] was used for atoms lying within a single layer and the Lennard-Jones potential [50] for interlayer interactions. The modeling studies were described in details in paper **P2**.

The theoretical $S(Q)$ and $PDF(r)$ calculated based on the big-model simulations that give the best agreement with experimental neutron and X-ray diffraction results are presented in Fig. 6 and 7. In paper **P2** the diffraction data calculated based on the big models are compared with the data for the optimized small models of averaged coherent scattering domains. The big models created by coalescence of small building blocks account for spatial correlations between atoms within single coherent scattering domain, as well as between atoms lying in different domains, and they match significantly better to both neutron and X-ray experimental diffraction data than the small models.
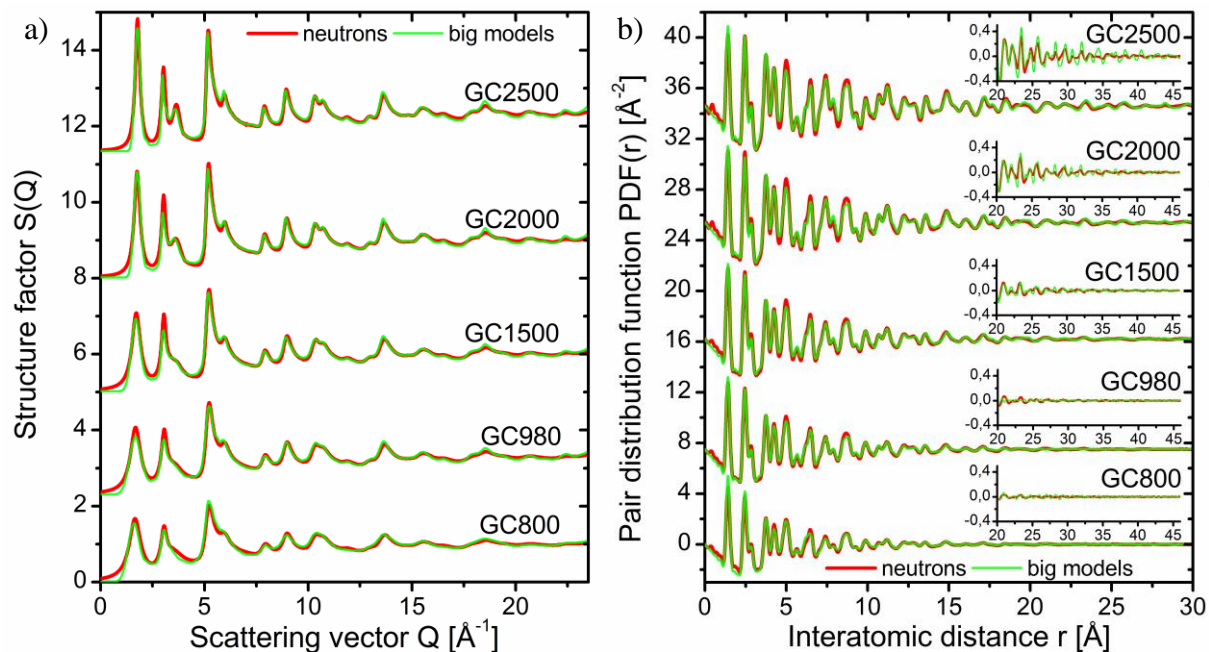
Fig. 6 Comparison of the structure factors (a) and the pair distribution functions (b) computed for big models of structure with the neutron diffraction experimental data [**P2**].
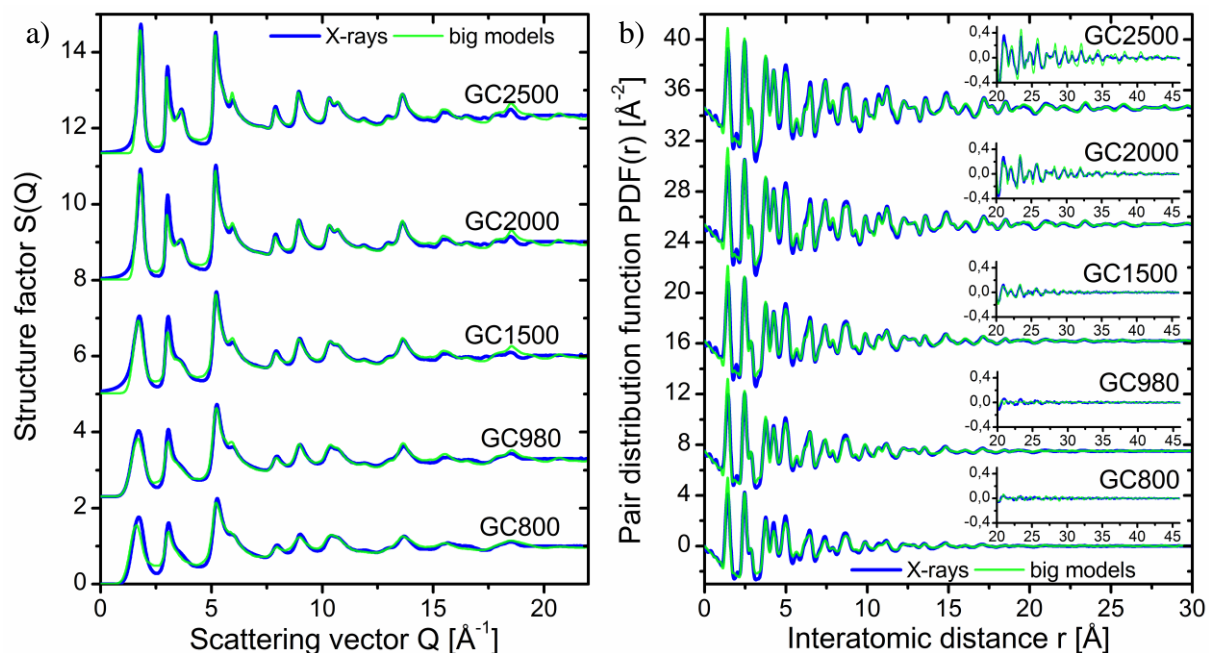
Fig. 7 Comparison of the structure factors (a) and the pair distribution functions (b) computed for big models structure with the X-ray diffraction experimental data [**P2**].

A visualization of the stored geometry for the optimized small and big models of the glassy carbon structure is displayed in Fig. 8 and 9, respectively. The models in Fig. 8 show a clear evolution of the averaged coherent scattering domains under heat treatment. One can observe the effect how the point defects (shown in panels (b-c) of Fig. 8) deform the

originally flat graphene layers. As for fullerene elements, the occurrence of non-hexagonal-membered carbon rings induces strains and is responsible for deviations from planarity. Consequently, in some regions the rippling brings closer of the graphene sheets and they can even merge together, as it is shown in panel (a) of Fig. 8. This behavior can explain the mechanism of closed porosity creation in the glassy carbons.
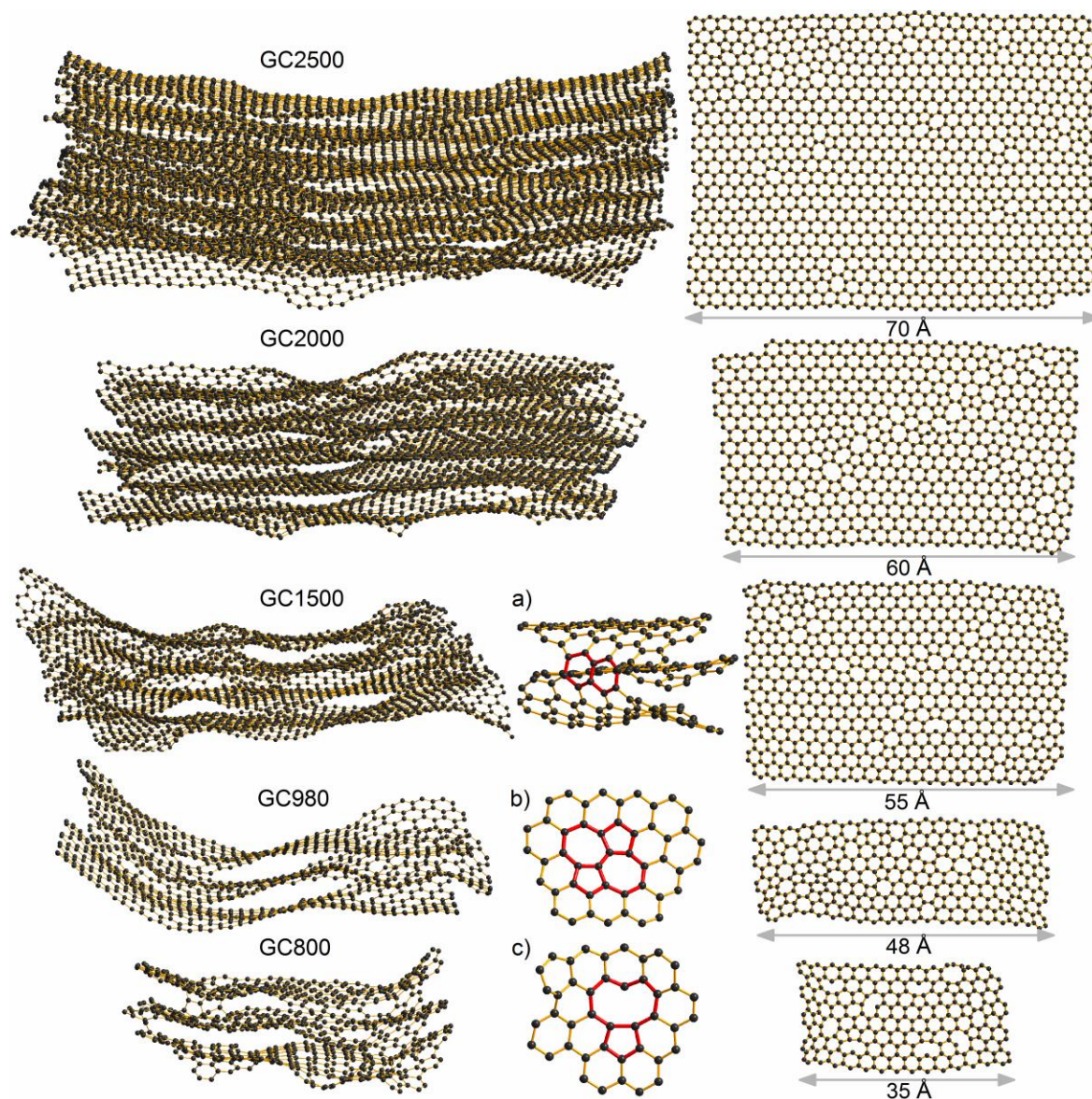
Fig. 8 Visualization of the proposed models of averaged coherent scattering domains (small models) for the glassy carbons, single layers randomly separated from the models (on right), fragment of GC1500 model with nonplanar sp^2 bonding (a), fragment of GC980 model with Stone-Thrower-Wales defect (b), fragment of GC800 model with monovacancy defect (c) [**P2**].

For the big models the boundaries of the linked domains are also a rich source of various types of defects that can be recognized in the fragments of the models in Fig. 9(a-d).

Among them non-six-memebered rings, multi-vacancies, isolated tetrahedral bonds and carbon chains can be distinguished. The presence of such agglomerated defective regions induces formation of curvature and interlayer bridges which may effectively inhibit the movement of the carbon layers and prevent graphitization. It is apparent that the heat treatment process reduces disorder and transforms the glassy carbon atomic structure toward more graphite-like structure. It should be pointed out that the disappearance of curvature as a function of the increase in pyrolysis temperature observed for the proposed models follows the changes in peak positions of the theoretical $PDFs(r)$ in a similar manner as for the experimental data in Fig 5.
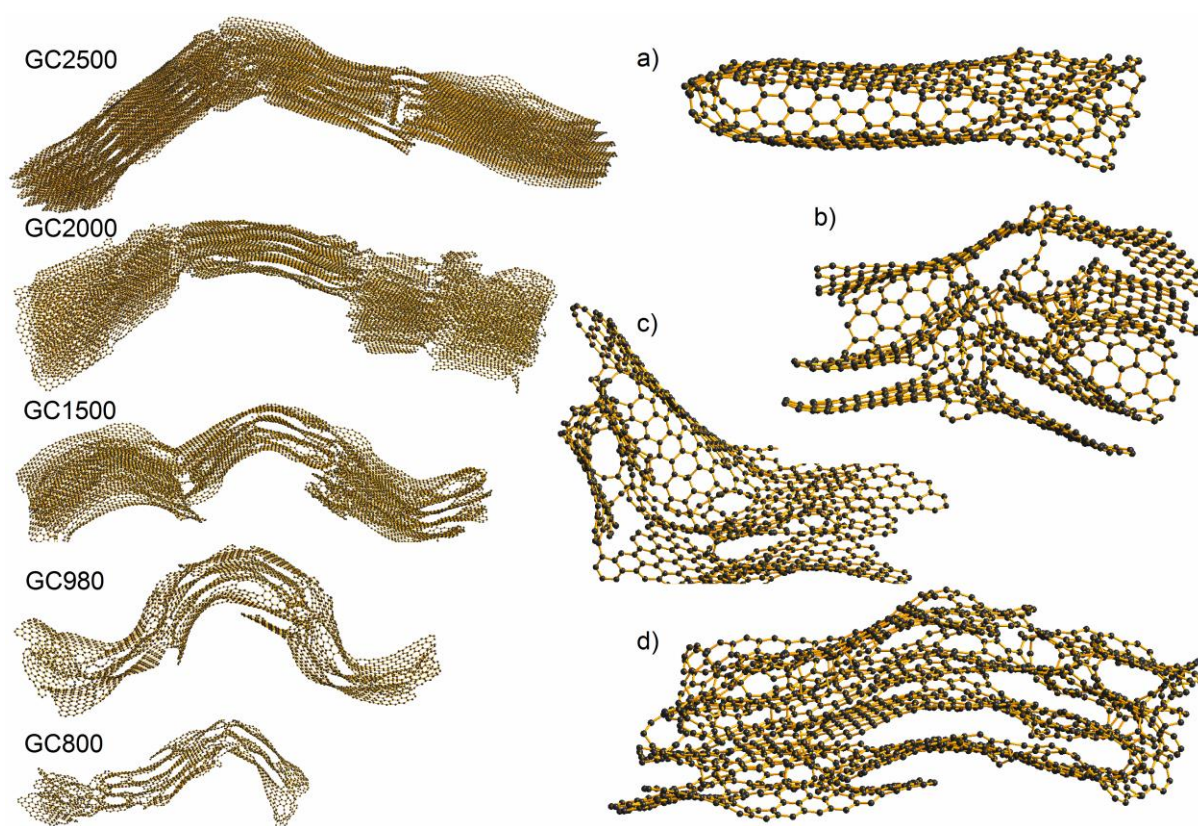

Fig. 9 Visualization of the proposed structural models for the glass-like carbons, and magnified selected fragments of the models for GC1500 (a), GC980 (b,c), and GC800 (d,m) [**P2**].

2.2. Complementary information on the structure from other experimental techniques

2.2.1. High-resolution transmission electron microscopy

In order to verify the correctness of the proposed models of the glass-like carbon atomic structure at different stages of the pyrolysis process the HRTEM images were recorded. HRTEM technique is only a local probe of structure, however, the obtained 'snapshots' of the glass-like carbons using HRTEM, are in good agreement with averaged models of the atomic structure reproducing all features of the diffraction data. The representative HRTEM images at different magnifications of the glassy carbon pyrolyzed at temperatures from the range 600 °C - 2500 °C are presented in Fig. 10. All information concerning the measurements was described in details in paper **P3**.

The pictures in Fig. 10 show the evolution from a network of randomly oriented, disordered carbon domains for low temperature GC600 to a more organized system for high temperature GC2500, resembling onion-like elements in which carbon layers are less rippled. With increasing the carbonization temperature above 600°C the curvature related with elements resembling fragments of nanotubes, fullerenes, onions or even completely closed fullerene-like particles is more prevalent. The different types of curved structural elements for the GC980 are marked with arrows in Fig. 10(h,i). During the heat treatment process the glassy carbon crystallites grow at the expense of the more disordered part of the microstructure. The less-organized regions are consumed by the domains with parallel layers resulting in their growth, both in width and height, and simultaneously in creation of empty voids. In the low-temperature glassy carbons the microporosity is a direct consequence of misalignment of the curved sheets or their packages. As the annealing temperature increases the bigger pores are formed due to joining of disordered fragments to more ordered domains. This leads to creation of isolated, non-connected voids such as these marked with circle frames in Fig. 10(n,r).
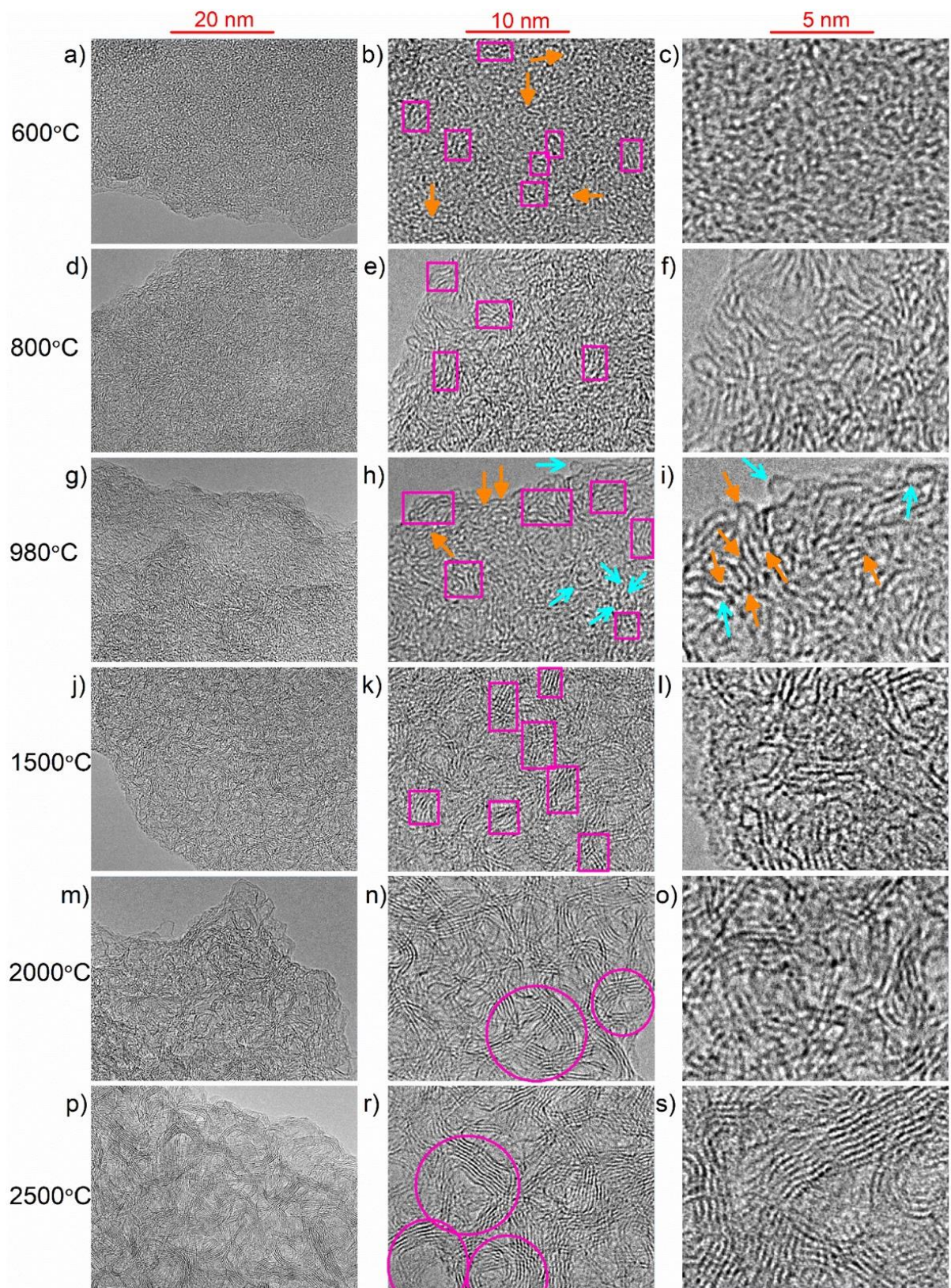
Fig. 10 Representative HRTEM images at various magnifications of different regions of glassy carbon samples pyrolyzed at temperatures from the range 600-2500°C. Rectangular frames expose domains with stacked graphene-like layers; round frames show onion-like structures enclosing pores; arrows indicate curved structural units [P3].

2.2.2.   Raman spectroscopy

For further examination of the structural changes in the glass-like carbon subjected to the thermal treatment the Raman scattering was measured. The analysis of the Raman spectra is widely described in paper **P3**. The first order Raman spectra display two main peaks, G and D marked in Fig. 11(a), which are characteristic features of graphitic carbons [51]. The spectra of the first-order Raman region normalized to the G band intensity are presented in Fig. 11(b). The intensity of the D band increases with respect to the G band intensity with increasing pyrolysis temperature up to 2500°C. Such dependence is in agreement with the rule proposed by Ferrari and Robertson [52] claimed that for amorphous and disordered carbons containing small clusters below about 25 nm the development of the D peak indicates their ordering and grow.
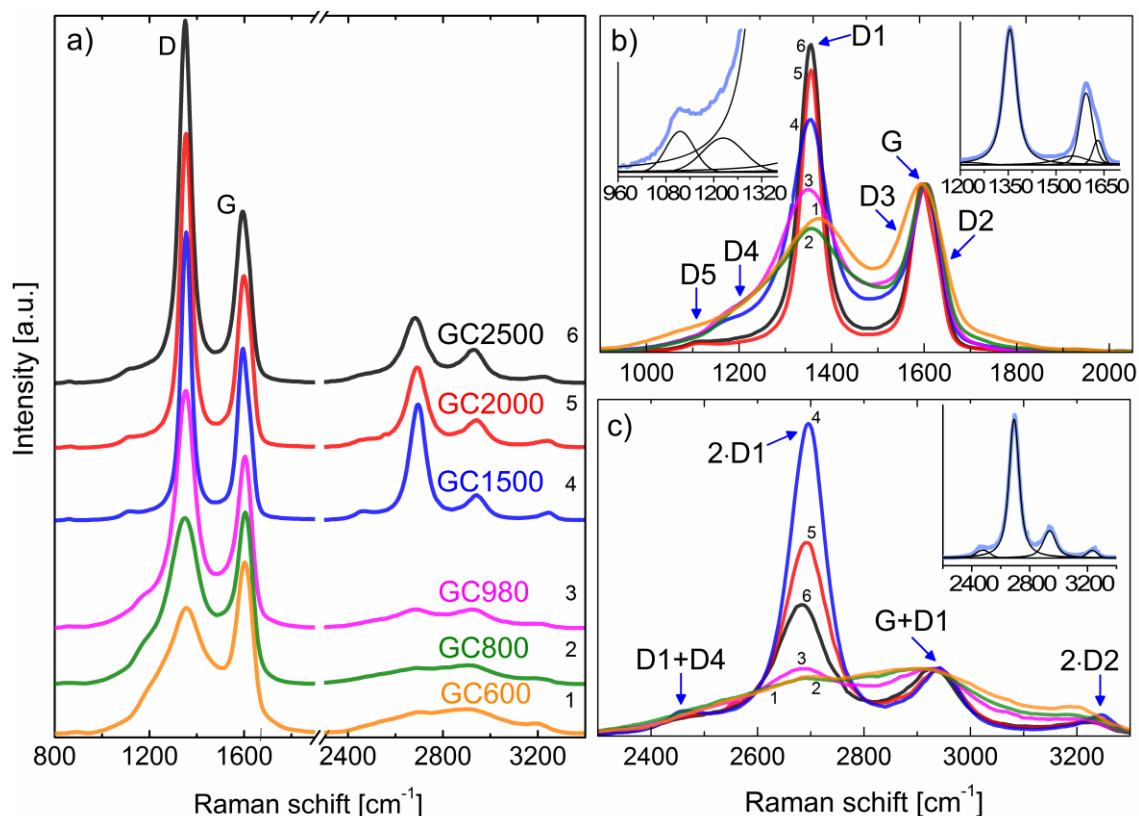
Fig. 11 Overview of the Raman spectra for glassy carbons pyrolyzed at different temperatures from the range of 600-2500°C (GC600-GC2500) (a); comparison of the normalized spectra for the first-order region (b) and the second-order region (c). The insets show the best fit of the experimental data for glassy carbon pyrolyzed at 1500°C (GC1500) [**P3**].

The D4 and D5 features around 1210 cm^{-1} and 1110 cm^{-1}, respectively, were taken into account for the total Raman spectra as showed in Fig. 11(b). They may come from the

vibrations of carbon atoms in non-hexagonal rings such as STW defects which are considered as the possible reason of the fullerene-like structure of glassy carbons. The signal from Stone-Thrower-Wales defects on single-walled carbon nanotubes were experimentally and theoretically identified just in the range of 1100-1200 cm^{-1} [53,54].

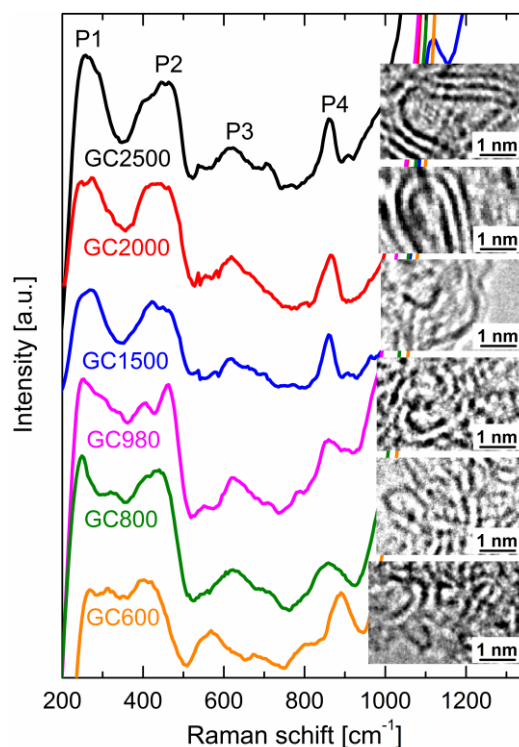Fig. 12 Low-frequency Raman modes for glassy carbons pyrolyzed up to different temperatures from the range of 600-2500°C (GC600-GC2500). The insets show selected HRTEM images with curved structural units of around 1 nm in diameter [**P3**].

The measured Raman spectra were also carefully examined in the low frequency region below 900 cm^{-1}. A number of Raman-active modes were observed is this region. They probably are an evidence of the curved structural units in the studied carbons. All studied here glassy carbons show peaks near 260 cm^{-1} (P1), 440 cm^{-1} (P2), 620 cm^{-1} (P3) and 860 cm^{-1} (P4), as can be seen in Fig. 12, while it is known that this Raman region is completely silent for graphite and diamond crystals according to the group theory [55]. Analogous bands in the low-frequency region of Raman spectra were found for carbon nanotubes, fullerenes or nanoonions [30-31,55-57], as well for more exotic non-planar carbon structures such as tubular cones, whiskers and polyhedral crystals [58]. The P1 peak around 260 cm^{-1} can be related to breathing modes of carbon atoms in curved structural units, analogous to the radial breathing modes in carbon nanotubes [59]. In paper **P3** it was qualified that the diameter of the nanotube-like fragments responsible for the breathing vibrations may be of approximately

1 nm. Interestingly, such nanotube-like elements of approximately 1 nm in diameter can be found in HRTEM images and their examples were shown as insets to the Fig. 12. The diameter of order of 1 nm fits the geometrical size of pores enclosed by the curled layers presented here in the proposed structural models, and in the HRTEM images, especially for the low-temperature glassy carbons.

Beside the P1 peak, the Raman spectra contain also broad features with maxima at around 440 cm^{-1} (P2), 620 cm^{-1} (P3) and 860 cm^{-1} (P4). They are analogues to the Raman features identified for carbon nanoonions [57] and nanotubes [30]. Two possible explanations for the origin of these peaks are that they are combination of the acoustic and optical phonon modes activated due to radial geometry, or they are defect-induced modes [60].

2.2.3.   *Electron energy loss spectroscopy*

The X-ray diffraction studies combined with computer simulations, HRTEM images, and Raman scattering results clearly evidenced that the structure of glass-like carbons have features of non-planar structure of nanocarbons such as fullerenes, nanotubes or nanoonions. The question that subsequently arises is what type of bonds between carbon atoms the curved layers contain. Particularly, it would be of great interest to estimate the amount of sp^3 diamond-like bonds, since they are very strong and could explain the glassy carbon high hardness. To verify the possible content of sp^3 bonds in the studied glassy carbons electron energy loss spectroscopy was employed. The experimental details on the EELS measurements, data treatment, and analysis can be found in paper **P3**.
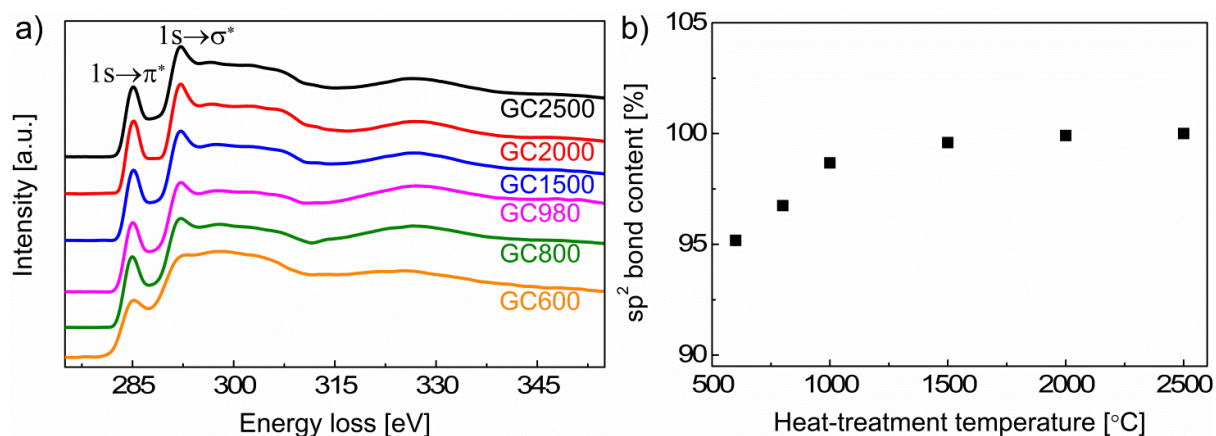

Fig. 13 Variation in the glassy carbon electron-energy loss in the C-K edge region (a), and in the determined sp^2-hybridized bond content (b) as a function of pyrolysis temperature from the range of 600-2500°C (GC600-GC2500) [**P3**].

The representative EELS spectra in the C K-edge region are shown in Fig 13(a). With increase in pyrolysis temperature the EELS spectra show an increase in the intensity of the π* peak in respect to the σ* peak intensity. Such a behavior is typical for conversion of disorder carbon structure towards graphitic sp^2 bond configuration [61]. The procedure developed by Berger, McKenzie and Martin [62] was used for determining the fraction of sp^2-bonded carbon atoms in respect to the total content of sp^2 and sp^3 bonds, results are presented in Fig. 13(b). The fraction of sp^2 bonds rises from about 95% for low temperature glassy carbon, GC600, up to almost 100% for high temperature GC2000.

The obtained EELS spectra gave also an opportunity to measure the amount of non-planar sp^2 bonds related with fullerene-like structure. The method described by [63] was used to determine the fraction of the sp^2 non-planar bonds to the total sp^2 bond content (fullerene-like non-planar and graphitic-like planar). The results presented in Fig. 14 show that the ratio of non-planar sp^2-bonded to all sp^2-bonded carbon atoms increases from approximately 25% for GC600 up to about 38% for GC980, and then a subsequent drop of this ratio is watched up to about 30% for GC2500.
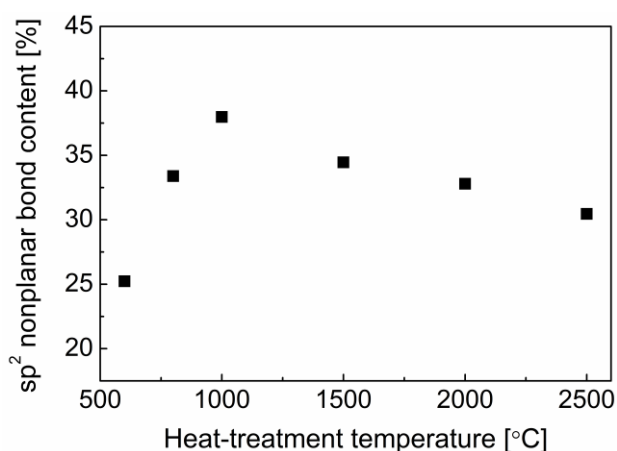
Fig. 14 The variation in the sp^2-hybridized non-planar bond content as a function of pyrolysis temperature from the range of 600-2500°C [**P3**].

2.3. Correlations preparation-structure-mechanical properties

At the last stage of this research a special emphasis has been placed on the correlations between glass-like carbon preparation, structure and mechanical properties. Particularly, I was focused on the explaining whether structural disorder makes these materials harder and

stronger, or softer and weaker, and also what is the optimal heat treatment temperature for applications of glassy carbon in mechanically demanding products.

Fig. 15 shows the effect of pyrolysis temperature on the mechanical properties, hardness (H) and reduced Young's modulus (E_r), of the glassy carbons measured using nanoindentation technique. The results of these studies were published in paper **P3**. The values of the determined hardness and reduced Young's modulus rise from around 3 GPa and 16 GPa, respectively, for glassy carbon carbonized at 600°C up to around 6 GPa and 38 GPa, respectively, for 980°C. With further increase in heat treatment temperature, a continues decrease in H and E_r is observed up to around 4 GPa and 27 GPa, respectively, for 2500°C. The changes in hardness and reduced Young's modulus follow the same trend as the changes in the content of non-planar to the total amount of sp^2 carbon bonds with increase in pyrolysis temperature, as described in previous section. Comparison of the data from EELS in Fig. 14 with nanoindentation results in Fig. 15 shows that the measured mechanical properties are a direct response of the structural transformation that undergoes with increase in heat treatment temperature. The fraction of sp^2 non-planar, fullerene-like or nanotube-like bonds with respect to the total content of sp^2 bonds between carbon atoms may be successfully used for glassy carbon hardness and Young's modulus rating.
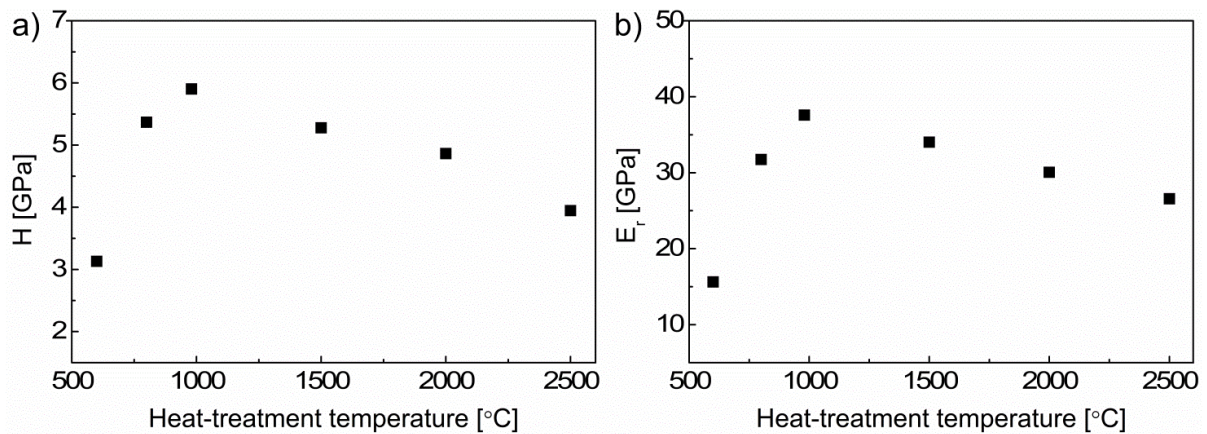
Fig. 15 Variation in the glass-like carbon nanoindentation hardness (a), and reduced Young's modulus (b) as a function of pyrolysis temperature from the range of 600-2500°C [**P3**].

Carbon nanotubes are one of the strongest materials nowadays known [64]. The presence of nanotube-like elements in the structure of non-graphitizing glass-like carbons can be responsible for their high hardness and strength comparing to graphitizing carbons. The nanotube-like bridges between neighboring carbon layers evident in HRTEM images of Fig. 10 bind the entire structure into a tight network. It is worth to mention that the proposed here

structural models of glass-like carbons display the possible configurations of such fullerene-like or nanotube-like interfaces. Based on the models it was established that the creation of such interlayer connections, or so-called crosslinks, is facilitated by the presence of defects in form of non-hexagonal rings, vacancies, isolated sp^3 bonds or chains which introduce curvature. The curved units may also effectively inhibit the movement of carbon layers and prevent the graphitization.

The optimal temperature of pyrolysis for the best mechanical performance of glass-like carbon prepared here as described in papers **P1**, **P2** and **P3** is around 1000 °C. When this carbon is processed at temperatures higher than 1000 °C, it becomes more ordered but less hard and elastic. It should be pointed out that the prepared glass-like carbons carbonized at different temperatures were also tested for use in heart valves. The results of tribological characteristics, as well as micromechanical properties were published in articles [65,66]. A correlation was observed between hardness, Young's modulus, and the stabilized friction coefficient. It was shown that the increase in the heat treatment temperature from 1000 °C to 2500 °C results in reduction of the stabilized friction coefficient with decrease in the microhardness and Young's modulus.

3. Concluding remarks

This thesis represents fundamental research connecting all three facets of synthesis, structure, and properties of glass-like carbons. These non-graphitizing, hard glass-like carbons produced by pyrolysis of polyfurfuryl alcohol at different temperatures from 600 °C up to 2700 °C have been thoroughly characterized using different experimental techniques such as wide-angle X-ray and neutron scattering, high-resolution transmission electron microscopy, Raman spectroscopy, electron energy loss spectroscopy, nanoindentation, and computer simulations of the atomic structure based on paracrystalline model and classical molecular dynamic method. The applied comprehensive approach allowed collecting broad range of information about their structure and its relations to properties and pyrolysis conditions.

The most significant achievements of this doctoral project, I would like to point out, are as follows:

- Proving by many different techniques that the atomic structure of glass-like carbons has much in common with the structure of non-planar nanocarbons such as fullerenes, nanotubes, and nanoonions.

- Proposing of structural models of the glassy carbons at different stages of pyrolysis process which are compatible with various experimental results and explain the observed properties.

- Exposing the possible type and amount of topological defects in these carbons, their changes during thermal treatment up to 2500 °C, and their effect on the topology of the atomic structure.

- Indicating that the Raman spectroscopy method can be used as a tool for verification of the presence and quantifying of curved-spaced structures in carbon materials.

- Demonstrating the insignificant amount of diamond-like sp^3-bonds in glassy carbons and excluding their presence as a main factor governing their mechanical properties.

- Exhibiting the scaling of the glassy carbon hardness and Young's modulus with the structure and pyrolysis conditions.

- Explaining the origin of the glass-like carbon microporosity, high hardness and strength comparing to graphitizing carbons, and resistance to graphitization in regards to their structure.

The fundamental knowledge about glass-like carbons flowing from this research could be impactful for design and fabrication of new carbon systems with tailored or even transformative properties for applications in many areas of life, such as medicine, aerospace and automotive industry or electrochemistry.

4. Publications with statements of co-authors on contribution

4.1.   P1: Paracrystalline structure of glass-like carbons

Jurkiewicz, K., Duber, S., & Burian, A. (2016). Paracrystalline structure of glass-like carbons. *International Journal of Applied Glass Science*, *7*(3), 355-363, DOI: 10.1111/ijag.12186.

Contribution of the first author to this publication was preparation of glass-like carbons, performing X-ray diffraction measurements, performing the data treatment, analysis and interpretation, performing computer simulations, writing and editing the manuscript.

Zakład Biofizyki i Fizyki Molekularnej   Chorzów, 04.11.2017 r.
Instytut Fizyki, Uniwersytet Śląski w Katowicach
Śląskie Międzyuczelniane Centrum Edukacji i Badań Interdyscyplinarnych
ul. 75 Pułku Piechoty 1A, 41-500 Chorzów

Statement on the contribution to publication

Publication:
Jurkiewicz, K., Duber, S., & Burian, A. (2016). Paracrystalline structure of glass-like carbons. *International Journal of Applied Glass Science*, 7(3), 355-363.
DOI: 10.1111/ijag.12186

We hereby state that the contribution to the work published jointly with Karolina Jurkiewicz is in accordance with the description below:

Karolina Jurkiewicz
Preparation of glass-like carbons, performing X-ray diffraction measurements, performing the data treatment, analysis and interpretation, performing computer simulations, writing and editing the manuscript.

Signature:

Stanisław Duber
Participation in preparation of carbon materials.

Signature:

Andrzej Burian
Providing scientific consultations and participation in editing the manuscript.

Signature:

INTERNATIONAL JOURNAL OF

Applied Glass
SCIENCE

Paracrystalline Structure of Glass-Like Carbons

Karolina Jurkiewicz* and Andrzej Burian

A. Chełkowski Institute of Physics, University of Silesia, Katowice, 40-007, Poland

Silesian Center for Education and Interdisciplinary Research, Chorzów, 41-500, Poland

Stanisław Duber

Laboratory of Structural Research, University of Silesia, Chorzów, 41-500, Poland

This study reports on structural characterization of a series of glass-like carbons obtained by pyrolysis of polyfurfuryl alcohol at 600, 800, 980, and 2700°C. The atomic scale structure of the prepared materials has been studied using wide-angle X-ray scattering technique. The acquired diffraction data were analyzed in reciprocal space as the structure factor and in real space in the form of the pair distribution function to reveal the structural attributes such as number of hexagonal network layers, size of the layers, interlayer correlations, interlayer and interatomic distances. The parameters have different effects on the diffraction intensity and the pair distribution function and are verified in reciprocal and real diffraction space simultaneously. The obtained results show that the structure of the glass-like carbons consists of defective graphite-like domains which size increase with the pyrolysis temperature. The heat treatment leads to a noticeable ordering of coherently scattering domains of glass-like carbon in directions perpendicular to graphene-like layers. However, paracrystalline type of disorder within individual layers manifesting itself in decrease in intensity and broadening of the diffraction lines is preserved in the atomic structure even at heat-treatment temperature of 2700°C.

Introduction

Glass-like carbons appeared as commercially available products in the early sixties.[1] Thereafter, most scientific investigations were concerned with the interesting properties of this material combining the features of graphite with those of glass: high temperature and chemical resistance, good electrical conductivity, closed porosity, high hardness, and excellent biocompatibility.[2–4] The unique combination of the properties

has drawn attention of many scientists to the atomic structure of this form of carbon. Over the years, many structural models have been put forward[1,5,6] but none has been entirely satisfactory in explaining the origin of the glass-like carbon properties. In principle, the structure of glass-like carbons at the atomic level remains still poorly understood. More research is needed to determine the arrangement of atoms in detail and to understand the relationship between the atomic scale structure and physical properties. However, due to the lack of long range atomic ordering, the structure of investigated materials cannot be probed by conventional methods used for crystalline materials. One of the most

powerful techniques to study noncrystalline structures is wide-angle X-ray scattering (WAXS). In the WAXS experiment, the distribution of coherently scattered radiation using incident X-rays with an appropriate wavelength is measured and used for obtaining structural information. The observed diffraction pattern may be converted by the Fourier transform to the pair distribution function which yields quantitative data for a direct modeling of the real space structures. The WAXS technique used together with the modeling studies has proved to be efficient tools for probing the structure of various noncrystalline carbon materials as reported in our previous studies.[7–11]

Among the proposed structural models of glass-like carbon, one of the most frequently mentioned is the model of turbostratic carbon[12–14] featured by alignment of flat graphite layers stacked without spatial correlations in the direction perpendicular to layers. The adjacent planes are shifted or rotated with respect to one another that results in lack of graphitic -ABAB- stacking sequence and increase in the interlayer spacing. The model was developed by Warren as a first approach to the structure of carbon black.[15] Warren showed that the orientations of stacked graphite domains in the investigated carbons are uncorrelated and described this arrangement as turbostratic. Early structural models of other type of carbon materials—activated carbons—have also assumed turbostratic disorder.[1,16] It has been previously reported that the theoretical pair distribution function calculated based on the turbostratic theory for activated carbons, prepared from a polymer of phenol formaldehyde resin, could not reproduce all the features of the experimental data.[17] Therefore, it has been realized that additional disorder should be imposed on the structural models to account for the experimental data. It has been assumed that network distortion propagates proportionally to the square root of the interatomic distances, according to the paracrystalline theory. This approach has been proposed and then developed by Hossemann and his group.[18,19] The model with the graphite-like arrangement within a single layer and paracrystalline-type disorder of the two-dimensional hexagonal structure has proved to be more appropriate description of the atomic scale structure of the activated carbons.[7,17]

The main purpose of this study was to verify whether the idea of turbostratic or paracrystalline disorder can be supported for the interpretation of the diffraction data for the prepared glass-like carbons. A comparison between theoretical and experimental diffraction data is used as a first examination of considered structural models.

Experimental Procedure

Sample Preparation

The investigated glass-like carbon samples were prepared from furfuryl alcohol as a precursor. The polymerization of furfuryl alcohol (from SAFC, ≥ 98% pure) was carried out by addition of 2% (v/v) of 0.1 M p-toluenesulfonic acid (from Acros Organics, 99% pure) solution in ethanol. The homogenization of the catalyst in the furfuryl alcohol was accomplished by magnetic stirring for 24 h. The catalyzed precursor was then cast in the molds and held at 120°C for 2 h for curing. After polymerization, the resin was divided into different batches and carbonized under Ar gas flow at different temperatures: 600, 800, 980, and 2700°C (samples 1–4, respectively; this enumeration of samples will be used when describing results). The heating rate was 10°C/h to 200°C and 5°C/h to the desired temperature. Upon reaching the final heat-treatment level, the temperature was held constant for 2 h. The samples were allowed to cool in Ar flow.

Wide-Angle X-Ray Scattering Measurements and Data Processing

The wide-angle X-ray scattering (WAXS) measurements were performed using a laboratory diffractometer (Rigaku-Denki D/MAX RAPID II-R) equipped with a rotating Ag anode ($\lambda_{K\alpha}$ = 0.5608 Å), an incident beam (*002*) graphite monochromator and an image plate in the Debye–Scherer geometry as a detector. The powder samples were measured at room temperature in glass capillaries with a diameter of 1.5 mm and wall thickness of 0.01 mm. The scattered X-ray radiation was recorded as two-dimensional diffraction patterns and then converted into a one-dimensional function of intensity versus the scattering vector $I(Q)$, where $Q = 4\pi\sin\theta/\lambda$, 2θ is the scattering angle and λ is the wavelength of the incident beam. The intensity functions were corrected for background, polarization, absorption, and incoherent Compton scattering and normalized using the data processing procedure developed for high energy X-rays.[20–22] In the next step, the diffraction data were expressed as the structure factor

which is related to the corrected and normalized (to the electron units) intensity $I(Q)$ divided by square of the carbon atomic scattering factor f^2 according to the following formula:

$$S(Q) = \frac{I(Q)}{f^2(Q)} \qquad (1)$$

The $S(Q)$ depends only on distribution of atoms, so on the structure of investigated object and not on the atomic scattering power. For an advanced analysis of the structural features of investigated carbons, the structure factor determined for each sample was converted to the real space representation of the diffraction data in the form of the pair distribution function PDF(r) as follows:

$$PDF(r) = \frac{2}{\pi} \int_0^{Q_{max}} Q[S(Q) - 1]\sin(Qr)\frac{\sin(\pi Q/Q_{max})}{\frac{\pi Q}{Q_{max}}} dQ \qquad (2)$$

where $Q_{max} = 22$ Å is the maximum value of scattering vector reached in the measurement, r is the interatomic distance in the real space and the last term refers to the Lorch function. The termination of Fourier integral at a finite value of Q_{max} introduces high-frequency ripples in the real space distribution function. The used Lorch modification function minimizes the unwanted effect of the finite Q_{max} value.

The pair distribution function is proportional to the probability of finding two atoms separated by a distance of r and is not centered in any specific atom, thus giving a structural description of local ordering around any atom in the structure. Successive PDF peaks correspond to nearest-, second-, and next-neighbor atomic distribution. The PDF approach is widely used to study the local structure of liquids, glasses, and disordered materials. The classical diffraction analysis methods are limited for such kinds of materials because, due to the lack of the crystalline order, only few atomic planes will be participating coherently in the diffraction. The advantage of the PDF method is that all the diffuse scattering is integrated and so the structural information inherent to it is recovered.

Modeling of Atomic Structure

The glass-like carbons investigated in this work have the structure intermediate between crystalline and amorphous. For predicting the scattered intensity in diffraction process from such kind of disorder materials, the Debye's formula within the kinematic theory of X-ray scattering can be used.[23] In the case of scattering by a system consisting of N atoms, the distribution of scattered intensities averaged over all orientation can be calculated as follows:

$$I_N(Q) = f^2 \sum_{i,j=1}^N \frac{\sin(Qr_{ij})}{Qr_{ij}} \qquad (3)$$

The $I(Q)$ is related to the structure factor $S_N(Q)$ in accordance with Eq. (1). For modeling of the atomic structure, the Debye's equation normalized to one atom was used. The final structure factor per one atom can be calculated as follows:

$$S(Q) = 1 + \frac{1}{N}\left[\sum_{i,j=1}^N \frac{\sin(Qr_{ij})}{Qr_{ij}} \exp\left(-\frac{\sigma^2_{ij}Q^2}{2} \right) \right]_{i \neq j} \qquad (4)$$

where the last exponential term describes the generalized Debye–Waller-type factor that characterizes attenuation of the intensity due to thermal vibrations of atoms and static disorder and σ_{ij} is the standard deviation of the interatomic distance r_{ij}. The small-angle X-ray scattering contribution to the diffraction pattern appearing in theoretical $S(Q)$ at small Q does not contain information about the atomic distribution and was eliminated as described by Mitchell.[24] In the next step, the scattering data were converted to the real space representation by the sine Fourier transform of $S(Q)$ according to the Eq. (2) yielding the theoretical pair distribution function PDF(r). Such an approach allows direct comparison of the simulation results with the experimental data in both reciprocal and real spaces.

In the modeling studies presented in this study, the intensity of the X-rays scattered by atoms arranged like in the graphite structure was calculated using the Debye's equation, and then, a disorder was imposed on the system. Two approaches to the disorder investigation were considered. In the first one, the turbostratic contribution was taken into account. The model was defined by as follows: the lattice constant a of the graphitic structure; the dimensions x and y of a rectangular graphitic layer; the number of layers n; the interlayer spacing d; and the standard deviations of interatomic distances due to thermal vibrations of atoms for atoms laying in the same layer σ_{intra} and for atoms lying in

different layers σ_{intra}. To fulfill the requirements of the turbostratic theory, neighboring graphitic planes were translated relative to each other by a distance t expressed as a fraction of the lattice constant.

In the second approach, the paracrystalline structure was generated. The paracrystalline theory is based on the assumption that the distances from any atom to adjacent atoms fluctuate without statistical correlations and these fluctuations propagate proportionally to the square root of the interatomic distance.[18,19,25] The sets of the Cartesian coordinates have been generated on the base of the input model parameters for the turbostratic structure. Then, the structure was disordered by means of the generalized Debye–Waller factor with $\sigma_{intra} = \sigma_0 \sqrt{r}$ and $\sigma_{inter} = \sigma_1 \sqrt{\Delta n}$, where σ_0 and σ_1 are adjustable parameters, $\Delta n = n_i - n_j$ (n_i and n_j label the layer position in the stack). Paracrystalline stacking

of layers was generated assuming Gaussian distribution of the interlayer spacing with the standard deviation denoted by σ_z. The final structure factor was computed by averaging over all structure factors determined for 200 statistically independent atomic arrangements in the form of the Cartesian coordinates with Gaussian distribution of the interplanar distance.

Results and Discussion

The experimental structure factors and pair distribution functions of the prepared glass-like carbons are compared with the simulated functions for turbostratic models in Fig. 1. The presented experimental data for all samples are typical for disordered carbons having the structure intermediate between crystalline and
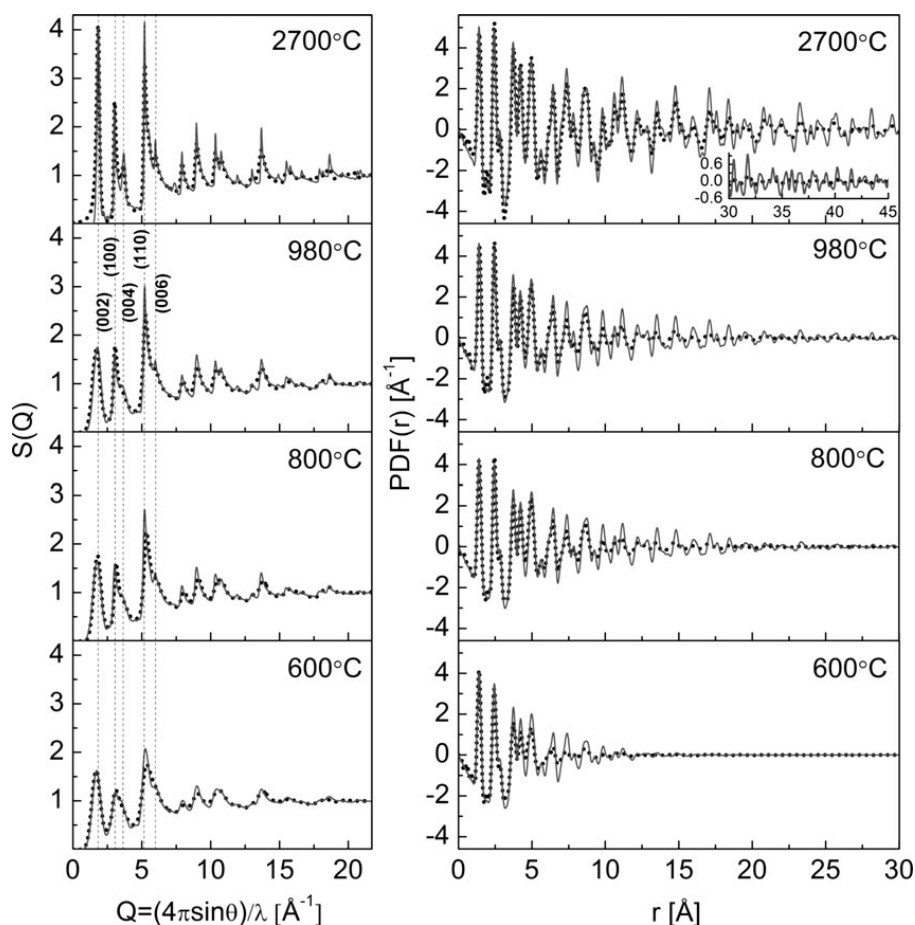

Fig. 1. Comparison of the experimental structure factors and pair distribution functions (dotted line) for the glass-like carbons carbonized at different temperatures with the simulated functions (solid line) for turbostratic models. The first few diffraction reflections were marked by the vertical dashed lines.

amorphous. The carbon heated at 600°C shows only broad diffraction peaks, and the corresponding pair distribution function exhibits features in a limited range of interatomic distances up to 10 Å. It should be pointed out that the region of the first three PDF peaks up to about 3 Å involves in the carbon–carbon bond distances in the aromatic-type hexagon of graphite. The next peaks correspond to the subsequent in-plane carbon–carbon bond distances of graphite-like structure. The presented structure factor for sample 1 resembles that of typical turbostratic carbon and contains only the (*00 2l*) and (*hk0*) graphite-type reflections. The first few diffraction reflections were identified and marked in Fig. 1. The lack of -ABAB- spatial correlations between individual graphitic layers in direction perpendicular to them is related to the absence of (*hkl*) diffraction lines. Furthermore, the (*hk0*)-type peaks are strongly asymmetric due to the Warren effect.[15,26] The observed Warren effect is related to 2D diffraction patterns typical for layered structures. For glass-like carbons prepared at higher temperatures, the features of turbostratic structure can also be noticed from analysis of the structure factors. A common attribute of the diffraction data for samples 1–3 is the intensity of the first diffraction peak (the (*002*) peak in graphite) occurring at about 1.7 Å^{-1}. The amplitude of this line depends on the number of stacked layers.[7] More than twice increase in intensity of this peak is observed for sample 4 and indicates a great extension of coherent scattering domain size in direction perpendicular to the carbon planes. With increasing the synthesis temperature, sharpening and rise of these peaks occur that can be explained by ordering of the atomic structure. As the carbonization process proceeds, the graphene-like planes continued to grow and rearranged to more ordered structural domains. However, by analyzing the diffraction patterns, it can be concluded that the investigated carbons are clearly nongraphitizing. The differences between structural orders of studied glass-like carbons are also clearly seen from the comparison of the pair distribution functions determined from Eq. 2. The range of PDF peaks and thereby the range of interatomic correlations expand as a function of heat-treatment temperature. For the material prepared at 2700°C, the structural coherence extends to approximately 45 Å. The amplitude of the subsequent PDF peaks depends on the coordination numbers and a degree of ordering. Different types of structural imperfections can easily suppress intensity of the PDF. On

the other hand, the heat-treatment process organizes the positions of atoms and can promote increase of the PDF peak amplitudes and such a behavior can be observed for the glass-like carbons.

The listed features indicate that the measured materials can be formally described as turbostratic graphite clusters with very weak correlations in the orientation of adjacent graphene layers and with nanosize of the coherently ordered domains. Therefore, an attempt was made to fit the experimental PDFs assuming their turbostratic structure. The numbers of layers in the created turbostratic models were adjusted to reproduce the amplitudes of the (*002*) first diffraction peak. The model size in direction perpendicular to the layers for the sample 4 is more than twice of that for samples 1–3. The values of the interplanar spacing have been picked out so that to estimate the positions of the (*002*) reflection. The adjusted interplanar distances (3.475, 3.42, 3.41, and 3.4 Å for sample 1–4, respectively) are clearly greater than that of graphite (3.35 Å) and also suggest the turbostratic nature of these carbons. The lattice constant for each model have been chosen so as to best reproduce the peak positions of the PDFs over the whole range of the interatomic distances. As an example, the model of the glass-like carbon structure consists of three layers is shown in Fig. 2. Playing with the values of standard deviations of interatomic distances σ_{intra}, the amplitudes of the first three PDFs lines were fitted. The values of σ_{intra} were taken the same as in case of σ_{intra}. To lose the graphitic -ABAB- correlations, the individual layers forming model have been shifted relative to each other by a distance from a range 0–t expressed as a fraction of the lattice constant. Fifty turbostratic configurations were generated and the computed structure factors were averaged. The created models have a limited size that was established in paracrystalline modeling and will be described afterward. All parameter of the simulated turbostratic models are summarized in Table I. The comparison of the experimental and computed structure factors and pair distribution functions clearly demonstrates that the turbostratic models are not able to describe correctly the atomic arrangements in the investigated samples. Peak positions are generally precisely reproduced by the constructed models but some features of experimental data are not satisfactorily reconstructed by calculated theoretical functions. The PDF peaks in the range of above 5 Å have much higher amplitudes than those of the experimental functions,
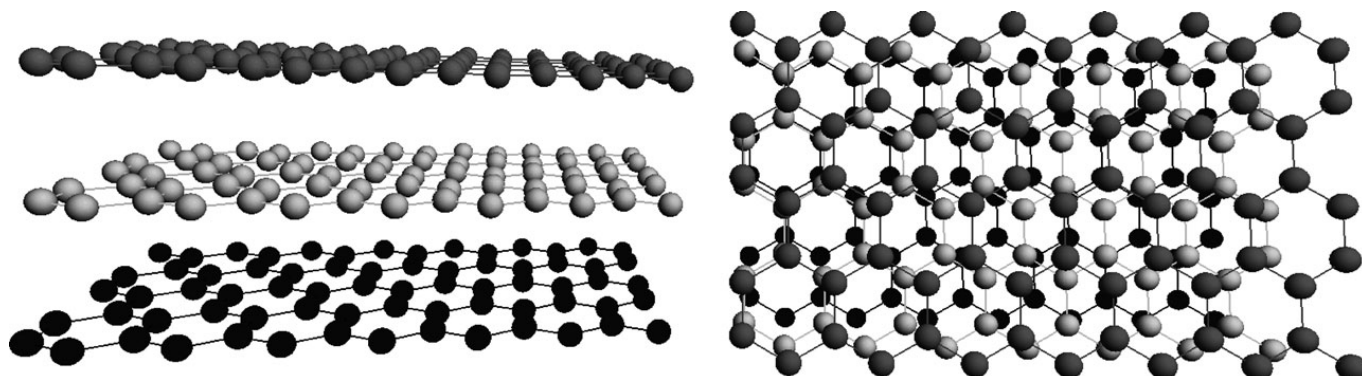
Fig. 2. *Example of geometry of the simulated glass-like carbon structures based on model for glassy carbon pyrolyzed at 600° C.*

Table I. Parameters of Simulated Models of Structure Based on Turbostratic Theory

	a [Å]	l [Å] k [Å]	n	σ_{intra} [Å] σ_{intra} [Å]	d [Å]	t
Sample 1	2.45	16	3	0.09	3.475	0.3
		9		0.09		
Sample 2	2.445	35	3	0.09	3.42	0.8
		18		0.09		
Sample 3	2.44	50	3	0.08	3.41	1.0
		18		0.08		
Sample 4	2.436	69	7	0.07	3.4	1.2
		51		0.07		

and no simple scaling of the Debye–Waller factors could improve the agreement with the experimental data both in reciprocal and real space. A general conclusion can be drawn from this analysis. The models based on the graphite structure, disordered only by the thermal vibrations of atoms and the turbostratic displacement of graphitic layers, cannot explain the real structure of glass-like carbons. Even the sample 4 prepared at 2700°C, expected as the most ordered and showing the higher degree of similarity to the structure of polycrystalline graphite, is characterized by a greater deviation from the atomic arrangement of perfect graphite. It should be noted that in such high temperature of synthesis, other noncarbon elements, which can be present in starting polymer, are removed and should not influence the disorder discussed.

In the second attempt of the analysis of the experimental WAXS data, disorder in the form of paracrystalline distortion of the atomic network was introduced into the models. The model parameters for investigated

samples 1–4 are listed in Table II. The numbers of graphitic layers for each model, the lattice constants and the values of interlayer spacing were adjusted previously by simulations of turbostratic structures. Moreover, the translation of neighboring layers in the stack was kept for describing the features of experimental data related to the turbostratic structure. The range of PDF peaks and their shape depend on the size of constructed model used for calculations. The chosen dimensions x and y of individual carbon layers as well as the adjustable parameters, σ_0 and σ_1, of standard deviations of interatomic distances result in the best agreement with experimental data. The paracrystalline distortion of graphene planes leads to a significant attenuation of the PDF peaks and hence to loss of longer-range ordering that cannot be achieved using only turbostratic-type disorder. The values of the standard deviation of interlayer spacing σ_c were estimated according to requirements of paracrystalline model. The so-called α^* relation in paracrystalline concept[18,25] determines the empirical relation between the paracrystalline domain size and degree of disorder as follows:

$$\alpha^* = \sqrt{n}\frac{\sigma_z}{d} \tag{5}$$

where $0.1 \leq \alpha^* \leq 0.2$. The formula given above means that real paracrystal has a limited size controlled by degree of disorder. The greater the size of system in direction perpendicular to stacked graphene layers, the more the regular distance between them. In the present calculations, the values of standard deviation of interplanar spacing σ_z vary from 0.25 to 0.15 Å for glass-like carbon samples 1–4, respectively. There is a closed correspondence between the expected changes in the structure of investigated carbons as a function of pyrol-

Table II.   Parameters of Simulated Models of Structure Based on Paracrystalline Theory

	a [Å]	l [Å] k [Å]	n	σ_0 [Å] σ_1 [Å]	d [Å]	σ_z [Å]	t	N
Sample 1	2.45	16 9	3	0.075 0.075	3.475	0.25	0.3	2.46
Sample 2	2.445	35 18	3	0.06 0.06	3.42	0.2	0.8	2.64
Sample 3	2.44	50 18	3	0.055 0.055	3.41	0.2	1.0	2.62
Sample 4	2.436	69 51	7	0.04 0.075	3.4	0.15	1.2	2.86

ysis temperature and the parameters of paracrystalline models. In general, the parameters that characterize disorder such as σ_0, σ_1, σ_z, and t decrease with increasing synthesis temperature. As can be seen in Fig. 3, the peak positions, their widths and amplitudes of the experimental and model functions in the reciprocal and real space are in good agreement. The paracrystalline models explain also the broadening of the pair distribution peaks with increasing the interatomic distance that can be observed for experimental functions.

The coordination numbers N for the first coordination spheres of the studied glass-like carbon structures
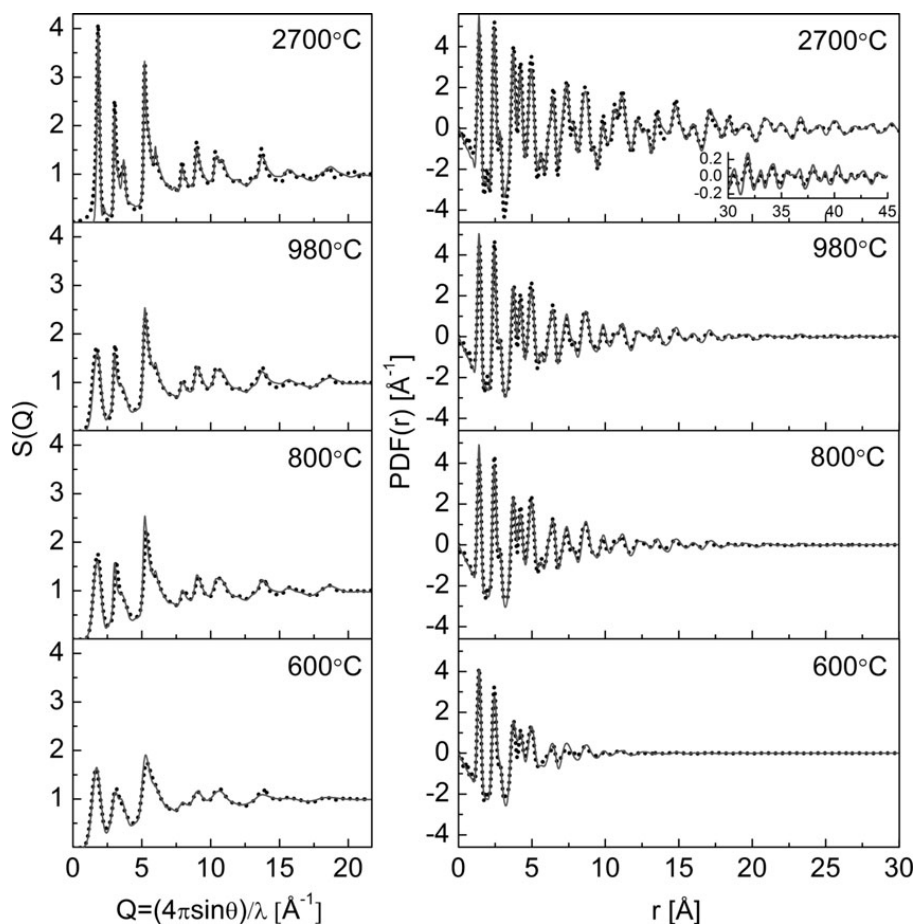

Fig. 3.   Comparison of the experimental structure factors and pair distribution functions (dotted line) for the glass-like carbons carbonized at different temperatures with the simulated functions (solid line) for paracrystalline models.

were determined from the experimental radial distribution functions by the curve-fitting method, as described in Ref. (17) and are listed in Table II. The obtained values of the coordination numbers are lower than the coordination number of a single layer graphene structure that equals three. Such a behavior is due to the "size effect" of limited coherent scattering domains in the studied materials and a significant contribution of atoms at plane edges that may be under-coordinated. At higher pyrolysis temperatures, leading to the growth of glassy carbon plane size, the determined near-neighbor coordination numbers increase and tend to the coordination number of infinite graphene network. Beside the not-compensated edge effects in the finite-sized models, different kind of structural defects may influence the atomic coordination increasing the atomic disorder.

The simulations of the structural models provided many details about the size of coherent scattering domains and the atomic arrangement within the single carbon layer and between layers. However, some discrepancies between experimental and theoretical data remain for the structure factors, as well as for the pair distribution functions. An exact analysis of these differences may require a physical implementation of disorder in the atomic structure. The recent ideas on the structure of glass-like carbons and other nongraphitizing carbons concern the presence of atomic dislocations, atom vacancies, the Stone–Thrower–Wales defects and/or graphene sheet curvature.[27–29] Such defects can lead to changes in the distribution of interatomic distances and attenuation of perfect graphitic order.

The model of the paracrystalline structure can be turned into another noncrystalline materials consisting of randomly oriented domains and containing disordered, defective atomic layers. In practice, experimental results for diffraction by glass systems should be always compared with theory/simulation in both r space and Q space, as well as with results from other experimental techniques, so as to create a complementary atomistic three-dimensional structural model.

Conclusions

In our work, we studied thermal evolution of atomic structure of glass-like carbon prepared by pyrolysis of polyfurfuryl alcohol using the wide-angle X-ray scattering and computer simulations with pair distribution function formalism. It is important to point out that neutron scattering provides data for which scattering cross section is Q independent.[30–32] While in the case of X-ray scattering, the measured intensity is strongly diminishing with Q and for carbon samples, the intensity in a higher Q range is dominated by the Compton scattering.[33] It may cause normalization problems but the carefully performed correction and normalization procedures allow getting reliable data that can be Fourier converted to the form of the pair distribution function as it was shown in our previous study.[33]

The simulations of structural models based on turbostratic and paracrystalline theory allowed calculation of the theoretical structure factors and the atomic pair distribution functions. The obtained X-ray diffraction data show that an increase in the pyrolysis temperature leads to a noticeable ordering of coherently scattering domains of glass-like carbon in directions parallel and normal to the graphene layers. However, the general type of disorder is preserved even at heat-treatment temperature of almost 3000°C. The experimental WAXS data remain some features of the turbostratic structure with very weak interlayer spatial correlations. Nevertheless, the considered models based on turbostratic theory could not be treated as a comprehensive specification of glass-like carbon nanoclusters. The results obtained from the modeling indicate the presence of more complex lattice distortion in studied materials that can be accurately described in terms of the paracrystalline theory. Now our challenge is therefore to create a realistic model of glass-like carbon atomic structure that would comply with all the diffraction data and other experimental results simultaneously. The physical implementation of paracrystalline perturbation in the structure can be related to the presence of different types of topological imperfections such as vacancies and Stone–Wales defects or atomic domain edges and boundaries. Moreover, glass-like carbons are regarded as porous materials for which special attention should be paid to the data analysis.[34,35]

The effect of the structural defects listed above on the diffraction data of glass-like carbons will be a subject of our future work.

Acknowledgments

References

1. P. J. F. Harris, "Fullerene-Related Structure of Commercial Glassy Carbons," *Philos. Mag.*, 84 [29] 3159–3167 (2004).

2. Z. Laušević and S. Marinković, "Mechanical Properties and Chemistry of Carbonization of Phenol Formaldehyde Resin," *Carbon*, 24 [5] 575–580 (1986).

3. A. Dekanski, J. Stevanovic, R. Stevanovic, B. Ž. Nikolic, and V. M. Jovanovic, "Glassy Carbon Electrodes: I. Characterization and Electrochemical Activation," *Carbon*, 39 [8] 1195–1205 (2001).

4. A. Braun *et al.* , "X-Ray Scattering and Adsorption Studies of Thermally Oxidized Glassy Carbon," *J. Non-Cryst. Solids*, 260 [1] 1–14 (1999).

5. G. M. Jenkins and K. Kawamura, "Structure of Glassy Carbon," *Nature*, 231 175–176 (1979).

6. L. A. Pesin and E. M. Baitinger, "A New Structural Model of Glass-Like Carbon," *Carbon*, 40 [3] 259–306 (2002).

7. A. Szczygielska, A. Burian, and J. C. Dore, "Paracrystalline Structure of Activated Carbons," *J. Phys.: Condens. Matter*, 13 [24] 5545–5561 (2001).

8. J. Koloczek, A. Brodka, A. Burian, J. C. Dore, V. Honkimaki, and T. Kyotani, "Structural Studies of Carbon Nanotubes Obtained by Template Deposition Using High-Energy X-Ray Scattering," *Diam. Relat. Mater.*,15 [4] 1036–1040 (2006).

9. L. Hawelek, A. Brodka, J. C. Dore, V. Honkimaki, S. Tomita, and A. Burian, "Structural Studies of Nanodiamond by High-Energy X-Ray Diffraction," *Diam. Relat. Mater.*, 17 [7] 1186–1193 (2008).

10. L. Hawelek, A. Brodka, J. C. Dore, V. Honkimaki, and A. Burian, "The Atomic Scale Structure of CXV Carbon: Wide-Angle X-Ray Scattering and Modeling Studies," *J. Phys.: Condens. Matter*, 25 [45] 454203 (2013).

11. L. Hawelek, A. Kolano-Burian, J. Szade, W. Maziarz, N. Woznica, and A. Burian, "The Atomic Scale Structure of Nanographene Platelets Studied by X-Ray Diffraction, High-Resolution Transmission Electron Microscopy and Molecular Dynamics," *Diam. Relat. Mater.*, 35 40–46 (2013).

12. F. C. Cowlard and J. C. Lewis, "Vitreous Carbon—A New Form of Carbon," *J. Mater. Sci.*, 2 [6] 507–512 (1967).

13. M. I. Nathan, J. E. Smith Jr., and K. N. Tu, "Raman Spectra of Glassy Carbon," *J. Appl. Phys.*, 45 [5] 2370–2370 (1974).

14. M. S. Dresselhaus, G. Dresselhaus, and P. C. Eklund, *Science of Fullerenes and Carbon Nanotubes: Their Properties and Applications*, Chapter 2, 24–24, Academic Press, San Diego, California, 1996.

15. B. E. Warren, "X-Ray Diffraction in Random Layer Lattices," *Phys. Rev.*, 59 [9] 693–698 (1941).

16. P. J. F. Harris, "New Perspectives on the Structure of Graphitic Carbons," *Crit. Rev. Solid State Mater. Sci.*, 30 [4] 235–253 (2005).

17. A. Burian, A. Ratuszna, J. C. Dore, and S. W. Howells, "Radial Distribution Function Analysis of the Structure of Activated Carbons," *Carbon*, 36 [11] 1613–1621 (1998).

18. R. Hosemann and S. N. Bagchi, *Direct Analysis of Diffraction by Matter*, North-Holland Publishing Co., Amsterdam, 1962.

19. R. Hosemann and A. M. Hindeleh, "Structure of Crystalline and Paracrystalline Condensed Matter," *J. Macromol. Sci. Phys. B*, 34 [4] 325–356 (1995).

20. H. Schlenz, J. Neuefeind, and S. Rings, "High-Energy X-Ray Diffraction Study of Amorphous (Si0.71Ge0.29)O2," *J. Phys.: Condens. Matter*, 15 [29] 4919–4926 (2003).

21. H. F. Poulsen, J. Neuefeind, H. B. Neumann, J. R. Schneider, and M. D. Zeidler, "Amorphous Silica Studied by High Energy X-Ray Diffraction," *J. Non-Cryst. Solids*, 188 [1–2] 63–74 (1995).

22. L. Hawelek, J. Koloczek, A. Burian, J. C. Dore, V. Honkimaki, and T. Kyotani, "Application of Image Plate for Structural Studies of Carbon Nanotubes By High-Energy X-Ray Diffraction," *J. Alloys Comp.*, 401 [1–2] 51–54, (2005).

23. P. Debye, "Zerstreuung von röntgenstrahlen," *Ann. Phys.*, 351 [6] 809–823 (1915).

24. G. R. Mitchell, "Eliminating the Small-Angle Component of the Scattering Calculated for Models," *Acta Crystallogr. Sect. A*, 37 [4] 488–490 (1981).

25. A. M. Hindeleh and R. Hosemann, "Paracrystals Representing the Physical State of Matter," *J. Phys. C: Solid State Phys.*, 21 [23] 4155–4170 (1988).

26. B. E. Warren and P. Bodenstein, "The Diffraction Pattern of Fine Particle Carbon Blacks," *Acta Crystallogr.*, 18 [2] 282–286 (1965).

27. S. J. Townsend, T. J. Lenosky, D. A. Muller, C. S. Nichols, and V. Elser, "Negatively Curved Graphitic Sheet Model of Amorphous Carbon," *Phys. Rev. Lett.*, 69 [6] 921–924 (1992).

28. P. J. F. Harris, "Imaging the Atomic Structure of Activated Carbon," *J. Phys.: Condens. Matter*, 20 [36] 362201 (2008).

29. P. J. F. Harris, "Fullerene-Like Models for Microporous Carbon," *J. Mater. Sci.*, 48 [2] 565–577 (2012).

30. P. Zhou, R. Lee, A. Claye, and J. E. Fischer, "Layer Disorder in Carbon Anodes," *Carbon*, 36 [12] 1777–1781 (1998).

31. M. Acharya *et al.* , "Simulation of Nanoporous Carbons: A Chemically Constrained Structure," *Philos. Mag. B*, 79 [10] 1499–1518 (1999).

32. V. Petkov, R. G. DiFrancesco, and S. J. L. Billinge, "Local Structure of Nanoporpus Carbons," *Philos. Mag. B*, 79 [10] 1519–1530 (1999).

33. L. Hawelek *et al.* , "Wide-Angle X-Ray Scattering as a Quality Test for Carbon Nanotubes," *Diam. Relat. Mater.*, 29 [1] 18–22 (2012).

34. D. F. R. Mildner and J. M. Carpenter, "The Normalization of Diffraction from Porous Non-Crystalline Systems," *J. Non-Cryst. Solids*, 69 [1] 27–37 (1984).

35. C. G. Summerfield, D. F. R. Mildner, and J. M. Carpenter, "Mixing of Phases in Non-Crystalline Materials: Application to Carbon," *J. Non-Cryst. Solids* 57 [2] 289–303 (1983).

4.2. P2: Modelling of glass-like carbon structure and its experimental verification by neutron and X-ray diffraction

Contribution of the first author to this publication was preparation of glass-like carbons, performing X-ray and neutron diffraction experiments, performing data treatment, analysis and interpretation, performing computer simulations of structure, writing and editing the manuscript.

.

Zakład Biofizyki i Fizyki Molekularnej
Instytut Fizyki, Uniwersytet Śląski w Katowicach
Śląskie Międzyuczelniane Centrum Edukacji i Badań Interdyscyplinarnych
ul. 75 Pułku Piechoty 1A, 41-500 Chorzów

Chorzów, 04.11.2017 r.

Statement on the contribution to publication

Publication:

We hereby state that the contribution to the work published jointly with Karolina Jurkiewicz is in accordance with the description below:

Karolina Jurkiewicz

Preparation of glass-like carbons, performing X-ray and neutron diffraction experiments, performing data treatment, analysis and interpretation, performing computer simulations, writing and editing the manuscript.

Signature: *Jurkiewicz*

Stanisław Duber

Participation in preparation of carbon materials.

Signature: *S. Duber*

Henry E. Fischer

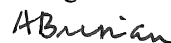Managing neutron diffraction experiment and participation in neutron data treatment.

Signature: *Henry E. Fischer*

Andrzej Burian

Providing scientific consultations and participation in editing the manuscript.

Signature: *A Burian*

Modelling of glass-like carbon structure and its experimental verification by neutron and X-ray diffraction

K. Jurkiewicz,[a,b]* S. Duber,[c] H. E. Fischer[d] and A. Burian[a,b]

[a]A. Chełkowski Institute of Physics, University of Silesia, ulica Uniwersytecka 4, Katowice, 40-007, Poland, [b]Silesian Center for Education and Interdisciplinary Research, ulica 75 Pułku Piechoty 1A, Chorzów, 41-500, Poland, [c]Laboratory of Structural Research, University of Silesia, Chorzów, 41-500, Poland, and [d]Institut Laue–Langevin, 71 Avenue des Martyrs, Grenoble, 38000, France. *Correspondence e-mail: kjurkiewicz@us.edu.pl

Glass-like carbon is a well known carbon form that still poses many challenges for structural characterization owing to a very complex internal atomic organization. Recent research suggests that glassy carbon has a fullerene-related structure that evolves with the synthesis temperature. This article reports on direct evidence of curved planes in glassy carbons using neutron and X-ray diffraction measurements and their analysis in real space using the atomic pair distribution function formalism. Changes in the structure including the degree of curvature of the non-graphitizing glassy carbons as a function of the pyrolysis temperature in the range 800–2500°C (1073–2773 K) are studied using optimized models of the atomic structure. Averaged models of single coherent scattering domains as well as larger structural fragments consisting of thousands of atoms were relaxed using classical molecular dynamics. For such models the diffraction intensities and the pair distribution functions were computed. The compatibility of the computer-generated models was verified by comparison of the simulations with the experimental diffraction data in both reciprocal and real spaces. On the basis of features of the developed structural models for glass-like carbons, the origin of the properties such as high strength and hardness and low gas permeability can be better understood.

1. Introduction

Glass-like carbon can be classified as non-graphitizing carbon according to criteria proposed by Rosalind Franklin in her earliest research involving studies of coal, carbon and graphite (Franklin, 1951). It is very hard, chemically inert and impermeable to gases, factors that make this material important from the point of view of applications such as electrodes and high-temperature crucibles. Although glass-like carbon has been produced since the early 1960s, and despite its commercial importance, the atomic structure of this carbon material is not well understood. Detailed reviews of glass-like carbon studies including earlier structural models have been reported by Harris (1997, 2005). The crucial point of new ideas concerning the atomic structure of non-graphitizing carbons is the presence of curved fragments that can be related to the formation of topological defects.

sp^2-Hybridized carbon layers can yield curved nanostructures such as fullerenes (Kroto *et al.*, 1985), nanotubes (Iijima, 1991), nanohorns (Iijima *et al.*, 1999) or nano-onions (Ugarte, 1992). The discovery of these special carbon forms prompted the realization that non-planar structures or their fragments may be thermodynamically stable. The presence of these curved elements in carbon nanomaterials can be related

GC980

to the formation of topological point-type defects in which non-hexagonal rings (pentagons, heptagons and higher-membered rings) occur (Terrones & Terrones, 2003). These are the Stone–Thrower–Wales (STW) and vacancy defects. In the simplest example of the STW defect, four hexagons are transformed into two pentagon–heptagon pairs by rotating one of the C—C bonds by 90° (Stone & Wales, 1986). When such a transformation occurs by simultaneous movement of the two involved atoms the defected structure retains the same number of atoms and no dangling bonds are created. The mono-vacancy defect is created when one atom is missing from the carbon network. From the geometrical point of view, this leads to the formation of one pentagon and one nine-membered ring with one dangling bond remaining. Therefore, the formation energy of this defect is higher owing to the presence of an under-coordinated C atom. The multi-vacancy defects can also appear in sp^2 carbon lattices when more C atoms are lost. Energetically favoured vacancy structures have an even number of missing atoms since if an odd number of C atoms are removed dangling bonds occur.

The presence of non-hexagonal rings as integral elements of atomic structure was also suggested by Harris and co-workers (Harris et al., 2000, 2008; Harris, 2004, 2013) for glassy and other non-graphitizing carbons on the basis of high-resolution transmission electron microscopy (HRTEM) investigations. Imaging the atomic structure of glassy carbon by HRTEM, Harris et al. showed that it consists of curved discrete carbon sheets and to some extent resembles the structure of fullerenes. The curvature is believed to be a natural consequence of the presence of the topological defects which produce saddle points and change the local topography. The studies of Harris provided evidence of completely closed particle-like carbon structures as well as their broken and imperfect parts, and in particular a high proportion of closed particles in the 'low-temperature' glassy carbons (those prepared at temperatures up to 1000°C; [°C] = [K] − 273). Single non-hexagonal carbon rings were also directly observed using HRTEM (Harris et al., 2008). As a result of these observations, a model of glassy carbon structure was proposed which is built from fragments of curved carbon sheets, in which pentagons and heptagons are randomly dispersed throughout the network of hexagons (Harris, 2004).

Obtaining high-quality atomic resolution images of glassy carbons is extremely challenging, owing to their highly disordered structure. As the number of point defects in the materials is low, there is little chance of observing them using a local probe such as HRTEM or scanning tunnelling microscopy (STM). Moreover, it is known that the irradiation of carbons by the electron beam in electron microscopy can create some defect sites and it is difficult to distinguish between the native and irradiation-induced defects (Suenaga et al., 2007). Apart from these difficulties, direct imaging techniques such as HRTEM or STM provide valuable information about the atomic scale structure of carbon materials. However, this knowledge concerns only a limited volume of the sample probed. In order to obtain information about the atomic arrangement of a larger sample volume it is desirable

to use another approach. Modelling studies of different types of porous carbons allow for the formation of non-six-membered rings in order to produce the curved fragments observed in HRTEM images (O'Malley et al., 1998; Jain et al., 2006). Diffraction methods do not provide unequivocal evidence that pentagons or other non-hexagonal rings are present. However, in our previous studies we successfully developed models of atomic structure for various types of carbons, including the presence of STW and vacancy defects, which described well all features of experimental diffraction data (Jurkiewicz et al., 2015; Woznica et al., 2015; Hawelek et al., 2008, 2011, 2012). It should be emphasized that such a kind of disorder imposed on the models produced a specific damping of the amplitude of diffraction data that could not be reproduced using entirely perfect sp^2-hybridized hexagonal carbon networks.

In this work, we present the results of combined wide-angle neutron and X-ray scattering (WANS and WAXS) studies of a series of glass-like carbons supported by computer modelling of atomic structure by the molecular dynamics method. The use of crystallographic methods suitable for materials exhibiting three-dimensional periodicity, such as Rietveld (Rietveld, 1969) or PDFgui (Farrow et al., 2007) refinement procedures, cannot be applied to non-graphitizing glass-like carbons. In this paper, modelling and comparison of the model-based simulations with the experimental data are proposed as a way of describing the atomic arrangement in the materials in question, taking into account the complexity of their structure at various temperatures. The diffraction data provide averaged structural information about the coherently scattering domain. Therefore, in the first step, models of the sizes of these domains have been computer generated. At this stage, it is assumed that the coherently scattering domains are arranged without spatial correlations. Then, in order to account for possible cross-correlations between such domains, larger models are constructed. The presence of such correlations may lead to the formation of the porous structure that has been established for glass-like carbons. Moreover, such an approach will allow description of these crosslinks, which may prevent graphitization even at high temperatures.

Therefore, analysis of experimental and simulated data is performed in both reciprocal and real space simultaneously, involving the pair distribution function (PDF) formalism. We noticed that the presence in glassy carbons of the postulated topological defects and curvature has a distinct manifestation in the diffraction data. A gradual reduction of curvature in fullerene-like fragments of structure and elimination of related defects that accompany the increase in heat-treatment temperature result in slight changes of atom-to-atom distances. On the basis of the developed structural models, which take into account the obtained information on the interatomic distance distribution, evolution of the glassy carbons as a function of synthesis temperature can be observed. The new structural models are of great value in understanding the properties of glassy carbon, such as resistance to graphitization, low chemical reactivity, great strength and hardness, and impermeability to gases.

research papers

2. Experimental details

2.1. Sample preparation

The glass-like carbon samples were prepared from furfuryl alcohol as a precursor. In the first step the furfuryl alcohol (from Sigma–Aldrich, ≥98% pure) was polymerized by the addition of 5%(v/v) of 0.1 M p-toluenesulfonic acid (from Acros Organics, 99% pure) solution in ethanol. The catalysts and furfuryl alcohol were mixed together for 24 h using magnetic stirring, resulting in a homogeneous composition. The catalysed precursor was then cast in moulds and held at 120°C for 2 h for curing. The structure of the furfuryl alcohol molecule and the assumed structure of the furfuryl alcohol polymer (Guigo et al., 2007) are presented in Scheme 1(a) and 1(b), respectively.
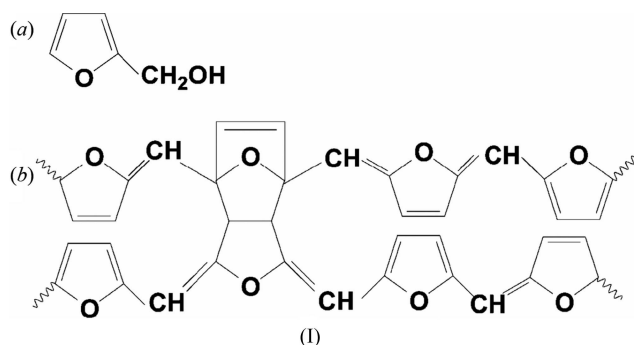
After the polymerization, the resin was divided into different batches and carbonized under protective Ar gas flow at 800 or 980°C in a quartz tube furnace (the samples will be denoted here as GC800 and GC980). The heating rate was $10°C\,h^{-1}$ to 200°C and $5°C\,h^{-1}$ to the desired temperature. Upon reaching the final heat-treatment level, the temperature was held constant for 2 h. The samples were allowed to cool in an Ar flow. Next, some of the samples carbonized at 980°C were further heat treated to 2500°C in an Ar atmosphere. For this purpose, a graphite electric furnace was used. The glassy carbon discs placed in the furnace were covered with carbon soot to prevent cracking due to thermal shock. The high-temperature processing was performed with a heating rate of $4°C\,min^{-1}$ between room temperature and the desired temperature of pyrolysis (1500, 2000 and 2500°C, respectively, corresponding to samples GC1500, GC2000 and GC2500), and the samples were allowed to soak for 2 h at the final temperature. Then the samples were cooled to room temperature under a flow of Ar gas and purified from the remaining soot particles. The performed diffraction measurements required samples in the form of a fine powder and thus the requisite number of prepared discs were ground in a steel mill.

2.2. Wide-angle neutron scattering

The neutron diffraction results reported here were collected on the disordered materials diffractometer D4 at the Institut Laue–Langevin in Grenoble, France (Fischer et al., 2002).

Total scattered intensities were recorded as a function of the scattering angle 2θ. The instrument was operated using an incident wavelength λ of 0.4989 Å from a Cu(220) monochromator that allowed a maximum momentum transfer Q_{max} of 23.5 Å^{-1}, where the scattering vector magnitude Q is related to λ according to the following formula: $Q = 4\pi \sin\theta/\lambda$. The samples were packed within a cylindrical vanadium container of 6.8 mm internal diameter, placed in the middle of an aluminium bell jar and measured at room temperature. Vertical slits placed only a few centimetres upstream of the sample position ensured that all samples had the same height of 50 mm, which is important for scattered intensity normalization. For detection of the scattering signal, an array of nine microstrip detectors was used. Additional measurements were carried out for the empty bell jar and the sample container. In order to normalize the diffraction intensity from the sample to an absolute scale accounting for its geometry, a vanadium rod was also measured. The final scattered intensities for each sample were obtained from the raw data, taking into account corrections for multiple scattering, attenuation and inelasticity using the CORRECT program (Howe et al., 1996). The initially processed functions of intensity versus the scattering vector magnitude, $I(Q)$, were used to calculate structure factors, $S(Q)$, according to the equation

$$S(Q) = \frac{I(Q)}{b^2}, \quad (1)$$

where b is the coherent scattering length of carbon and the isotopic effect is neglected (Fischer et al., 2006).

The structure factor is related to the coherent scattering intensity $I(Q)$ in counts per second as measured by a detector of solid angle $d\Omega$ normalized by the incident flux per atom in the sample:

$$I(Q) = \frac{d\sigma}{d\Omega}(Q)\,d\Omega, \quad (2)$$

where $d\sigma/d\Omega$ is the differential scattering cross section for diffraction (Fischer et al., 2006).

The structure factor will be used in this work as a representation of diffraction data in reciprocal space. The measured wide-angle scattering was also analysed in a real-space representation of diffraction data in the form of the atomic pair distribution function PDF(r), which is related to $S(Q)$ through the sine Fourier transform according to

$$PDF(r) = \frac{2}{\pi} \int_0^{Q_{max}} Q[S(Q) - 1]\sin(Qr)\frac{\sin(\pi Q/Q_{max})}{\pi Q/Q_{max}}\,dQ. \quad (3)$$

Here r indicates the interatomic distance and the last fraction denotes the Lorch modification function, reducing effects arising from the finite value of the upper Q limit.

2.3. Wide-angle X-ray scattering

The X-ray diffraction measurements were performed using a laboratory Rigaku Denki D/max RAPID II-R diffractometer equipped with a rotating Ag anode producing X-rays with wavelength $\lambda_{K\alpha}$ of 0.5608 Å. The maximum value of

momentum transfer available with this setup is $Q_{max} = 22$ Å^{-1}. The incident beam was monochromated by a graphite (002) crystal and formed with a 0.3 mm collimator. An image plate in Debye–Scherrer geometry was used as a detector. The samples were measured at room temperature in glass capillaries with a diameter of 1.5 mm and wall thickness of 0.01 mm. The empty capillary was also measured and then the background was subtracted. The scattered X-ray radiation was recorded as two-dimensional diffraction patterns and then converted to $I(Q)$ after integration over azimuthal angles. The intensity functions were then corrected for polarization, absorption and incoherent Compton scattering [computed as described by Balyuzi (1975)] and subsequently normalized using a processing procedure developed for high-energy X-rays (Schlenz *et al.*, 2003; Poulsen *et al.*, 1995; Hawelek *et al.*, 2005). The structure factors were computed as follows:

$$S(Q) = \frac{I(Q)}{\overline{f}^2}, \qquad (4)$$

where f in this case is the atomic form factor for carbon and $I(Q)$ indicates the scattered intensity corrected and normalized to electron units. The PDFs were calculated for each carbon sample, converting the X-ray scattering data according to equation (3).

3. Modelling procedure

When combined with computer-based modelling analysis of the structure factors, the PDF allows quantitative information about the structure to be extracted from the neutron and X-ray diffraction data. Here, the classical molecular dynamics (MD) technique was used to match structural models containing many atoms to experimental diffraction data. In the case of a partially ordered system consisting of N atoms of the same type, the scattered intensity averaged over all orientations can be calculated using the Debye equation (Debye, 1915):

$$I_N(Q) = b^2 \,(\text{or}\, f^2) \sum_{i,j=1}^{N} \frac{\sin(Qr_{ij})}{Qr_{ij}}, \qquad (5)$$

where r_{ij} denotes the distance between the ith and jth atoms. The Debye equation is related to the structure factor as follows:

$$S_N(Q) = \frac{I_N(Q)}{b^2 \,(\text{or}\, f^2)}. \qquad (6)$$

In order to compare the model-based simulations with experimental data, the structure factor normalized to one atom is used:

$$S(Q) = 1 + \frac{1}{N}\left[\sum_{i,j=1}^{N} \frac{\sin(Qr_{ij})}{Qr_{ij}} \right]_{i \neq j}. \qquad (7)$$

Starting positions of C atoms were obtained from the ideal graphite structure with a nearest C—C distance of 1.42 Å and an interlayer spacing of 3.4 Å. The models consist of the

Cartesian coordinates of the constituent C atoms from which the interatomic distances are then calculated according to equation (7). The successive graphene layers were randomly translated in the direction perpendicular to their stacking, bringing a turbostratic kind of disorder into the models. Additional distortion of the graphitic lattice was generated by introducing STW and vacancy defects. In order to obtain stable atomic configurations and minimize the energy of the models, they were relaxed using a suitable C—C potential interaction. The reactive empirical bond order potential (Brenner *et al.*, 2002) was used for atoms lying within a single layer and the Lennard–Jones potential (Girifalco *et al.*, 2000) for interlayer interactions. Taking into account the interactions described by the above potentials, the forces acting on the C atoms were calculated and used to solve the Newtonian equations of motion, applying the predictor–corrector method with a time step of 0.2 ps. The temperature of 27°C was kept constant during the simulations by a Berendsen thermostat, which allows for thermal vibrations of C atoms. The procedure of structure optimization using MD leads to a realistic representation of the bond lengths and energy. Such prepared sets of Cartesian coordinates of atoms were used for calculation of theoretical structure factors according to equation (7) and PDFs according to the Fourier transformation presented in equation (3). The agreement between the experiment and the simulation was evaluated in both reciprocal and real diffraction spaces, from the values of the discrepancy factor computed as follows:

$$R = \left[\frac{\sum (F_{exp} - F_{the})^2}{\sum F_{exp}^2} \right] \times 100\%, \qquad (8)$$

where F_{exp} and F_{the} are the experimental and theoretical structure factors in reciprocal-space representation or PDFs in real-space representation, respectively (Wright, 1993).

4. Results and discussion

The aim of the neutron and X-ray wide-angle scattering experiments was to compare the diffraction results determined by different techniques using a large-scale facility and a laboratory diffractometer, for different amounts of sample used in the measurement, and by performing different procedures of data correction. The phenomena of the elastic scattering of neutrons by nuclei and the scattering of X-rays by electron clouds are described essentially by the same theoretical equations. The difference in Q dependency of the scattering length and the atomic scattering factor for neutrons and X-rays, respectively, favours neutron diffraction. In this particular case of disordered carbon materials, neutron diffraction is preferred since the neutron form factor does not decrease with diffraction angle and, consequently, the structural oscillations in the high-Q range are more noticeable. The greatest limitation of X-ray scattering is the rapidly decaying X-ray form factor signal compared with the growing Compton background contribution at high Q values, making the accurate extraction of $S(Q)$ more difficult (Fischer *et al.*, 2006).

Accurate determination of the structure factor and PDF requires neutron or X-ray diffraction data measured with a large momentum transfer which are then subjected to data processing as described above. In order to estimate reliably the goodness of agreement between the modelling results and the experimental data, it is important to quantify possible inaccuracies resulting from both statistical and systematic errors as discussed by Thijsse (1984) and Toby & Egami (1992). The error levels were estimated as discrepancies between the structure factors and the PDFs determined experimentally and computed for polycrystalline nickel and silicon powder standards for the neutron and X-ray measurements, respectively. Both functions are shown together with the errors in Figs. S1 and S2 in the supporting information.

The comparison of the structure factors and the PDFs determined from neutron and X-ray scattering measurements for the series of glassy carbons is shown in Figs. 1 and 2. Both diffraction experiments provided data with similar high quality, making their further analysis reasonable. The comparison shows that carefully performed normalization and correction procedures for X-ray data allow one to obtain reliable results, despite the strongly diminishing intensities of the X-ray scattering with Q. Neutron diffraction patterns were collected in a slightly wider range of Q than the X-ray data, but the difference between the maximum value of Q accessible in the two experiments is too small to significantly affect the resolution of the PDF(r) peaks, as can be seen from Fig. 2. Only small changes in the peak amplitudes appear, as a result of the differences in the data recording and processing.

The general features of the experimental diffraction data in both reciprocal and real spaces for the glassy carbons produced by the pyrolysis of polyfurfuryl alcohol were described in our previous paper (Jurkiewicz *et al.*, 2016). In that work, the considered X-ray diffraction studies showed that the non-graphitizing glass-like carbons have a structure intermedi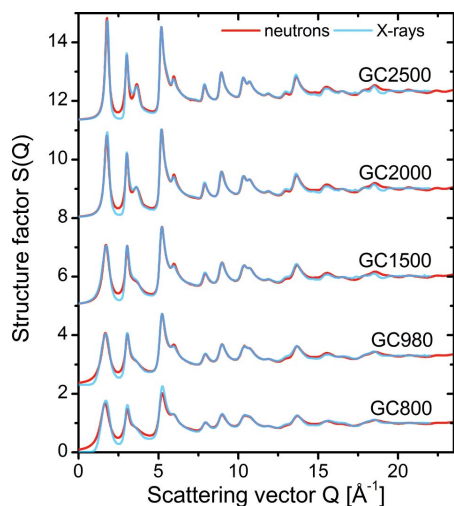ate between amorphous and crystalline, completely lacking crystalline periodicity. The broad and damped diffraction peaks at higher Q values suggest the presence of disorder in the investigated materials. An increase in the heat-treatment temperature leads to an ordering of the glassy carbon structure in the directions parallel and normal to the graphene planes. However, a kind of structural disorder is partly preserved even after heat treatment of the material at 2700°C, and it can be accurately described in terms of the paracrystalline theory. The paracrystalline disorder assumes that the nearest-neighbour atom–atom distances fluctuate randomly without spatial correlations, leading to a network distortion which propagates proportionally to $r^{1/2}$ (Hosemann & Hindeleh, 1995). Here, in order to specify the source of such fluctuations, the presence of the postulated topological defects in the structure will be considered.

From a comparison of the experimental PDFs for the glassy carbon samples carbonized at different temperatures in the range 800–2500°C with the function calculated for an unstrained single graphitic layer, shown in Fig. 3, systematic shifts of peaks can be seen. As can be perceived from Fig. 3(a), the peak positions of the PDF(r) appearing in the range of 1–6 Å are practically the same as those of the perfect hexagonal layer, but the peaks for higher r values seen in Fig. 3(b) shift towards longer interatomic distances characteristic of the intralayer graphitic structure. At 2500°C the peak positions approach the r values for unstrained graphite. At lower temperatures the interatomic distances in the investigated glass-like carbons are shorter when compared with graphite. This finding can be directly related to the curvature of the atomic structure and its gradual flattening under the influence
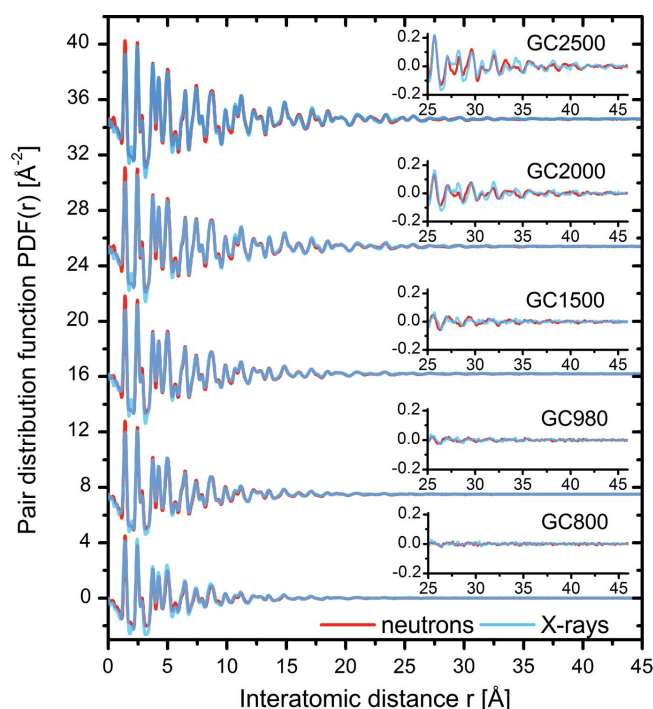

Figure 1
Comparison of the structure factors from the neutron and X-ray diffraction experiments for the glassy carbons.

Figure 2
Comparison of the pair distribution functions from the neutron and X-ray diffraction experiments for the glassy carbons.
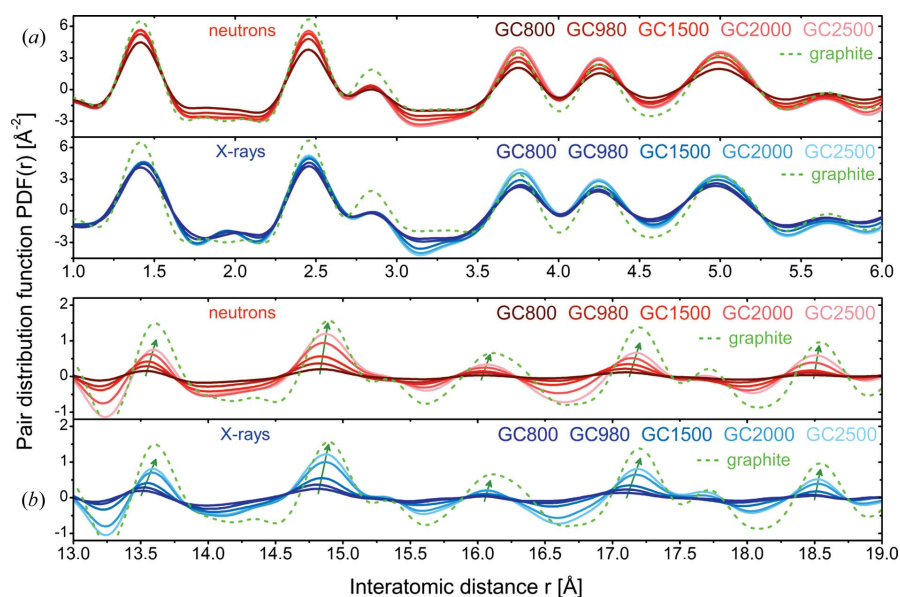
Figure 3
Comparison of the interatomic distances of the experimental pair distribution functions for the glassy carbons with the function calculated for a single unstrained graphite layer in the short-range order (*a*) and in the intermediate-range order (*b*).

stacking sequence. The density of atomic pairs in distinct layers is governed by the pair density of single layers, leading to a step-like contribution to the total radial distribution function (Mildner & Carpenter, 1974; Burian *et al.*, 1998). Therefore, the PDF peaks at larger distances can be related to intralayer correlations.

In order to specify the degree of the curvature manifesting itself in the diffraction data, the energy of computer-simulated models of the atomic structure was optimized using the MD method. In the first step of the simulations, models representing averaged coherent scattering domains were sought. The important parameters of the models, which were adjusted to fit the experimental data, are the number of graphitic layers, their size and shape, and the degree of disorder imposed on the models by the generated defects. At this stage it is assumed that these domains are arranged in space without correlations and therefore scatter independently with respect to one another. Within domains of the glass-like carbons the graphitic layers are stacked without correlations in the direction perpendicular to their planes. Moreover, the atomic arrangement within the layers is defective (Ergun, 1970; Ergun & Schehl, 1973; Mildner & Carpenter, 1974). For such materials the diffraction pattern contains two types of peaks: the (0 0 2*l*) graphitic peaks appearing at about 1.8 and 3.6 Å^{-1} due to the interlayer correlations and the remaining (*hk*0) ones originating from the intralayer correlations in the form of two-dimensional diffraction peaks exhibiting right-side asymmetry (Warren, 1941; Warren & Bodenstein, 1965). The amplitude and the
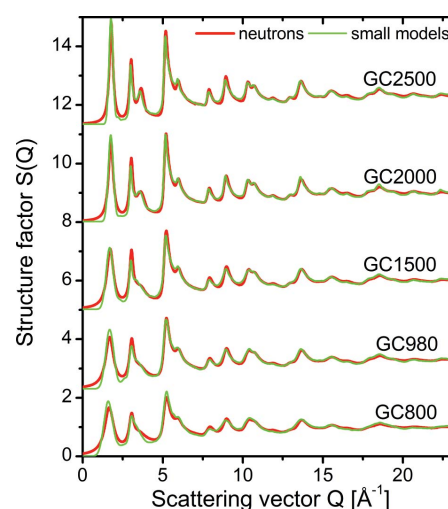
of the heat treatment. When two atoms occupy positions on the opposite sides of a circle, then the shortest distance between the pair of atoms is greater for the less curved surface. Depending on the degree of curvature relative to the size of the coherently scattering objects, its effect may have a significant manifestation in the diffraction data or may be negligible. The simulations performed by Koloczek & Burian (2004) for carbon nanotubes with different chirality demonstrated that calculated diffraction profiles are sensitive to the tube diameter. When the diameter is large (around 70 Å), and the curvature is small, the diffraction data lose the three-dimensional spatial correlations and resemble those of flat graphene sheets for each type of nanotube chirality. In the case of nanotubes with a small diameter (around 7 Å) the diffraction patterns differ for the armchair, zigzag and helical nanotubes and it is possible to distinguish between them.

The behaviour of the PDFs for the glass-like carbons suggests that, on a very local scale extending to the first few coordination spheres, the curvature effect can be observed since the maxima of the PDF(*r*) are in almost the same positions for all C atoms. The only contrast between the first few PDF(*r*) peaks is their amplitude and full width at half-maximum. Considering the greater interatomic correlations of the PDF(*r*), exhibited in Fig. 3(*b*), one can notice the apparent shifts towards greater atom-to-atom distances becoming more distinct with increasing carbon synthesis temperature. This, therefore, suggests that the structure evolves. It is important to point out that in the layered structure of glass-like carbon there are two types of distances: intralayer and interlayer. It has been established that for this type of structure the graphitic layers are stacked without spatial correlations, and this structure is called turbostratic (Warren, 1941; Mildner & Carpenter, 1974), in contrast to the graphitic –*ABAB*–

Figure 4
Comparison of the structure factors computed for models of coherent scattering domains with the neutron experimental data.

position of the (0 0 2*l*)-type peaks depend on the number of layers and their mean interlayer spacing. Their broadening provides information about the size of the domains in the direction normal to the layers and disorder in their stacking. Broadening of the (*hk*0)-type peaks and the *r* range in which oscillations of the PDFs disappear can be used for estimation of the in-layer model size and in-layer disorder. Therefore, the starting models of the investigated glass-like carbons at different temperatures were constructed taking into account the above-mentioned parameters.
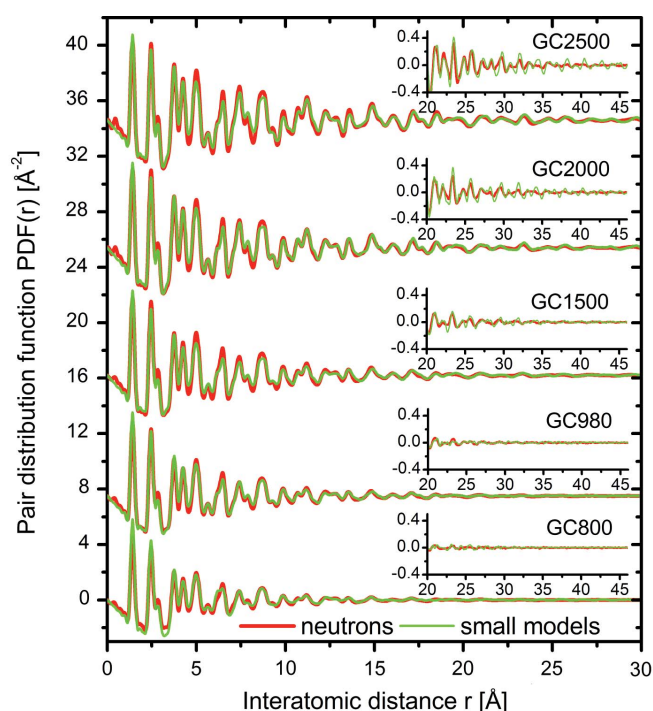
The number of layers and the interlayer spacing were chosen to reconstruct the amplitude and the position of the (002)-type peak at each temperature. The layer sizes were estimated as the value of the in-layer interatomic distance where the PDF oscillations disappear. Then, topological defects were introduced to the perfect hexagonal carbon network assuming their random distribution. The energy of such constructed models was optimized to find a minimum energy configuration. The intention, at the end of this procedure, is that the model-based simulation fits the diffraction data in both reciprocal and real spaces. The choice of the number of model defects is a trial-and-error procedure. The theoretical *S*(*Q*) and PDF(*r*) calculated from the relaxed atomic configurations that were found to give the best agreement with experimental results are shown in Figs. 4–7. The agreement between the experimental data and the simulation results is quantified using the discrepancy factor defined by equation (8). The calculated discrepancy factors are presented in Table 1. Both peak positions and amplitudes are well reproduced by the models. Insets to Figs. 5 and 7 display the range of the interatomic distances 20–45 Å. Even for such great distances the theoretical curves reconstruct the experimental data in a satisfactory way. The discrepancy factors have slightly lower values for the neutron scattering data, which can be explained by small differences between the neutron and X-ray results. This indicates that neutron diffraction is favourable for the atomic structure determination, possibly because of the better statistics collected for a greater amount of material.

Figure 5
Comparison of the pair distribution functions computed for models of coherent scattering domains with the neutron experimental data.
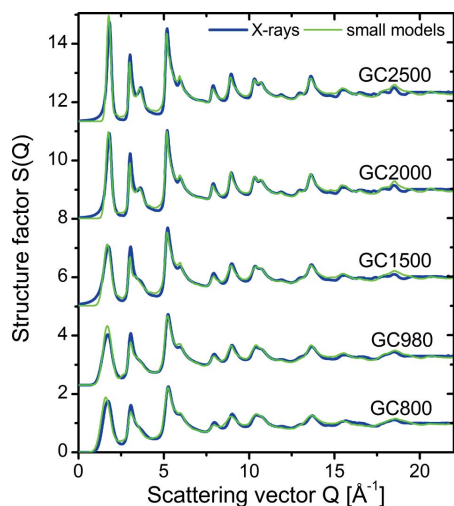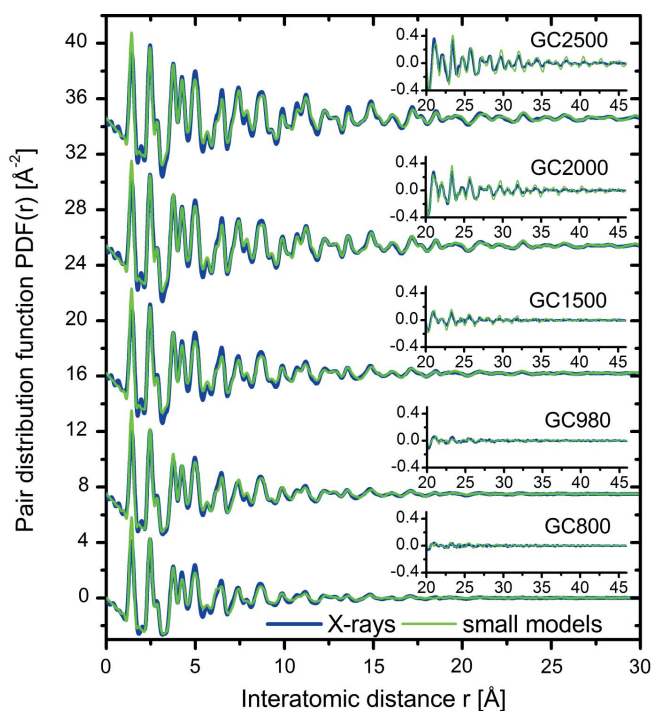

Figure 6
Comparison of the structure factors computed for models of coherent scattering domains with the X-ray experimental data.

Figure 7
Comparison of the pair distribution functions computed for models of coherent scattering domains with the X-ray experimental data.

Table 1
Discrepancy factors R (%) between simulated and experimental neutron and X-ray diffraction data.

	Small models				Big models			
	$S(Q)$		PDF(r)		$S(Q)$		PDF(r)	
	Neutron	X-ray	Neutron	X-ray	Neutron	X-ray	Neutron	X-ray
GC800	8.5	8.9	26.8	25.7	7.0	8.4	22.0	25.0
GC980	6.8	8.2	18.2	21.9	6.5	6.9	15.5	21.2
GC1500	8.3	9.6	21.1	24.4	7.5	9.4	16.5	21.8
GC2000	9.4	9.5	19.1	21.7	8.7	9.6	18.1	21.4
GC2500	9.8	10.9	22.1	23.9	9.0	9.7	18.0	21.5

It should be pointed out that the generation of the structural model for each glassy carbon required testing of many configurations of defects and their numbers, types and distribution among the simulated arrangements of carbon hexagons. It was found that for GC800 the defects that introduce the proper attenuation of the diffraction data are mono-vacancies. The model used for GC800 consists of 777 atoms arranged in three graphene-like layers with 30 randomly distributed mono-vacancy defects. For GC980 the best-suited

model is built from 1122 atoms divided into three layers with six introduced mono-vacancies and 15 STW defects. The results obtained for GC1500, GC2000 and GC2500 favour the models with STW defects; however, the presence of mono- or multi-vacancies cannot be completely ruled out. The number of atoms forming the models are 3123, 4587 and 8398, respectively, for GC1500, GC2000 and GC2500, while the numbers of randomly distributed STW defects are 70, 75 and 127 for these respective systems. The final sets of Cartesian coordinates of C atoms in the optimized models are available in the supporting information (as .xyz-type files). In principle, the experimental diffraction results do not provide an unequivocal answer to the question of what type of topological defect dominates. However, the simulations are strong evidence that the low-temperature glassy carbons may consist of graphene sheets deficient in C atoms. As the heat-treatment temperature increases the missing atoms can be healed or replaced by STW defects, which are energetically favourable (Guo *et al.*, 2012). The question arises as to the origin of the vacancies and STW defects. Possibly they are created during the coalescence of small graphene-like fragments and the growth process of glassy carbon structural units. The atomic rearrangement at grain boundaries in graphene has already been typified by the formation of topological defects (Banhart *et al.*, 2011; Jacobson *et al.*, 2012). Moreover, the vacancies can migrate and initiate the STW transformation and thus local structural changes (Kotakoski *et al.*, 2011).

A visualization of the geometry for the optimized models of the glassy carbon structure, as well as the atomic configurations in single layers separated randomly from each model, is presented in Fig. 8. The comparison of the models shows a clear evolution of the averaged coherent scattering domains with the rise in the heat-treatment temperature. The domains increase in size in the directions parallel and perpendicular to the defective graphene planes. One can observe how the point defects (shown in Figs. 8*b* and 8*c*) deform the originally flat graphene layers and produce positive and negative curvature which is seen in HRTEM images (Harris *et al.*, 2000, 2008; Harris, 2004, 2013). As for fullerene elements, the occurrence of non-hexagonal-membered carbon rings within the hexagonal carbon network induces strains and is responsible for deviations from planarity and irregular interlayer spaces. Consequently, in some regions the rippling brings the graphene sheets closer and they can even merge
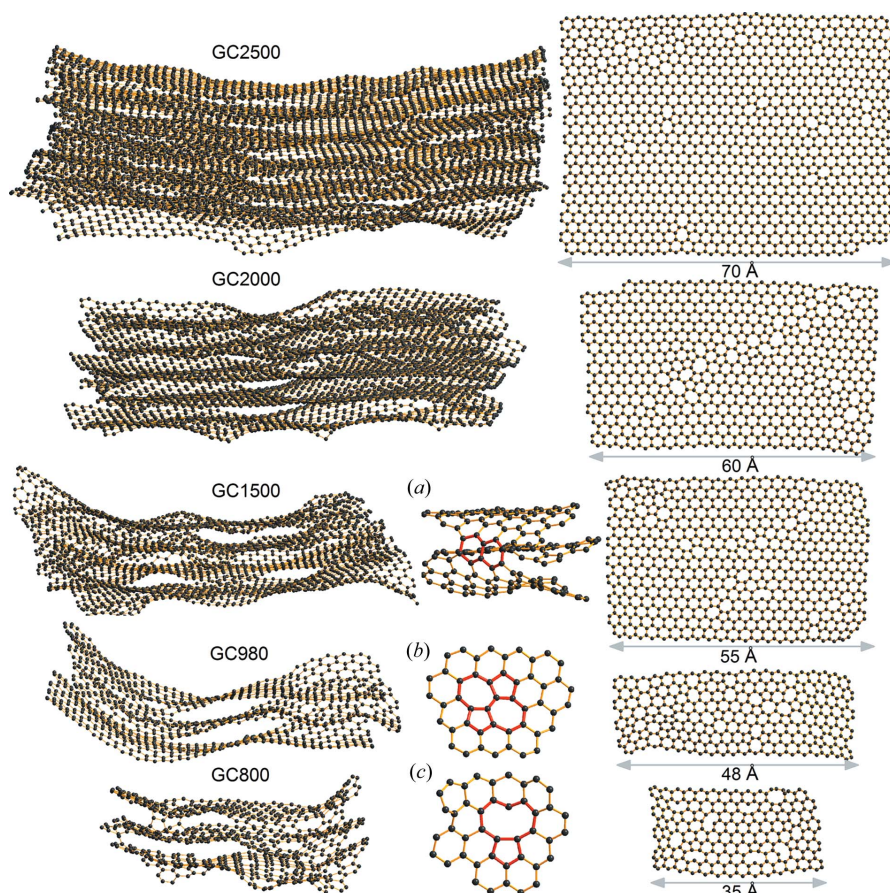

Figure 8
Visualization of the proposed models of averaged coherent scattering domains (small models) for the glassy carbons and the atomic configuration of single layers randomly separated from the models (on the right). Fragment of GC1500 model with non-planar sp^2 bonding (*a*), fragment of GC980 model with an STW defect (*b*), and fragment of GC800 model with a mono-vacancy defect (*c*).

together, as shown in Fig. 8(a). The above-described behaviour can explain the mechanism of pore creation in the microporous carbons.

For the models with sizes representing the extent of the coherently scattered domains, it is assumed that they diffract independently. Such an assumption was suggested by Franklin (1951) in her model of non-graphitizing carbons in which graphitic microcrystallites are joined together by crosslinks, of an unspecified nature. In order to see if these crosslinks can influence the diffraction data, larger models consisting of several smaller models were constructed. These models will be
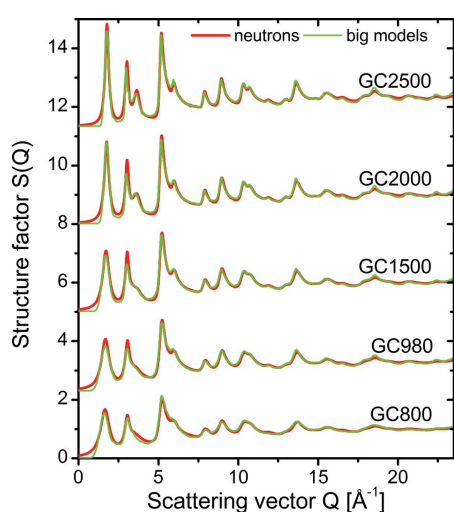
called 'big models' in the next part of this paper. The main aim of this procedure is to collect more quantitative information about the structure of the studied glass-like carbons. The larger fragments of structure should account for spatial correlations between atoms within a single coherent scattering domain, as well as between atoms lying in different domains. A particularly important issue that should be discussed for the big models is the nature of the linkage between smaller structural units. Moreover, a model of closed porous structure can emerge from the optimized three-dimensional big structural blocks. In order to prepare the big models of glassy carbon structure, the previous models of coherent scattering domains were employed. As a starting configuration for the MD geometry optimization three coherent scattering domains were moved closer to each other and set at different angles relative to their basal planes. In some cases, additional fragments of the domains or single graphene layers were added to the big models and randomly distributed. The theoretical $S(Q)$ and $PDF(r)$ calculated from the big-model simulations that give the best agreement with experimental results are presented in Figs. 9–12. The computed discrepancy factors for the diffraction data calculated from the big models are compared with the R values for the small models of single domains in Table 1. The big models match both neutron and X-ray experimental diffraction data in reciprocal and real spaces significantly better than the small models. Moreover, it is important to note that the differences between the experimental data and the simulations are lower than the estimated uncertainties, as shown in the supporting information. In the case of the big models the amplitude of the first $PDF(r)$ peak around 1.41 Å slightly decreases, while in the range of 5–15 Å medium interatomic distances the amplitude of the $PDF(r)$ correlations is higher and better fits the experimental results. These variations can be justified on the basis of the relaxed atomic configurations in these models. A visualization of the big models of glassy carbon structure is given in Fig. 13. Figs. 13(a)–13(d) present magnified selected fragments of the

Figure 9
Comparison of the structure factors computed for models of large structural blocks with the neutron experimental data.
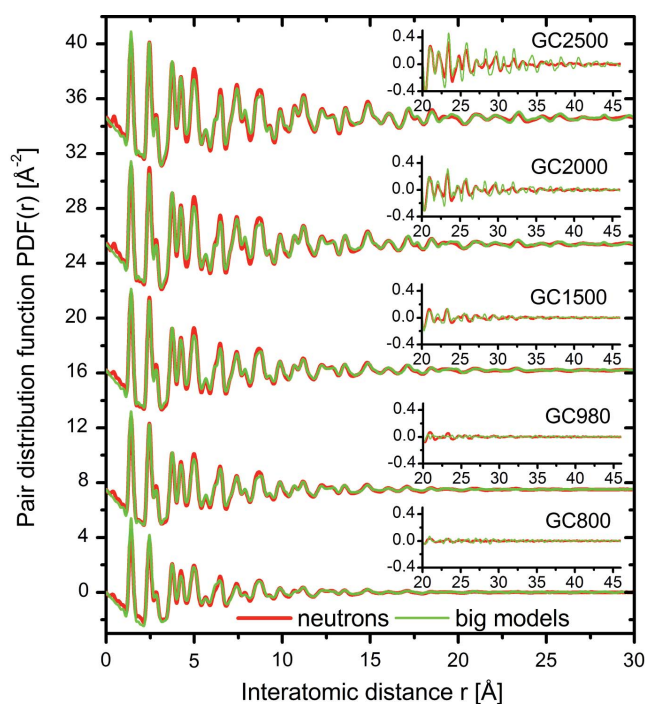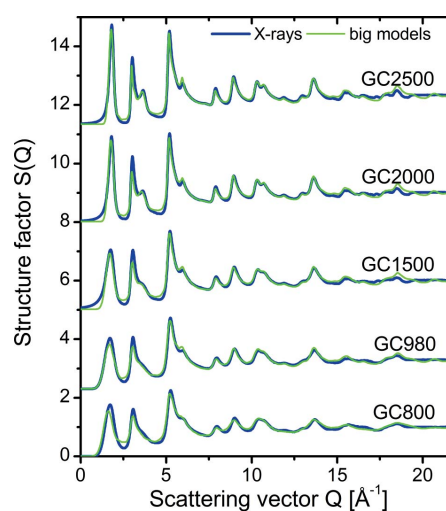

Figure 10
Comparison of the pair distribution functions computed for models of large structural blocks with the neutron experimental data.

Figure 11
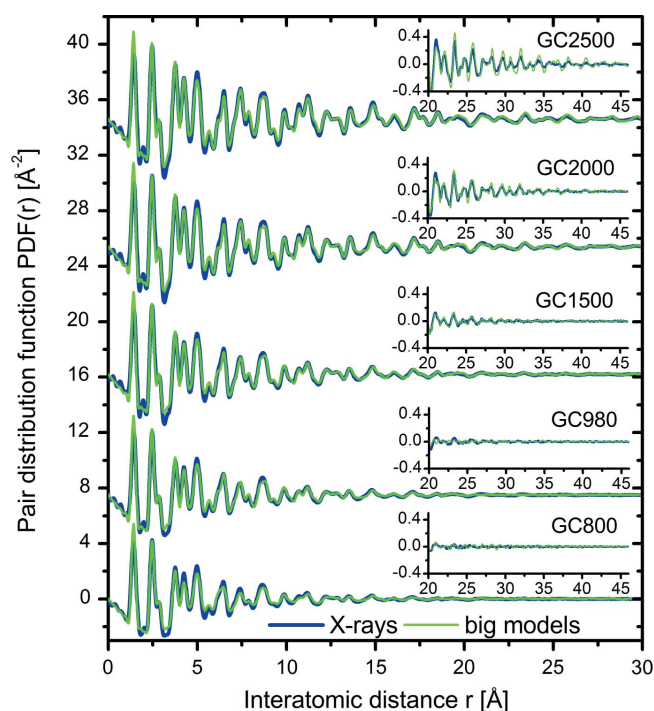Comparison of the structure factors computed for models of large structural blocks with the X-ray experimental data.

Figure 12
Comparison of the pair distribution functions computed for models of large structural blocks with the X-ray experimental data.

with planar sp^2 C atoms, non-planar sp^2 sites, non-six-membered rings, multi-vacancies, isolated tetrahedral bonds and carbon chains can be distinguished. These kinds of imperfections introduce disorder in the distribution of the interatomic distances within the first coordination shell and cause damping of the first PDF(r) peak. Considering the models consisting of several coherent scattering domains, the contribution resulting from a possible correlation between them is taken into account. Thus, the simulated diffraction data can better describe the real structure of the material.

The presence of agglomerated defective regions induces the formation of curvature. More precisely, buckling of the simulated models can occur owing to elastic strains created by the defects. During the process of atomic structure rearrangement induced by high-temperature heat treatment, some of the defective agglomerates are ordered. It can be expected that this process causes changes in the degree of curvature, which are reflected in the measured diffraction data, as observed in Fig. 2. It should be pointed out that the disappearance of curvature as a function of the increase in pyrolysis temperature observed for the proposed models follows the changes in peak positions of the theoretical PDF(r) in a similar manner as for the experimental data. The effect of the heat treatment on the glassy carbons apparently is to reduce disorder and transform the atomic structure towards the graphite structure. However, it seems that many topological defects are left intact and they prevent the graphitization process. Summarizing the performed computer simulations, the prepared big models show the evolution of the curvature of glassy carbon structure. The 'low-temperature' glassy carbons are built from fine structural units which are rich in defects and characterized by a high degree of curvature. The tightly curled carbon layers can enclose micropores. The 'high-temperature' glassy carbons contain more layers of greater size. There are fewer defects in the structure and a lower proportion of closed surfaces. However, fullerene-like features occur enclosing pores, which can be larger than those in the 'low-temperature' glassy carbons.

These findings may be reinforced by consideration of the bond length and valence angle distributions shown in Fig. 14. At lower temperatures the nearest-neighbour C—C distances exhibit a broad distribution around the value of 1.42 Å, covering the bond lengths of 1.39 and 1.46 Å which were found for C_{60} fullerene as double and single C—C bonds (David *et al.*, 1991; Li *et al.*, 1991), respectively. For the big model at 800°C this range is even extended to longer distances. As the temperature increases the distributions tend to be narrower which is particularly evident for the big models. The

models. The large structural units are created through a coalescence of small building blocks. The boundaries of the linked domains are a rich source of various types of defects that can be recognized in the fragments of the models in Fig. 13. Among the deviations from the hexagonal structure
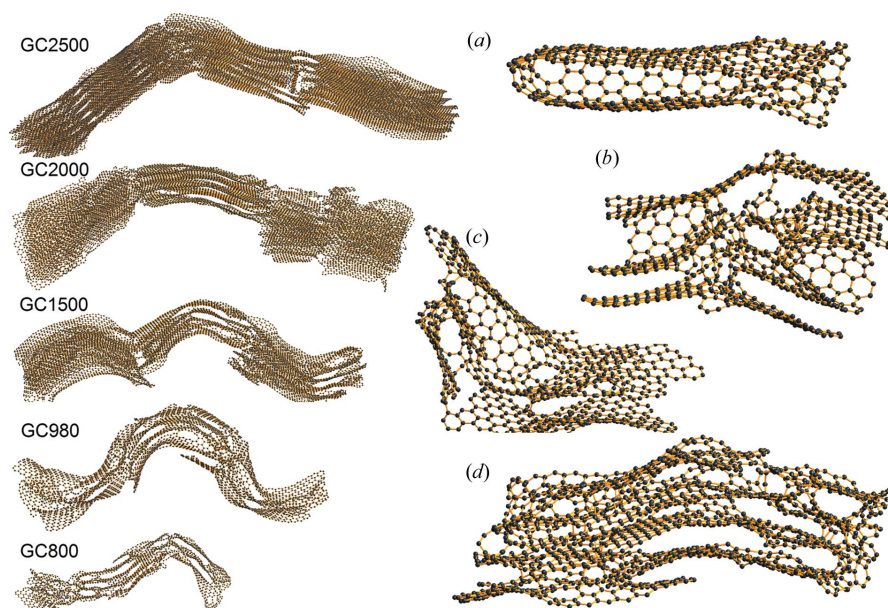

Figure 13
Visualization of the proposed models of large structural blocks (big models) for the glassy carbons and magnified selected fragments of the models for GC1500 (*a*), GC980 (*b*), (*c*), and GC800 (*d*).

distribution of the C—C bond lengths originates from both defect-induced distortion and layer curvature. Moreover, for smaller models undercoordinated edge atoms can also lead to a greater degree of disorder. From the modelling results presented above, it is concluded that larger models contain fewer defects and their layers are flatter. Taking into account these findings and considering that for big models the relative number of edge atoms is less, the behaviour of the presented distributions can be explained. A similar tendency can be observed for the valence angle distributions. The histograms shown in Fig. 14 show that the valence angle is concentrated around the value 120°, typical for sp^2 bonding, and exhibits broader distributions for smaller models and lower temperatures, and significantly narrower distributions at higher temperatures and for bigger models. The results concerning the bond lengths and the valence angles are consistent.

It is crucial to establish reliable structure–property relationships in glassy carbon to fully make use of its remarkable
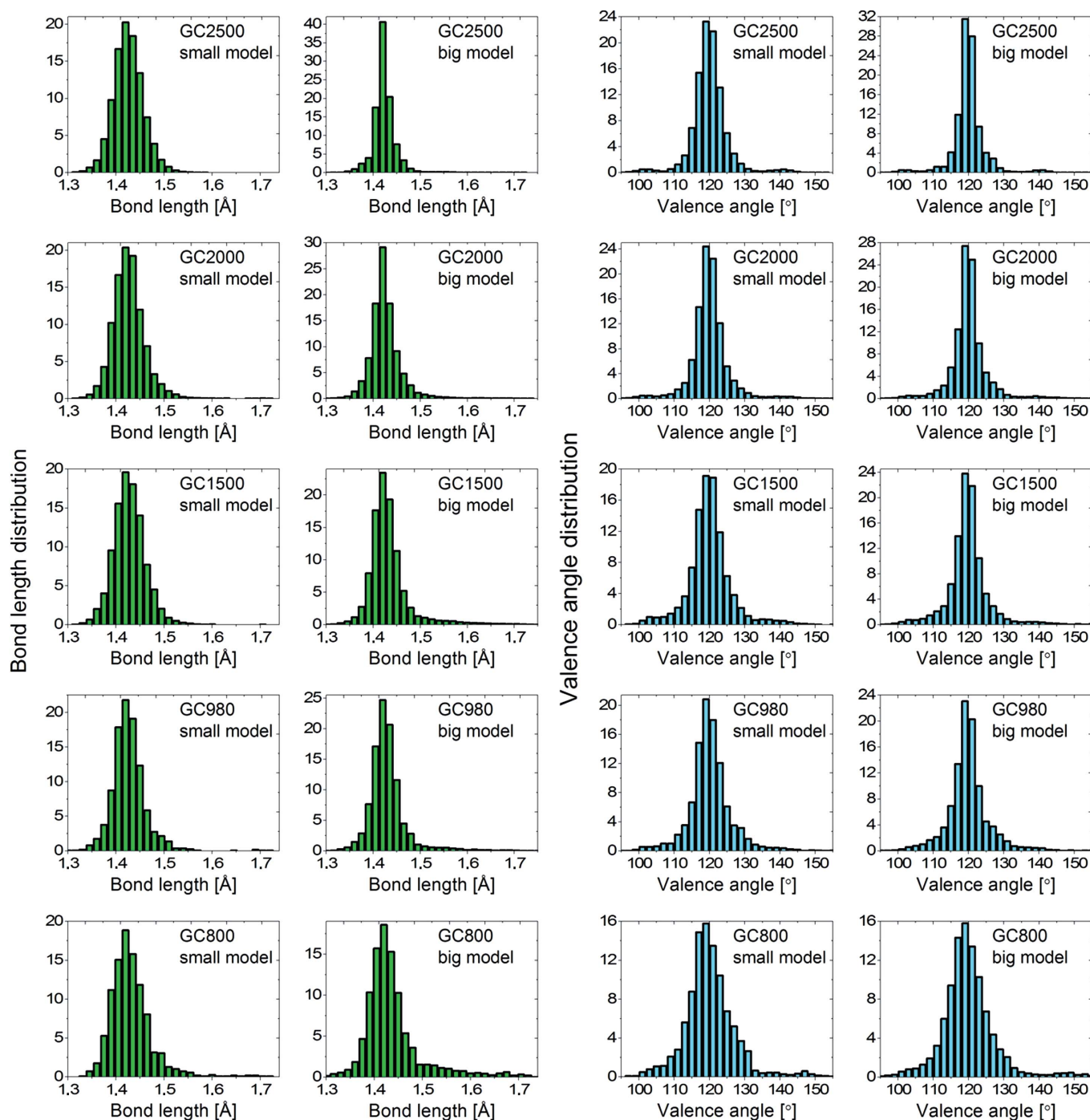

Figure 14
Bond length and valence angle distributions in per cent for small and big models of glassy carbons heat treated at 800–2500°C.

properties. The properties of the simulated models appeared to be generally consistent with the experimentally verified attributes of glassy carbons. The origin of the microporosity, hardness and resistance to graphitization may be well justified on the basis of the characteristic features of the proposed structural models. The three-dimensional pore structure is conditioned by the shape and layout of the carbon layers containing topological defects. The pores, which can be seen in Fig. 13, have elongated shapes closed by graphene-like planes and fullerene-like curved fragments. The numerous bridges between curved layers form a kind of cavity, explaining the tendency of glassy carbon to contain closed nanopores. By analysis of the evolution of the structural models, it can be imagined that the voids agglomerate and grow when the building domains are merged. Interestingly, the presence of the larger voids suggested by these simulations for the 'high-temperature' glassy carbons would explain to some extent the reduction of their hardness and strength in comparison with the 'low-temperature' glassy carbons. According to the literature (Jenkins & Kawamura, 1976), the hardness of glassy carbon rises rapidly above the heat-treatment temperature of 500°C to reach a maximum at 1500°C, and then the hardness decreases considerably during further heating. It is obvious that the variations of the mechanical properties are dependent not only on the final temperature of carbonization, but also on the heat-treatment duration. Therefore, the changes in hardness as a function of heat-treatment temperature can be slightly different, depending on the whole pyrolysis profile. In this particular case of the studied glassy carbons, it can be suspected that the 'low-temperature' samples (GC800 and GC980) may have the highest tensile strength and hardness. The modelling of atomic configurations performed for GC800 and GC980 shows that they can consist of crosslinked bunches of layers that are highly folded. The closed interconnected units make the structure very mechanically resistant. Since the structure is thermally stable and impermeable to gases and liquids, the ability of glassy carbon to react with chemical compounds is limited. The development of atomic structure–property relationships for glassy carbon can lead to a better understanding of this complex material. The description of the accurate representation of the atomic structure will help in predicting the behaviour of the material under certain conditions, its properties and possible applications.

5. Conclusions

The presented experimental wide-angle neutron and X-ray scattering and theoretical molecular dynamics studies of the series of glass-like carbons complemented information on their defective atomic structure already predicted on the basis of high-resolution transmission electron microscopy. The investigation of the glassy carbons formed at different temperatures was motivated by the differences in their structure and related properties, such as high hardness and strength, low reactivity, and closed porosity. Close examination of the experimental diffraction results provided direct proof for changes in the topology of the atomic structure

during heat treatment. The constructed structural models represent atomic arrangements averaged over the whole sample volume measured in the diffraction experiment and they support the idea of a fullerene-like structure of glassy carbons. As the carbonization temperature is increased from 800 to 2500°C, the carbon–carbon bond distribution in glassy carbon becomes more uniform, the domain size rises, the curvature disappears and the atomic structure tends towards the graphite structure. However, it can never reach the crystalline three-dimensional order of graphite. The proposed models give a reliable picture of why this happens. If the C atoms form fullerene-like or nanotube-like fragments, the graphene planes are linked to each other and have a limited mobility. Numerous interlayer bridges may effectively inhibit the movement of the carbon layers. Under the influence of energy supplied to the material with temperature, some of the defects can be healed, reducing the curvature and non-planarity. This kind of significant structural transformation must therefore be accompanied by changes in porosity and mechanical properties.

The complexity of the glassy carbon structure makes its characterization an extremely difficult task. The problem is, therefore, best tackled by obtaining a coherent set of results from complementary techniques which include experimental work and theoretical simulations. The experimental neutron and X-ray diffraction studies combined with molecular dynamics modelling carried out in this study provided highly detailed information on the structural building blocks and their degree of curvature for glassy carbons under differing synthesis conditions. Future advances in neutron and X-ray techniques and the development of computational methods could lead to a more accurate description of the disordered structure of various carbon materials. This certainly will help to complete the knowledge of the mechanism of structural changes in glass-like carbons and the origin of their properties. It is expected that it should be possible to tailor the properties of glassy carbon structure if its structure can be controlled by the synthesis conditions. The use of the proposed neutron or X-ray diffraction techniques is crucial for large-scale (industrial) characterization of carbon materials as they are the only methods capable of providing accurate information on the structure on the bulk scale.

References

Balyuzi, H. H. M. (1975). *Acta Cryst.* A**31**, 600–602.
Banhart, F., Kotakoski, J. & Krasheninnikov, A. V. (2011). *ACS Nano*, **5**, 26–41.
Brenner, D. W., Shenderova, O. A., Harrison, J. A., Stuart, S. J., Ni, B. & Sinnott, S. B. (2002). *J. Phys. Condens. Matter*, **14**, 783–802.
Burian, A., Ratuszna, A. & Dore, J. C. (1998). *Carbon*, **36**, 1613–1621.

David, W. I. F., Ibberson, R. M., Matthewman, J. C., Prassides, K., Dennis, T. J. S., Hare, J. P., Kroto, H. W., Taylor, R. & Walton, D. R. M. (1991). *Nature*, **353**, 147–149.

Debye, P. (1915). *Ann. Phys.* **351**, 809–823.

Ergun, S. (1970). *Phys. Rev. B*, **1**, 3371–3380.

Ergun, S. & Schehl, R. R. (1973). *Carbon*, **11**, 127–138.

Farrow, C. L., Juhas, P., Liu, J. W., Bryndin, D., Bozin, E. S., Bloch, J., Proffen, T. & Billinge, S. J. L. (2007). *J. Phys. Condens. Matter*, **19**, 335219.

Fischer, H. E., Barnes, A. C. & Salmon, P. S. (2006). *Rep. Prog. Phys.* **69**, 233–299.

Fischer, H. E., Cuello, G. J., Palleau, P., Feltin, D., Barnes, A. C., Badyal, Y. S. & Simonson, J. M. (2002). *Appl. Phys. Mater. Sci. Process.* **74**, s160–s162.

Franklin, R. E. (1951). *Proc. R. Soc. London Ser. A*, **209**, 196–218.

Girifalco, L. A., Hodak, M. & Lee, R. S. (2000). *Phys. Rev. B*, **62**, 13104–13110.

Guigo, N., Mija, A., Vincent, L. & Sbirrazzuoli, N. (2007). *Phys. Chem. Chem. Phys.* **9**, 5359–5366.

Guo, J., Morris, J. R., Ihm, Y., Contescu, C. I., Gallego, N. C., Duscher, G., Pennycook, S. J. & Chisholm, M. F. (2012). *Small*, **8**, 3283–3288.

Harris, P. J. F. (1997). *Int. Mater. Rev.* **42**, 206–218.

Harris, P. J. F. (2004). *Philos. Mag. 84*, 3159–3167.

Harris, P. J. F. (2005). *Crit. Rev. Solid State Mater. Sci.* **30**, 235–253.

Harris, P. J. F. (2013). *J. Mater. Sci.* **48**, 565–577.

Harris, P. J. F., Burian, A. & Duber, S. (2000). *Philos. Mag. Lett.* **80**, 381–386.

Harris, P. J. F., Liu, Z. & Suenaga, K. (2008). *J. Phys. Condens. Matter*, **20**, 362201.

Hawelek, L., Brodka, A., Dore, J. C., Honkimäki, V. & Burian, A. (2008). *Diamond Relat. Mater.* **17**, 1633–1638.

Hawelek, L., Koloczek, J., Burian, A., Dore, J. C., Honkimäki, V. & Kyotani, T. (2005). *J. Alloys Compd*, **401**, 51–54.

Hawelek, L., Woznica, N., Brodka, A., Fierro, V., Cezard, A., Bulou, A. & Burian, A. (2012). *J. Phys. Condens. Matter*, **24**, 495303.

Hawelek, L., Wrzalik, W., Brodka, A., Dore, J. C., Hannon, A. C., Iijima, S., Yudasaka, M., Ohba, T., Kaneko, K. & Burian, A. (2011). *Chem. Phys. Lett.* **502**, 87–91.

Hosemann, R. & Hindeleh, A. M. (1995). *J. Macromol. Sci. Phys. B*, **34**, 325–356.

Howe, M., McGreevy, R. & Zetterström, P. (1996). Internal Report. NFL Studsvik, Nykoping, Sweden.

Iijima, S. (1991). *Nature*, **354**, 56–58.

Iijima, S., Yudasaka, M., Yamada, R., Bandow, S., Suenaga, K., Kokai, T. & Takahashi, K. (1999). *Chem. Phys. Lett.* **309**, 165–170.

Jacobson, P., Stöger, B., Garhofer, A., Parkinson, G. S., Schmid, M., Caudillo, R., Mittendorfer, F., Redinger, J. & Diebold, U. (2012). *J. Phys. Chem. Lett.* **3**, 136–139.

Jain, S. K., Pellenq, R. J. M., Pikunic, J. P. & Gubbins, K. E. (2006). *Langmuir*, **22**, 9942–9948.

Jenkins, G. M. & Kawamura, K. (1976). *Polymeric Carbons – Carbon Fibre, Glass and Char.* New York: Cambridge University Press.

Jurkiewicz, K., Duber, S. & Burian, A. (2016). *Int. J. Appl. Glass Sci.* **7**, 355–363.

Jurkiewicz, K., Hawełek, L., Balin, K., Szade, J., Braghiroli, F. L., Fierro, V., Celzard, A. & Burian, A. (2015). *J. Phys. Chem. A*, **119**, 8692–8701.

Koloczek, J. & Burian, A. (2004). *J. Alloys Compd*, **382**, 123–127.

Kotakoski, J., Meyer, J. C., Kurasch, S., Santos-Cottin, D., Kaiser, U. & Krasheninnikov, A. V. (2011). *Phys. Rev. B*, **83**, 245420.

Kroto, H. W., Heath, J. R., O'Brien, S. C., Curl, R. F. & Smalley, R. E. (1985). *Nature*, **318**, 162–163.

Li, F., Ramage, D., Lannin, J. S. & Conceicao, J. (1991). *Phys. Rev. B*, **44**, 13167–13170.

Mildner, D. F. R. & Carpenter, J. M. (1974). *Proceedings of the 5th International Conference on Amorphous and Liquid Semiconductors*, Garmisch-Partenkirchen 2013, edited by J. Stuke & W. Brening, Vol. 1, pp. 463–477. London: Taylor and Francis.

O'Malley, B., Snook, I. & McCulloch, D. (1998). *Phys. Rev. B*, **57**, 14148–14157.

Poulsen, H. F., Neuefeind, J., Neumann, H. B., Schneider, J. R. & Zeidler, M. D. (1995). *J. Non-Cryst. Solids*, **188**, 63–74.

Rietveld, H. M. (1969). *J. Appl. Cryst.* **2**, 65–71.

Schlenz, H., Neuefeind, J. & Rings, S. (2003). *J. Phys. Condens. Matter*, **15**, 4919–4926.

Stone, A. J. & Wales, D. J. (1986). *Chem. Phys. Lett.* **128**, 501–503.

Suenaga, K., Wakabayashi, H., Koshino, M., Sato, Y., Urita, K. & Iijima, S. (2007). *Nat. Nanotechnol.* **2**, 358–360.

Terrones, H. & Terrones, M. (2003). *New J. Phys.* **5**, 126.

Thijsse, B. J. (1984). *J. Appl. Cryst.* **17**, 61–76.

Toby, B. H. & Egami, T. (1992). *Acta Cryst.* A**48**, 336–346.

Ugarte, D. (1992). *Nature*, **359**, 707–709.

Warren, B. E. (1941). *Phys. Rev.* **59**, 693–698.

Warren, B. E. & Bodenstein, P. (1965). *Acta Cryst.* **18**, 282–286.

Woznica, N., Hawelek, L., Fischer, H. E., Bobrinetskiy, I. & Burian, A. (2015). *J. Appl. Cryst.* **48**, 1429–1436.

Wright, A. C. (1993). *J. Non-Cryst. Solids*, **159**, 264–268.

4.3.   P3: Evolution of glassy carbon under heat treatment: correlation structure-mechanical properties

Contribution of the first author to this publication was preparation of glass-like carbons, participation in Raman spectroscopy measurements, performing transmission electron microscopy, electron energy loss spectroscopy, Raman spectroscopy, and nanoindentation data treatment, analysis and interpretation, writing and editing the manuscript.

Zakład Biofizyki i Fizyki Molekularnej   Chorzów, 04.11.2017 r.
Instytut Fizyki, Uniwersytet Śląski w Katowicach
Śląskie Międzyuczelniane Centrum Edukacji i Badań Interdyscyplinarnych
ul. 75 Pułku Piechoty 1A, 41-500 Chorzów

Statement on the contribution to publication

Publication:
Jurkiewicz, K., Pawlyta, M., Zygadlo, D., Chrobak, D., Duber, S., Wrzalik, R., Ratuszna, A. & Burian, A. Evolution of glassy carbon under heat treatment: correlation structure-mechanical properties. *Journal of Materials Science.*
DOI: 10.1007/s10853-017-1753-7.

We hereby state that the contribution to the work published jointly with Karolina Jurkiewicz is in accordance with the description below:

Karolina Jurkiewicz
Preparation of glass-like carbons, participation in Raman spectroscopy measurements, performing transmission electron microscopy, electron energy loss spectroscopy, Raman spectroscopy, and nanoindentation data treatment, analysis and interpretation, writing and editing the manuscript.
Signature: *Jurkiewicz*

Mirosława Pawlyta
Performing high-resolution transmission electron microscopy observations and electron energy loss spectroscopy measurements.
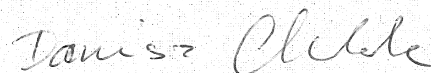Signature: *Pawlyta*

Dorota Zygadło
Performing Raman spectroscopy measurements.
Signature: *Dorota Zygadło*

Dariusz Chrobak
Performing nanoindentation measurements
Signature: *Dariusz Chrobak*

Stanisław Duber
Participation in preparation of carbon materials and providing scientific consultations.
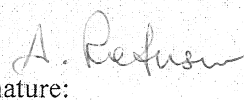Signature:

Roman Wrzalik
Providing scientific consultations.
Signature:

Alicja Ratuszna
Providing scientific consultations.
Signature: *A. Ratuszna*

Andrzej Burian
Providing scientific consultations and participation in editing the manuscript.
Signature: *A Burian*

CrossMark

Evolution of glassy carbon under heat treatment: correlation structure–mechanical properties

K. Jurkiewicz[1,2,*] (iD), M. Pawlyta[3] (iD), D. Zygadło[1,2] (iD), D. Chrobak[2,4] (iD), S. Duber[5] (iD),
R. Wrzalik[1,2] (iD), A. Ratuszna[1,2] (iD), and A. Burian[1,2] (iD)

[1] *A. Chełkowski Institute of Physics, University of Silesia, ul. Uniwersytecka 4, 40-007 Katowice, Poland*
[2] *Silesian Center for Education and Interdisciplinary Research, ul. 75 Pułku Piechoty 1A, 41-500 Chorzow, Poland*
[3] *Institute of Engineering Materials and Biomaterials, Silesian University of Technology, ul. Konarskiego 18A, 44-100 Gliwice, Poland*
[4] *Institute of Materials Science, University of Silesia, ul. 75 Pułku Piechoty 1A, 41-500 Chorzow, Poland*
[5] *Laboratory of Structural Research, University of Silesia, 41-500 Chorzow, Poland*

ABSTRACT

In order to accommodate an increasing demand for glassy carbon products with tailored characteristics, one has to understand the origin of their structure-related properties. In this work, through the use of high-resolution transmission electron microscopy, Raman spectroscopy, and electron energy loss spectroscopy it has been demonstrated that the structure of glassy carbon at different stages of the carbonization process resembles the curvature observed in fragments of nanotubes, fullerenes, or nanoonions. The measured nanoindentation hardness and reduced Young's modulus change as a function of the pyrolysis temperature from the range of 600–2500 °C and reach maximum values for carbon pyrolyzed at around 1000 °C. Essentially, the highest values of the mechanical parameters for glassy carbon manufactured at that temperature can be related to the greatest amount of non-planar sp^2-hybridized carbon atoms involved in the formation of curved graphene-like layers. Such complex labyrinth-like structure with sp^2-type bonding would be rigid and hard to break that explains the glassy carbon high strength and hardness.

Introduction

The disordered, non-graphitizing glassy carbons, also called glass-like carbons, are typically synthesized by pyrolysis of polymeric precursor such as phenolic resins or polyfurfuryl alcohol [1–4]. Due to their relative ease of production and a diverse range of physical properties, such as high thermal resistance, extreme chemical stability, low density and great hardness compared with other carbons, gases impermeability, and high electrical conductivity, these carbons have been extensively industrially applied since decades. In addition, glassy carbons exhibit excellent biologic compatibility with blood and tissues, meaning that they have a high potential for use in medicine [5]. The most recent studies have

🖄 Springer

suggested that glassy carbons have a fullerene-related structure. Such model of the structure, proposed by Harris [2, 6–8], consists of broken and imperfect fullerene fragments in the form of curved sp^2-bonded graphene-like planes, which can be multilayered and which often surround closed pores. The presence of curvature has been attributed to the topological defects in the form of non-hexagonal carbon rings such as pentagons and heptagons that were directly observed by the high-resolution transmission electron microscope (HRTEM) [9]. When glassy carbons are exposed to the temperature, the building structural blocks start ordering within individual graphene-like layers and the number of layers increases [2, 6–8, 10, 11]. Ordering within the layers is accompanied by increase in their sizes. However, even after heat treatment at temperatures of 3000 °C and above the glassy carbons cannot be transformed into crystalline graphite [7, 10] and preserve the general type of atomic disorder remaining features of the paracrystalline structure [12].

The structure is a key factor determining glassy carbon porosity, mechanical, and electronic properties. Therefore, the possibility to control the temperature-induced structural transformation is critically important for the fabrication of the glassy carbon products with desired functional features. It is essential to note that novel glassy carbon applications, such as micro-electro-mechanical systems [13, 14], that can be used for medical prostheses [15, 16] require comprehensive characterization of the properties–structure relationships at both, bulk- and nanoscale level. But up to now, the knowledge on how the manufacturing temperature, that is, how the internal structure affects the properties of glassy carbons is insufficient. Herein, high-resolution transmission electron microscopy, Raman spectroscopy, electron energy loss spectroscopy (EELS), and nanoindentation measurements were performed on a series of glassy carbons prepared by pyrolysis of polyfurfuryl alcohol at different temperatures from the range 600–2500 °C to shed more light on the evolution of their structure and properties during the heat treatment. The main aim of this work is investigation of correlations between the structure of the glassy carbons changing under the thermal treatment and their mechanical characteristics.

Experimental details

Preparation of glassy carbons

The glassy carbons studied here were prepared from furfuryl alcohol as a precursor. Polymeric furfuryl alcohol-based samples were pyrolyzed under protective Ar gas flow. The heating rate was 10 °C/h to 200 °C and 5 °C/h to the different desired temperatures: 600, 800, and 980 °C. Upon reaching the final heat treatment level, the temperature was held constant for 2 h. Then, the carbonized samples were allowed to cool in Ar flow. Next, some of the samples carbonized at 980 °C were further heat treated at 1500, 2000, and 2500 °C in Ar atmosphere. The high-temperature processing was performed with the heating rate of 4 °C/min from the room temperature up to the maximum pyrolysis temperature with the samples residence time 2 h at the final temperature. The glassy carbons heat treated as described above at different temperatures ranging from 600 to 2500 °C are labeled here according to the maximum annealing temperature as GC600, GC800, GC980, GC1500, GC2000, and GC2500, respectively. The chemical composition of the prepared carbons was examined using the X-ray fluorescence spectroscopy. The C content, included in Table 1, increases monotonically and tends toward 100% for high-temperature carbonization. The presence of elements other than C and O was below 0.1 at.%. The densities of the samples were monitored using helium pycnometer and are presented in Table 1. The density is observed to be the highest at temperature of 800 °C. Above 800 °C, the density decreases significantly due to rearrangement of the structure, formation, and growth of closed pores and for GC2500 is around 1.51 g/cm^3. The observations of density changes with pyrolysis temperature are generally in agreement with behavior reported by Zhang et al. [17] for glassy carbons from phenolic resins.

High-resolution transmission electron microscopy and electron energy loss spectroscopy

TEM investigations were done on a probe Cs-corrected S/TEM Titan 80-300 FEI microscope, equipped with a Gatan Tridiem 863 spectrometer. The preparation of samples was performed as follows: The pyrolyzed glassy carbon disks were ground in a steel

Table 1 C content and helium density of the glass-like carbons pyrolyzed at different temperatures from the range 600–2500 °C

Glass-like carbon	C content ± 1 [%]	He density ± 0.01 [g/cm^3]
GC600	94	1.60
GC800	96	1.88
GC980	97	1.77
GC1500	98	1.55
GC2000	100	1.52
GC2500	100	1.51

mill, the obtained powders were dispersed in ethanol using an ultrasonic bath, and then droplets of such prepared dispersions were put onto a carbon—coated lacey substrate supported by a copper grid and dried at room temperature. HRTEM imaging was obtained at 300 kV. The images were recorded with 1 s exposure time to avoid radiation damage of samples.

EELS spectra were acquired at 80 kV in STEM mode. Lower acceleration voltage of the electron was applied to exclude the influence of the electron beam on the structure of the material under test [18, 19]. The measurements were performed in STEM mode, allowing for the proper selection of fragments for analysis—sufficiently thin and homogeneous. The fitting procedure of EELS bands was performed with the Fityk software [20].

Raman spectroscopy

The Raman spectra of the series of glassy carbons were obtained using WITec Alfa 300R Raman spectrometer equipped with a confocal microscope, a 532-nm Nd:YAG diode laser and a highly sensitive back-illuminated Newton-CCD camera. The data were collected at room temperature with a 50 × objective (NA = 0.5), accumulated with 10 s exposure time and 100 repetitions in the spectral range between 200 and 3500 cm^{-1}. For each glassy carbon sample, the Raman scattering was measured at different places to make sure that the probed materials are homogeneous and the collected spectra provide representative structural information of bulk material. The fitting procedure of Raman bands was performed with the Fityk software [20].

Nanoindentation

Nanoindentation tests were performed with the Hysitron TriboIndenter TI-950 system. We have used Berkovich diamond tip to conduct the mechanical tests. The maximum load applied to the indenter was 0.8 mN, while the load function was composed of three parts: 5 s loading, 2 s dwell time, and 5 s unloading. The thermal drift rate was less than 0.1 nm/s. All experiments were performed in a constant ambient temperature and humidity, shielding the equipment from external vibrations. The Berkovich tip was calibrated using the fused quartz as a standard. The key parameters obtained during the nanoindentation experiment were hardness (H) and reduced Young's modulus (E_r). They were estimated using the well-known Oliver–Pharr method [21] as follows:

$$H = \frac{P_{max}}{A_r},\tag{1}$$

where P_{max} is the maximum load and A_r is the residual indentation area;

$$\frac{1}{E_r} = \frac{1 - v^2}{E} + \frac{1 - v_{ind}^2}{E_{ind}},\tag{2}$$

where E and v are the elastic modulus and Poisson's ratio of the sample, respectively, E_{ind} and v_{ind} are the same parameters of the diamond indenter tip.

Results

Comparative characterization of glassy carbon structural organization by HRTEM

The representative HRTEM images at different magnifications of the glassy carbons pyrolyzed at various temperatures, 600, 980, 1500, 2000, and 2500 °C are presented in Fig. 1. Black lines in these pictures represent parts of the carbon sheets which lie approximately parallel to the incident electron beam. The pictures show the evolution from a network of randomly oriented, disordered carbon domains to a more organized system resembling onion-like elements in which carbon layers are less rippled. The glassy carbon microstructure passes through a few
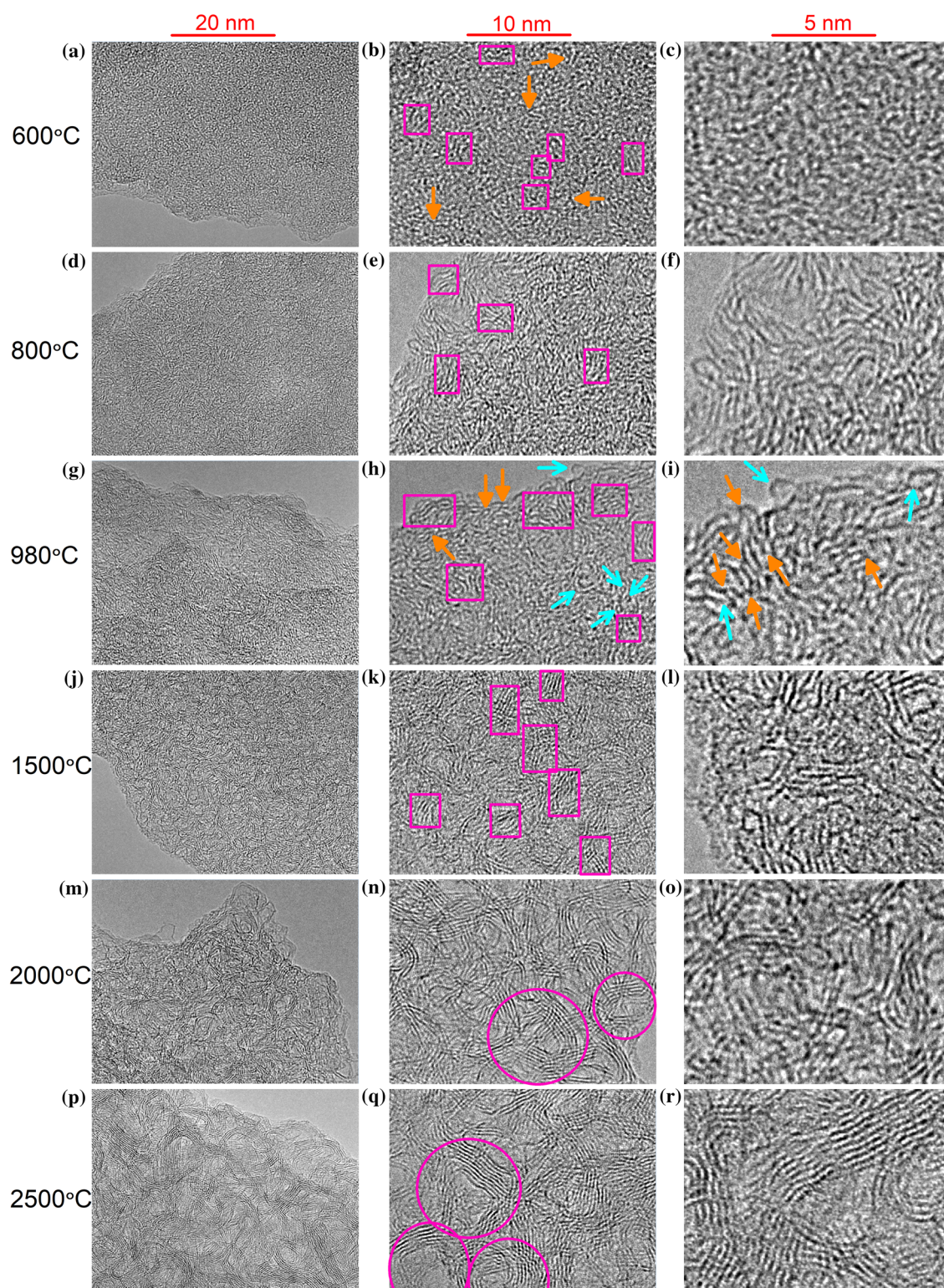
Figure 1 Representative HRTEM images at various magnifications of different regions of glassy carbon samples pyrolyzed at temperatures from the range 600–2500 °C. Rectangular frames expose domains with stacked graphene-like layers; round frames show onion-like structures enclosing pores; arrows indicate curved structural units.

phases during the conversion to its high-temperature form. The low-temperature glassy carbon (this pyrolyzed at 600 °C) is comprised of curled layers, as can be seen in Fig. 1a–c. Such curvature can arise from both, defects in the graphene-like domains and connections between them. The presence of bridges between the neighboring carbon domains is a natural consequence of the starting polymer network which undergoes extensive cross-linking [22] that was postulated by Franklin in early models of graphitizing and non-graphitizing carbons [10]. The microstructure of the GC600 sample is homogeneous. However, clusters of two, three, or even four layers of about 1–2 nm long that are arranged in stacks can be distinguished (marked in Fig. 1b by rectangular frames) in the overall tangle of randomly distributed carbon layers. Most of these carbon segments up to 1–2 nm long are bent. Completely flat layers are very rare. The distance between neighboring layers is irregular not only due to their curvature, but also cross-links and branches they create and which are marked in Fig. 1b with arrows. The gaps created between the curved layers may result in slit-shaped nanometer pores.

In the case of the GC800 and GC980 samples, in the HRTEM images (Fig. 1d–i) one can notice that some changes in the structure have been undergone due to the higher annealing temperature. Like the GC600, some of the layers are stacked in groups. In the case of the GC800 and GC980, however, the stacks are longer and there are definitely more packages of three, four, or even more layers which are aligned roughly parallel to each other (Fig. 1e, h). As regards the structural curvature, a few types of the curvature-related behavior can be distinguished. The first type refers to the corrugation of surface observed for almost every carbon layer in the structure. The expected source of such curvature is the presence of structural defects in the form of vacancies and non-hexagonal carbon rings causing the graphene-like sheet to transform from a planar to curved geometry [6, 23, 24]. The different types of defects may be created during the coalescence of structural units [25]. During pyrolysis, atoms are not in the thermodynamic equilibrium and many dangling bonds occur. The structure is allowed to eliminate them in the non-equilibrium conditions by the formation of polygons such as pentagons or heptagons or higher-membered rings resulting in the folding of carbon layers. It should be noted that the pentagon rings are

also originally present in the initial structure of the furfuryl alcohol polymer [22, 26] and they can partly survive at the later stages of heat treatment, as confirmed by Tondi et al. [27], causing out-of-plane ripples. In parallel, the curvature is created by the carbon layers which branch out or link together by forming the specific tubular caps, marked in Fig. 1h, i with filled arrows. Such type of bridges between adjacent carbon layers creates compact 3D network which may prevent graphitization and make the material strong.

With increasing the carbonization temperature above 800 °C, the curvature related with elements resembling fragments of fullerenes, onions or even completely closed fullerene-like particles is more prevalent. The different types of curved structural elements for the GC980 are marked with arrows in Fig. 1h, i.

On the further heat treatment up to 1500 °C, one can notice in Fig. 1j–l that within the microstructure of glassy carbon two parts mixing with each other can be clearly distinguished. The first part, more organized, consists of groups of stacked and more or less parallel planes, while the second part, globally disordered, is characterized by randomly oriented and twisted layers of various sizes. We observe that the glassy carbon crystallites grow at the expense of the more disordered part of the microstructure. The less-organized regions are consumed by the domains with parallel layers resulting in their growth, both in width and height, and simultaneously in creation of empty voids. In the low-temperature glassy carbons, the microporosity is a direct consequence of misalignment of the curved sheets or their packages. As the annealing temperature increases, the bigger pores are formed due to joining of disordered fragments to more ordered domains. This leads to the creation of isolated, non-connected voids such as these marked with circle frames in Fig. 1n, r. The HRTEM images pretty clearly exhibit that dimensions of the micropores are tunable by the heat treatment in the range of few angstroms to several nanometers. Up to the maximum annealing temperature 2500 °C, the gradual elongation of graphene-like layers, increase in their number in the stacks and growth of pores are observable. As the pyrolysis temperature increases, the onion-like carbon structures become more prevalent. The high-temperature GC2500 is mostly composed of well-organized great fragments of onions or even entire onions (Fig. 1p–r).

They are made up of the curved and faceted graphite-like crystallites up to around 10 nm long and 10 layers thick. The onion-like elements are interwoven together and limit pores which are much larger than in the low-temperature glass-like carbons.

Correlation of first- and second-order Raman peaks behavior with the structural transformation

The first-order Raman spectra display two main peaks between 1200 and 1700 cm^{-1}, as shown in Fig. 2a, which are characteristic features of graphitic carbons [28]. The peak at around 1600 cm^{-1} is called graphitic or simply G band and is due to optical phonon mode with E_{2g} symmetry associated with an in-plane stretching of sp^2-bonded carbon atoms. The peak at around 1350 cm^{-1} is called disorder-induced or D band and is not observed for single-crystal perfect graphite [29]. The origin of the D mode had long been debated, and more recently it was attributed to the double-resonant Raman scattering [30]. The spectra of the first-order Raman region normalized to the D band intensity and overlapped to better distinguish differences between them are presented in Fig. 2b. The main characteristic feature of these spectra is the increase in the D intensity (I_D) with respect to the G peak intensity (I_G) and sharpening of

the D peak width with increasing pyrolysis temperature up to 2500 °C. The ratio of intensities I_D/I_G or corresponding integrated areas upon D and G peaks is sometimes used to calculate the averaged in-plane size of graphitic domains (L_a). According to the formula proposed by Tuinstra and Koenig: $I_D/I_G \sim 1/L_a$ (the so-called T-K rule) [28]. In the case of the studied here glassy carbons by HRTEM images, we observe continuous growth of carbon layers with the heat treatment temperature. Therefore, the T-K rule does not appear to be fulfilled in this case. Ferrari and Robertson [31] showed that for amorphous and disordered carbons the development of the D peak indicates ordering, exactly opposite to the case of graphite. They argued that the T-K formula should not be valid at very small values of L_a, because for small L_a the D band strength is proportional to the probability of finding a sixfold aromatic ring in the carbon cluster that is proportional to the cluster area L_a^2. Therefore, they submitted a new dependence of the I_D to I_G ratio on the L_a size, namely $I_D/I_G \sim L_a^2$ for carbons containing small clusters with L_a below about 25 nm and suggested that such a behavior of Raman spectra would be possible for non-crystalline graphite progressively defected resulting in its amorphization. Experimental example of this behavior has been found, i.e., for glassy carbon implanted with ions, which exhibited decreasing I_D/I_G ratio

Figure 2 Overview of the Raman spectra for glassy carbons pyrolyzed at different temperatures from the range of 600–2500 °C (GC600–GC2500) (**a**); comparison of the normalized spectra for the first-order region (**b**) and the second-order region (**c**). The insets show the best fit of the experimental data for glassy carbon pyrolyzed at 1500 °C (GC1500).
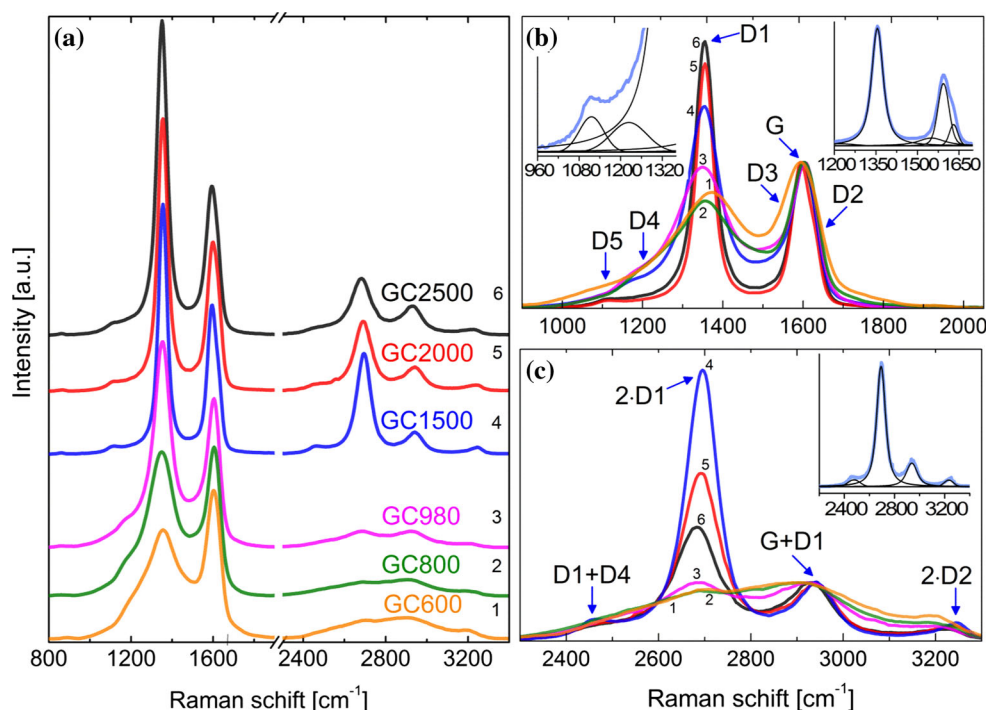
with higher ion doses due to loss in order and decrease in crystallite size [32]. Here, we observe a reverse process—the more disordered and fine carbon nucleuses are transformed during pyrolysis to less defected, better organized and greater packages of graphene layers and the I_D/I_G ratio increases with higher temperature. Similar tendency has been already observed for carbonized polyfurfuryl alcohol [33], cellulose [34], or wood [35].

In order to accurately recognize other bands contributing to Raman scattering for the glassy carbons, the spectra were fitted with the Voigt line shapes. A representative example of the fitting of the first- and second-order Raman spectra is showed for the glassy carbon heat treated at 1500 °C as insets in Fig. 2b, c. As a result of the fitting, we can distinguish six components contributing to the first-order Raman spectrum: (1) graphitic G peak at 1595 cm^{-1}, (2) disordered D1 peak at 1355 cm^{-1}, (3) D2 peak at 1630 cm^{-1} described in [29, 36], (4) D3 peak at 1549 cm^{-1} described in [28], (5) D4 peak at 1212 cm^{-1}, and (6) D5 peak at 1110 cm^{-1}. The D4 and D5 features must account for the total spectra during fitting of Raman data for all glassy carbon heat treated between 600 and 2500 °C; however, they weaken in intensity during the progressive heat treatment. Recently, Couzi et al. [37] showed that in the spectral range 1000–1300 cm^{-1} of various defective carbon materials three different components participate to the scattered signal and assigned them to the different defect-induced double resonance inter-valley processes. The idea of the defect-related history of the reported here D4 and D5 peaks seems to be reasonable. Interestingly, Fujimori et al. [38] experimentally identified a Raman signal from Stone–Thrower–Wales (STW) defects on single-walled carbon nanotubes in the range of 1100–1200 cm^{-1}. Moreover, according to theoretic calculations of the STW defect in a flat graphene two characteristic Raman modes at 1122 and 1173 cm^{-1} are predicted [39]. We assume that the D4 and D5 peaks observable here for the glassy carbons can also come from the vibrations of carbon atoms in non-hexagonal rings such as STW defects which are considered as the reason of the fullerene-like structure of glassy carbons [6–8].

The second-order Raman spectra compared in Fig. 2c reveal four peaks: (1) 2·D1 peak at 2695 cm^{-1}, (2) G + D1 peak at 2940 cm^{-1}, (3) 2·D2 at 3250 cm^{-1}, and (4) D1 + D4 at 2450 cm^{-1}. They are the overtones or the combined tones of the first-order bands.

For the low-temperature glassy carbons up to 1000 °C, the 2·D1 band merges with the other surrounding bands to form a small modulated bump. The intensity of the 2·D1 peak increases roughly six times for GC1500 in comparison with the GC980 and then decreases gradually for GC2000 and GC2500. It should be mentioned that the 2·D1 peak, named historically the G' peak, for graphene is more intense than the G band compared to bulk graphite [39–42]. Increasing the number of graphene layers in the stack leads to a significant decrease in the 2·D1 to G intensity ratio [43, 44]. Indeed, for the glassy carbons we observe a systematic drop of the 2·D1 intensity with increase in the heat treatment temperature above the 1500 °C. That is probably the effect of increase in number of layers in the graphite-like domains, as can be seen in the electron microscopic images in Fig. 1. The lack of clearly pronounced peaks in the second-order region for the glassy carbons at 600, 800, and 980 °C may be due to a much lower intensity of the first-order Raman modes. Moreover, the low intensity of the 2·D1 bands for the low-temperature glassy carbons GC600–GC980 may be explained by the small lateral size of the graphene-like layers and/or very high defect densities causing strong distortion of graphene-like clusters. Further formation of greater and more uniform carbon hexagonal network for the GC1500 causes significant rise in the 2·D1 intensity.

Evidence of curved structural units in low-frequency Raman spectra

In the low-frequency region below 900 cm^{-1} of the measured spectra, a number of Raman-active modes were observed. All glassy carbons show peaks near 260 cm^{-1} (P1), 440 cm^{-1} (P2), 620 cm^{-1} (P3), and 860 cm^{-1} (P4), as can be seen in Fig. 3, while this Raman region is completely silent for graphite and diamond crystals according to the group theory [45]. Analogous bands in the low-frequency region of Raman spectra were found for carbon nanotubes, fullerenes, or nanoonions [46–50] as well for more exotic non-planar carbon structures such as tubular cones, whiskers, and polyhedral crystals [51]. Therefore, we assume that the observed modes are markers of curvature-related geometry in the investigated glassy carbons, which has been already confirmed by the HRTEM images.
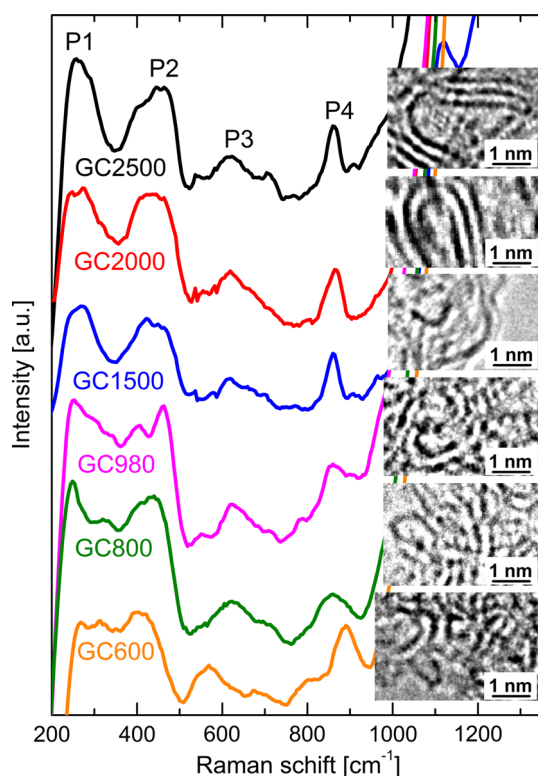
Figure 3 Low-frequency Raman modes for glassy carbons pyrolyzed up to different temperatures from the range of 600–2500 °C (GC600–GC2500). The insets show selected HRTEM images with curved structural units of around 1 nm in diameter.

It is known that a band in the range 100–350 cm^{-1} is a signature of single-walled carbon nanotubes (SWCNTs) and is related to their radial breathing modes (RBMs) unique to cylindrical symmetry [52]. The RBMs correspond to the coherent vibration of the carbon atoms where all the tube atoms vibrate radially in phase. Zhao et al. [53] established that the RBMs can also give active Raman peaks in the 100–600 cm^{-1} region for multi-walled carbon nanotubes (MWCNTs). These RBM frequencies (ω_{RBM}) are therefore very useful for identifying whether a given carbon material contains curved, nanotube-like elements. The ω_{RBM} depends on the nanotube diameter d as:

$$\omega_{RBM} = \frac{A}{d} + B, \qquad (3)$$

where A and B are experimentally determined constants dependent on environment in which nanotube is present. The reported glassy carbon building blocks are multilayer nanostructures which can be classified as fragments of MWCNTs. It was

determined that for SWNTs of 1.5 nm in diameter measured in bundles $A = 234$ cm^{-1} and $B = 10$ cm^{-1} [53]. If we take the values of A and B parameters as mentioned above and we assume that recorded P1 peaks are 10% up-shifted due to interlayer interactions in multilayered domains [29], we are able to estimate the diameter of the nanotube fragments possibly responsible for the breathing vibrations to be of approximately 1 nm. Such nanotube-like elements of approximately 1 nm in diameter can be easily found in HRTEM images and their examples were attached as insets to Fig. 3.

Beside the P1 peak around 260 cm^{-1}, the Raman spectra contain also broad features with maxima at around 440 cm^{-1} (P2), 620 cm^{-1} (P3), and 860 cm^{-1} (P4). Herein reported low-frequency Raman modes for glassy carbons are analogs to the Raman features identified by Roy et al. [50] for carbon nanoonions produced by the arc discharge of graphite electrodes. Tan et al. [51] also observed Raman peaks at ∼ 470, 620, and 860 cm^{-1} in ion-implanted highly oriented pyrolytic carbon and in turbostratically stacked particles. Moreover, it was showed first time by Rao et al. [47] that SWCNTs exhibit numerous Raman modes in the region 300–1400 cm^{-1}. Two possible explanations for the origin of these peaks were proposed. One claims that these modes are combination of the acoustic and optical phonon modes activated due to nanotube geometry, and the other that they arise from structural defects [54]. Hence, it is clear that disorder and defects strongly influence the Raman spectra of carbon materials and the features reported here for glassy carbons in the range 350–900 cm^{-1} can be defect-induced Raman modes.

Bonding character of carbon atoms at different stages of thermal treatment

HRTEM and Raman spectroscopy results showed that glassy carbons at different stages of pyrolysis contain curved structural units. The question that arises is what type of bonds between carbon atoms the buckled layers contain. The presence of diamond-like sp^3-bonded atoms would explain the high hardness and resistance to graphitization of glassy carbons, and in the past an idea appeared that the sp^3-bonded carbons may act as potential cross-linking [55]. We used electron energy loss spectroscopy to estimate the amount of the possible sp^3 bonds as well

as to evaluate the *sp²-type* bond character at different stages of the pyrolysis process.

The representative EELS spectra in the C-K edge region after background subtraction by fitting a power-low curve shown in Fig. 4a have two main features: the π* peak around 285 eV, caused by transitions from the carbon 1s core level to the anti-bonding state of π bonding, and the σ* peak around 291 eV, caused by transitions from the carbon 1s core level to the anti-bonding state of σ bonding. For GC600, the π* feature is broad and the σ* peak is poorly defined. With increase in pyrolysis temperature, the EELS spectra show an increase in the intensity of the π* peak in respect to the σ* peak intensity. Simultaneously, the σ* signal becomes more noticeable with rising temperature and the appearance of another weak features on the high energy side of the σ* peak, indicating an increase in longer range order [56]. Such a behavior of these spectra is typical for conversion of disorder carbon structure toward graphitic *sp²* bond configuration. However, the near-edge fine structure above 295 eV is less pronounced than in case for graphitic samples with three-dimensional crystalline order [56]. We used a procedure developed by Berger et al. [57] for determining the fraction of *sp²*-bonded carbon atoms in the glassy carbons. This method is based on estimation of the ratio of integrated window centered upon the π* peak ($I_{\pi*}$) to the integrated area containing both, π* and σ* peaks ($I_{\pi*+\sigma*}$), according to the following equation:

$$\frac{sp^2}{sp^2 + sp^3} = \frac{I_{\pi*}}{I_{\pi*+\sigma*}} \tag{4}$$

Here, for calculations we used 6 eV window centered at 292 eV over the both π* and σ* peaks. The ratio obtained according to the (4) is usually normalized to the factor determined from spectra of a 100% *sp²*-hybridized material. The most often highly oriented pyrolytic graphite (HOPG) is used [56, 58]. However, an open discussion is correctness of such technique [59, 60]. Therefore, in order to avoid the uncertainty related with the choice of reference material we used the GC2500 sample as a reference in this series of glassy carbons. Based on recent studies by X-ray and neutron diffraction combined with molecular dynamic simulations [61] and the resulting optimized models of the glassy carbon atomic structures (available as .xyz files in the supporting information of the Ref. [61]), we determined the percentage amount of *sp³* carbon bonds in the proposed model of the GC2500 atomic structure to be about 0.5%. Therefore, we treat the glassy carbon heated at 2500 °C as a material containing near 100% *sp²* carbon hybridization. The computed changes in the *sp²*-bonded C atoms content as a function of pyrolysis temperature with respect to the GC2500 reference are presented in Fig. 4b. The dispersion of the determined *sp²* fractions does not exceed 6% of the mean values. The fraction of *sp²* bonds is definitely over the fraction of *sp³* bonds, starting from about 95% for low-temperature glassy carbon GC600 and monotonically rising to almost 100% for GC2000. For low-temperature samples containing hydrogen, it is possible that we include intensity from electronic transition to the C–H(σ*) orbital giving signal about 287–289 eV, and the resulting content of *sp²* bonds determined by the procedure described above may be erroneously higher, as noticed by Daniels et al. [62].

Figure 5a shows example of a Gaussian fit to the C-K edge of glassy carbon pyrolyzed at 980 °C. Similar fits were employed for spectra of other glassy carbons. It is generally not possible to fit just one Gaussian peak to the 1s to π* transition range. An additional peak about 287 eV must be included even for high-temperature glassy carbons. It is unlikely that a significant amount of hydrogen can survive at

Figure 4 Variation in the glassy carbon electron energy loss in the C-K edge region (**a**), and in the determined *sp²*-hybridized bond content (**b**) as a function of pyrolysis temperature from the range of 600–2500 °C (GC600–GC2500).
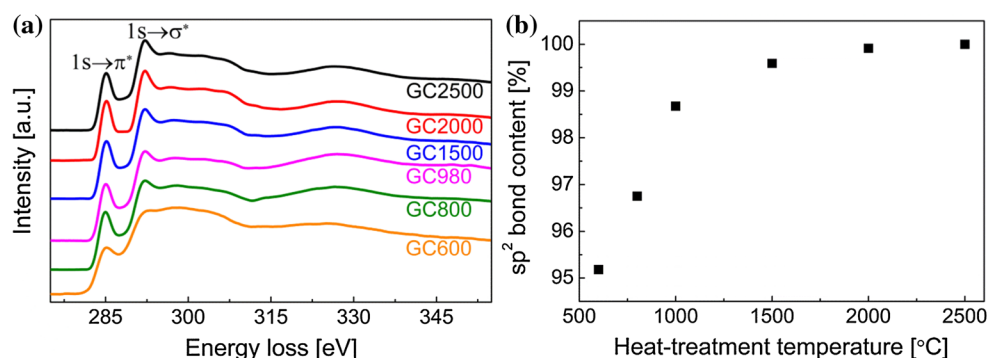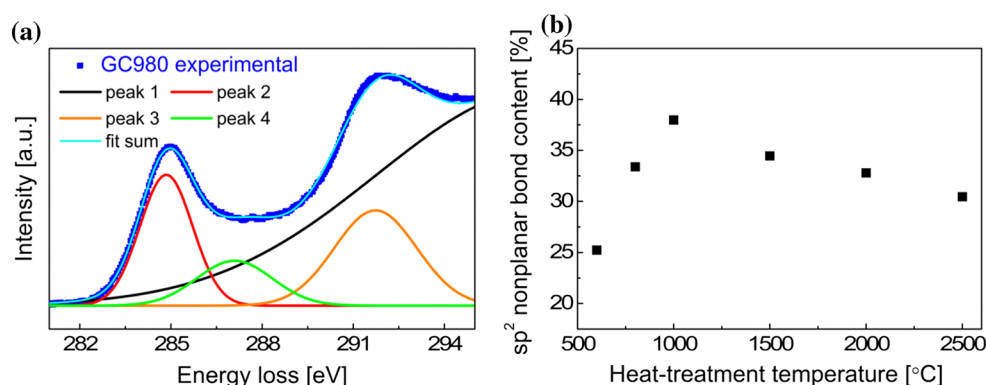
Figure 5 Example of a Gaussian fit to the C-K edge of glassy carbon pyrolyzed at 980 °C (GC980) (**a**), and variation in the sp^2-hybridized non-planar bond content as a function of pyrolysis temperature from the range of 600–2500 °C (**b**).

such high temperature as 2500 °C. Thus, the origin of the feature around 287 eV due to hydrogen content can be questionable. Other idea explaining the additional residual feature is that it can be due to the presence of curved fullerene-like bond configuration. Nyberg et al. [63] found that C-K absorption spectra of C_{60} and C_{70} fullerenes consist of double-peaked π^* component. The shoulder on the high energy side of the 1s to π^* peak centered at 287 eV was also confirmed in spectra of fullerenes by other researches [57, 60]. Bearing in mind the results from HRTEM and Raman spectroscopy which indicate that the structure of glassy carbon at different stages of pyrolysis has features of fullerene-like units, we suggest that the EELS spectra of glassy carbons can resemble the spectra of fullerenes. Therefore, we used the ratio of the integrated intensity upon the 287 eV peak ($I_{\pi*np}$) to the area under both 285 and 287 eV peaks ($I_{\pi*total}$) related with the 1s to π^* signal, as a measure of the sp^2 non-planar bond content (sp^2_{np}) to the total (fullerene-like non-planar and graphitic-like planar) sp^2 carbon bonds content (sp^2_{total}), according to the following formula:

$$\frac{sp^2_{np}}{sp^2_{total}} = \frac{I_{\pi*np}}{I_{\pi*total}} \tag{5}$$

This intensity ratio should reflect the degree of curvature of glassy carbon structure due to non-planar, strained sp^2 bonds. The results are presented in Fig. 5b. The dispersion of such determined non-planar sp^2 bond fractions does not exceed 13% of the mean values.

According to the obtained results, the ratio of non-planar sp^2-bonded to all sp^2-bonded carbon atoms increases from approximately 25% for GC600 up to about 38% for GC980 and then a subsequent drop of this ratio is observed to about 30% for GC2500. The

initial increase in the fraction of fullerene-like non-planar sp^2 bonds seems to be a consequence of coalescence of carbon domains. Under the increasing temperature, disordered layers within the glassy carbon merge and connect in various ways, as can be seen in the HRTEM images displayed in Fig. 1. The creation of the postulated non-hexagonal rings during the structure reorganization with heat treatment would explain the revealed rise to the non-planar, strained sp^2 bond content associated with the buckled units. With further increase in the heat treatment temperature, however, more and more defects could be healed progressively providing layers with higher fraction of planar graphitic-like sp^2 bonds.

Mechanical properties and their correlations with the structure

A schematic comparison of the force–displacement response of the studied glassy carbons upon indentation with 800 µN terminal force is shown in Fig. 6. For the sample carbonized at the lowest temperature,
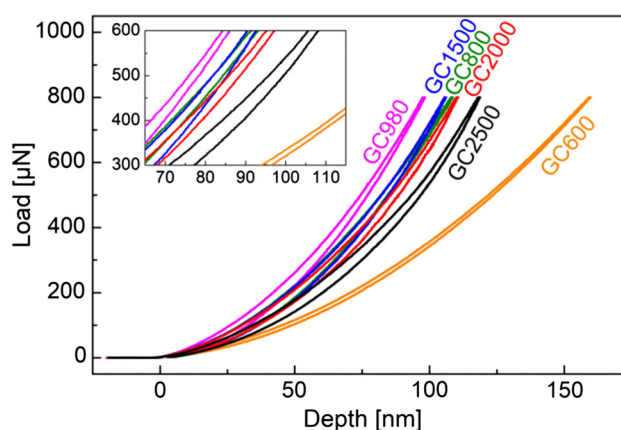

Figure 6 Indentation hysteresis curves of the glassy carbons pyrolyzed at different temperatures from the range of 600–2500 °C (GC600–GC2500).

GC600, the penetration by the indentation is the deepest. A progressive increase in the slope of the load–displacement curve and decrease in the penetration depth are observed up to carbonization at 980 °C. Interestingly, with further increase in carbonization temperature from 980 up to 2500 °C, the material response is reverse and the penetration depth increases gradually. Similar behavior in the temperature range from 1000 to 3000 °C was previously reported by Iwashita et al. [64, 69]. This can be simply explained taking into account the previously described structural changes with increasing pyrolysis temperature. Easier penetration of glassy carbon by indenter can be due to softening of the material during development of more graphitic structure and growth of pores with elevation of heat treatment temperature above around 1000 °C. The unloading paths do not completely retrace the loading paths but return to the origin forming hysteresis loops. The area of the hysteresis loop corresponds to the energy loss during the deformation of the sample surface by the indentation. For the low-temperature glassy carbon, GC600, there is only very small difference between loading and unloading curves, what demonstrates nearly perfect elastic deformation. Moreover, any residual indentation impression after complete loading was observed. This means that the position of indentation tip of the impression at the maximum load goes back to the original sample surface level. The energy dissipation is mostly related with the elastic reversible deformation.

Figure 7 shows the effect of pyrolysis temperature on the hardness and the reduced Young's modulus of the glassy carbons. These mechanical properties for each sample were calculated as averaged values over around 24 measurements of material ability to resist deformation after applying local force. Uncertainties estimated as standard deviations were not greater than 4% for H and 3% for E_r. The values of the determined hardness and reduced Young's modulus rise from around 3.1 and 15.6 GPa, respectively, for glassy carbon carbonized at 600 °C up to around 5.9 and 37.6 GPa, respectively, for 980 °C. With further increase in heat treatment temperature, a continuous decrease in H and E_r is observed up to around 4 and 26.6 GPa, respectively, for 2500 °C. Thus, the effect of pyrolysis temperature on mechanical properties of these polyfurfuryl alcohol-derived glassy carbons in the range of 600–2500 °C can be separated into two ranges: until reaching the temperature of 1000 °C and upon reaching the 1000 °C.

Franklin [10] proposed that the great hardness of the non-graphitizing carbons must be attributed to the strong cross-links between neighboring domains, which may be partially destroyed at high temperatures resulting in hardness decrease. The work of Jenkins and Kawamura [65] shed more light on the changes of glassy carbon mechanical properties during carbonization process. They demonstrated that the hardness increases approximately linearly with the decrease in H/C ratio during material decomposition up to 1500 °C, what is followed by, as they suggested, creation of cross-links and intermolecular forces. Further decrease in mechanical performance for higher heat treatment temperatures is related with breaking some of the cross-link bonds during development of more graphitic structures. Similar conclusions were generally given also by other authors in more recent reports [64, 66, 67].

In the present work, we revealed that the changes in hardness and reduced Young's modulus follow the same trend as the changes in the content of non-planar to the total amount of sp^2 carbon bonds with increase in pyrolysis temperature. Comparison of the data from EELS in Fig. 5b with nanoindentation results in Fig. 7a, b shows that the measured

Figure 7 Variation in the glassy carbon nanoindentation hardness (**a**), and reduced Young's modulus **b** as a function of pyrolysis temperature from the range of 600–2500 °C.
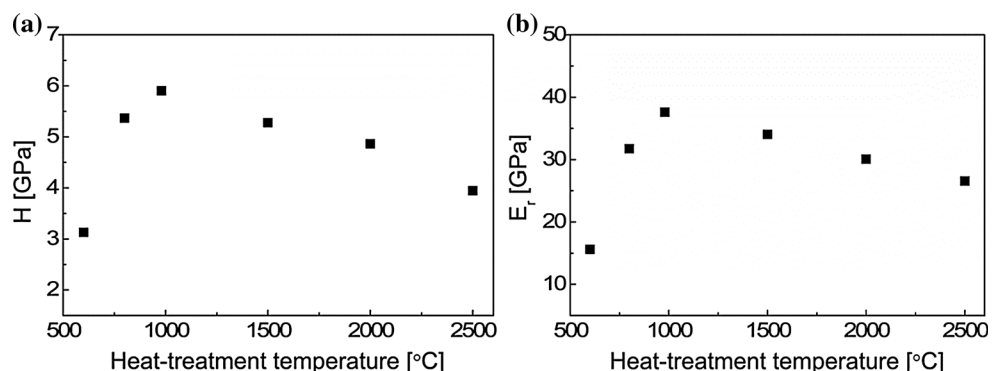
mechanical properties are a direct response of the structural transformation that undergoes with increase in heat treatment temperature. The fraction of sp^2 non-planar, fullerene-like or nanotube-like bonds with respect to the total content of sp^2-hybridized bonds between carbon atoms in structural units can be used for hardness and Young's modulus rating. It is known that carbon nanotubes are one of the strongest materials known [68]. They are also very elastic. It is due to the interlocking carbon-to-carbon covalent bonds. The presence of nanotube-like elements in the structure of glassy carbons can be responsible for their high hardness and strength. The nanotube-like bridges between neighboring carbon layers evident in HRTEM images bind the entire structure into a tight network. It is worth to mention that recently proposed structural models of glassy carbons [60] display the possible configurations of such fullerene-like or nanotube-like interfaces. Based on the models, it was established that the creation of such interlayer connections, or so-called cross-links, is facilitated by the presence of defects in the form of non-hexagonal rings, vacancies, isolated sp^3 bonds or chains which introduce curvature. The curved units may also effectively inhibit the movement of carbon layers and prevent the graphitization.

Conclusions

In this work, the detailed structure studies of the non-graphitizing glassy carbons prepared by pyrolysis of polyfurfuryl alcohol at different temperatures from 600 to 2500 °C and its effect on the mechanical properties of these materials were reported. It was proven that the mechanical properties (hardness and reduced Young's modulus) of the glassy carbons measured via nanoindentation as a function of the pyrolysis temperature are a direct reflection of their internal structure. The presence of fullerene-like or nanotube-like elements in the structure of glassy carbons is considered to be responsible for their high hardness and strength. The hardness and the reduced Young's modulus scale non-monotonically as a function of the pyrolysis temperature reaching maximum values of 5.9 and 37.6 GPa, respectively, for glassy carbon pyrolyzed at 980 °C. The peculiar mechanical behavior of the glassy carbon around 1000 °C is attributed to the greatest amount of non-planar sp^2-hybridized carbon atoms involved in the

building of curved and often interconnected fullerene-like elements at this temperature. The structural curvature seems to be gradually formed at the early stages of the pyrolysis process (at temperatures up to $\sim$ 1000 °C) due to merging of the initial small carbon domains. The cross-links between neighboring graphene-like layers may have nature of non-planar sp^2-type bonds whose content was quantified by EELS measurements. It was demonstrated that at the initial stages of pyrolysis up to 1000 °C the amount of fullerene-like non-planar to total sp^2 carbon bonds increases. Then, with higher heat treatment temperatures the structure is transformed into units composed of greater and less-defected graphite-like domains resulting in decrease in non-planar sp^2 bond content and drop in mechanical performance. In other words, when the material is heated at temperatures higher than 1000 °C, it becomes more ordered but weaker. Therefore, the fraction of sp^2 non-planar fullerene-like or nanotube-like bonds with respect to the total content of sp^2-bonds in the glass-like carbons can be used for evaluation of their mechanical properties.

The knowledge of the structure–property correlations is essential to manufacture glassy carbon products with tailored features. Undoubtedly, one of the most promising glassy carbon's uses is the fabrication of glassy carbon-based super lightweight and strong microlattices. They represent a significant step forward in the field of lightweight mechanical metamaterials and can exert a great impact for medical applications. Due to glassy carbon's good mechanical properties, electrical conductivity, and biocompatibility, this material is interesting for microimplants in the line of microstents, microscaffolds for bone regeneration, and microelectrodes. We hope that the developed here quantitative relationships between the structure and mechanical properties will benefit the further design of the glassy carbon systems.

Acknowledgements

References

[1] Yamada S, Sato H (1962) Some physical properties of glassy carbon. Nature 193:261–262. https://doi.org/10.1038/193261b0

[2] Harris PJF (2004) Fullerene-related structure of commercial glassy carbons. Philos Mag 84:3159–3167. https://doi.org/10.1080/14786430410001720363

[3] Jenkins GM, Kawamura K (1971) Structure of glassy carbon. Nature 231:175–176. https://doi.org/10.1038/231175a0

[4] Jenkins GM, Kawamura K (1976) Polymeric carbons: carbon fibre, glass and char. Cambridge University Press, Cambridge

[5] Driver M (2012) Coatings for biomedical applications. Elsevier, Amsterdam

[6] Harris PJF, Tsang SC (1997) High-resolution electron microscopy studies of non-graphitizing carbons. Philos Mag A 76:667–677. https://doi.org/10.1080/01418619708214028

[7] Harris PJF (1997) Structure of non-graphitising carbons. Int Mater Rev 42:206–218. https://doi.org/10.1179/imr.1997.42.5.206

[8] Harris PJF (2013) Fullerene-like models for microporous carbon. J Mater Sci 48:565–577. https://doi.org/10.1007/s10853-012-6788-1

[9] Harris PJF, Liu Z, Suenaga K (2008) Imaging the atomic structure of activated carbon. J Phys Condens Matter 20:362201–362206. https://doi.org/10.1088/0953-8984/20/36/362201

[10] Franklin RE (1951) Crystallite growth in graphitizing and non-graphitizing carbons. Proc R Soc Lond A Math Phys Eng Sci 209:196–218. https://doi.org/10.1098/rspa.1951.0197

[11] Petkov V, DiFrancesco RG, Billinge SJL, Acharya M, Foley HC (1999) Local structure of nanoporous carbons. Philos Mag B 79:1519–1530. https://doi.org/10.1080/13642819908218319

[12] Jurkiewicz K, Duber S, Burian A (2016) Paracrystalline structure of glass-like carbons. Int J Appl Glass Sci 7:355–363. https://doi.org/10.1111/ijag.12186

[13] Lentz CM, Samuel BA, Foley HC, Haque MA (2011) Synthesis and characterization of glassy carbon nanowires. J Nanomater 2011:129298–129306. https://doi.org/10.1155/2011/129298

[14] Li X, Gao H (2016) Mechanical metamaterials: smaller and stronger. Nat Mater 15:373–374. https://doi.org/10.1038/nmat4591

[15] Kassegne S, Vomero M, Gavuglio R, Hirabayashi M, Özyilmaz E, Nguyen S, Rodriguez J, Özyilmaz E, Niekerk P, Khosla A (2015) Electrical impedance, electrochemistry, mechanical stiffness, and hardness tunability in glassy carbon MEMS µECoG electrodes. Microelectron Eng 133:36–44. https://doi.org/10.1016/j.mee.2014.11.013

[16] Vomero M, Castagnola E, Ciarpella F, Maggiolini E, Goshi N, Zucchini E, Carli S, Fadiga L, Kassegne S, Ricci D (2017) Highly stable glassy carbon interfaces for long-term neural stimulation and low-noise recording of brain activity. Sci Rep 7:40332–40346. https://doi.org/10.1038/srep40332

[17] Zhang ZL, Brydson R, Aslam Z, Reddy S, Brown A, Westwood A, Rand (2011) Investigating the structure of non-graphitising carbons using electron energy loss spectroscopy in the transmission electron microscope. Carbon 49:5049–5063. https://doi.org/10.1016/j.carbon.2011.07.023

[18] Zobelli A, Gloter A, Ewels CP, Seifert G, Colliex C (2007) Electron knock-on cross section of carbon and boron nitride nanotubes. Phys Rev B 75:245402–245411. https://doi.org/10.1103/PhysRevB.75.245402

[19] Jinschek JR, Yucelen E, Calderon HA, Freitag B (2011) Quantitative atomic 3-D imaging of single/double sheet graphene structure. Carbon 49:556–562. https://doi.org/10.1016/j.carbon.2010.09.058

[20] Wojdyr M (2010) Open source GPL'd peak profiling program Fityk. J Appl Crystallogr 43:1126–1128. http://www.unipress.waw.pl/fityk

[21] Oliver WC, Pharr GM (1992) An improved technique for determining hardness and elastic modulus using load and displacement sensing indentation experiments. J Mater Res 7:1564–1583. https://doi.org/10.1557/JMR.1992.1564

[22] Burket CL, Rajagopalan R, Marencic AP, Dronvajjala K, Foley HC (2006) Genesis of porosity in polyfurfuryl alcohol derived nanoporous carbon. Carbon 44:2957–2963. https://doi.org/10.1016/j.carbon.2006.05.029

[23] Cortijo A, Vozmediano MA (2007) Effects of topological defects and local curvature on the electronic properties of planar graphene. Nucl Phys B 763:293–308. https://doi.org/10.1016/j.nuclphysb.2006.10.031

[24] Banhart F, Kotakoski J, Krasheninnikov AV (2010) Structural defects in graphene. ACS nano 5:26–41. https://doi.org/10.1021/nn102598m

[25] Acharya M, Strano MS, Mathews JP, Billinge SJ, Petkov V, Subramoney S, Foley HC (1999) Simulation of nanoporous carbons: a chemically constrained structure. Philos Mag B 79:1499–1518. https://doi.org/10.1080/13642819908218318

[26] Guigo N, Mija A, Vincent L, Sbirrazzuoli N (2007) Chemorheological analysis and model-free kinetics of acid catalysed furfuryl alcohol polymerization. Phys Chem Chem Phys 9:5359–5366. https://doi.org/10.1039/B707950H

[27] Tondi G, Pizzi A, Pasch H, Celzard A, Rode K (2008) MALDI-ToF investigation of furanic polymer foams before and after carbonization: aromatic rearrangement and surviving furanic structures. Eur Polym J 44:2938–2943. https://doi.org/10.1016/j.eurpolymj.2008.06.029

[28] Tuinstra F, Koenig JL (1970) Raman spectrum of graphite. J Chem Phys 53:1126–1130. https://doi.org/10.1063/1.1674108

[29] Pimenta MA, Dresselhaus G, Dresselhaus MS, Cancado LG, Jorio A, Saito R (2007) Studying disorder in graphite-based systems by Raman spectroscopy. Phys Chem Chem Phys 9:1276–1290. https://doi.org/10.1039/B613962K

[30] Thomsen C, Reich S (2000) Double resonant Raman scattering in graphite. Phys Rev Lett 85:5214–5217. https://doi.org/10.1103/PhysRevLett.85.5214

[31] Ferrari AC, Robertson J (2000) Interpretation of Raman spectra of disordered and amorphous carbon. Phys Rev B 61:14095–14107. https://doi.org/10.1103/PhysRevB.61.14095

[32] McCulloch DG, Prawer S, Hoffman A (1994) Structural investigation of xenon-ion-beam-irradiated glassy carbon. Phys Rev B 50:5905–5917. https://doi.org/10.1103/PhysRevB.50.5905

[33] Nakamizo M, Kammereck R, Walker PL (1974) Laser Raman studies on carbons. Carbon 12:259–267. https://doi.org/10.1016/0008-6223(74)90068-2

[34] Rhim YR, Zhang D, Fairbrother DH, Wepasnick KA, Livi KJ, Bodnar RJ, Nagle DC (2010) Changes in electrical and microstructural properties of microcrystalline cellulose as function of carbonization temperature. Carbon 48:1012–1024. https://doi.org/10.1016/j.carbon.2009.11.020

[35] Zickler GA, Smarsly B, Gierlinger N, Peterlik H, Paris O (2006) A reconsideration of the relationship between the crystallite size La of carbons determined by X-ray diffraction and Raman spectroscopy. Carbon 44:3239–3246. https://doi.org/10.1016/j.carbon.2006.06.029

[36] Sze SK, Siddique N, Sloan JJ, Escribano R (2001) Raman spectroscopic characterization of carbonaceous aerosols. Atmos Environ 35:561–568. https://doi.org/10.1016/S1352-2310(00)00325-3

[37] Couzi M, Bruneel JL, Talaga D, Bokobza L (2016) A multi wavelength Raman scattering study of defective graphitic carbon materials: the first order Raman spectra revisited.

Carbon 107:388–394. https://doi.org/10.1016/j.carbon.2016.06.017

[38] Fujimori T, Radovic LR, Silva-Tapia AB, Endo M, Kaneko K (2012) Structural importance of Stone–Thrower–Wales defects in rolled and flat graphenes from surface-enhanced Raman scattering. Carbon 50:3274–3279. https://doi.org/10.1016/j.carbon.2011.12.010

[39] Wu G, Dong J (2006) Raman characteristic peaks induced by the topological defects of carbon nanotube intramolecular junctions. Phys Rev B 73:245414–245422. https://doi.org/10.1103/PhysRevB.73.245414

[40] Piscanec S, Lazzeri M, Mauri F, Ferrari AC (2007) Optical phonons of graphene and nanotubes. Eur Phys J ST 148:159–170. https://doi.org/10.1140/epjst/e2007-00236-2

[41] Charlier JC, Eklund P, Zhu J, Ferrari A (2007) Electron and phonon properties of graphene: their relationship with carbon nanotubes. In: Jorio A, Dresselhaus G, Dresselhaus MS (eds) Carbon Nanotubes. Topics in Applied Physics, vol 111. Springer, Berlin, Heidelberg, pp 673–709. doi:10.1007/978-3-540-72865-8_21

[42] Childres I, Jauregui LA, Park W, Cao H, Chen YP (2013) Raman spectroscopy of graphene and related materials. In: Jang JI (ed) New Developments in Photon Materials Research, vol 1. Nova Science Publishers, New York, pp 1–20

[43] Gupta A, Chen G, Joshi P, Tadigadapa S, Eklund PC (2006) Raman scattering from high-frequency phonons in supported n-graphene layer films. Nano Lett 6:2667–2673. https://doi.org/10.1021/nl061420a

[44] Ferrari AC (2007) Raman spectroscopy of graphene and graphite: disorder, electron–phonon coupling, doping and nonadiabatic effects. Solid State Commun 143:47–57. https://doi.org/10.1016/j.ssc.2007.03.052

[45] Dresselhaus MS, Pimenta MA, Eklund PC, Dresselhaus G (2000) Raman scattering in fullerenes and related carbon-based materials. In: Weber WH, Merlin R (eds) Raman scattering in materials science. Springer, Berlin Heidelberg, pp 314–364. 10.1007/978-3-662-04221-2_10

[46] Dresselhaus MS, Dresselhaus G, Saito R, Jorio A (2005) Raman spectroscopy of carbon nanotubes. Phys Rep 409:47–99. https://doi.org/10.1016/j.physrep.2004.10.006

[47] Rao AM, Richter E, Bandow S, Chase B, Eklund PC, Williams KA, Fang S, Subbaswamy KR, Menon M, Thess A et al (1997) Diameter-selective Raman scattering from vibrational modes in carbon nanotubes. Science 275:187–191. https://doi.org/10.1126/science.275.5297.187

[48] Dresselhaus MS, Dresselhaus G, Eklund PC (1996) Science of fullerenes and carbon nanotubes: their properties and applications. Academic press, Cambridge

[49] Chase B, Herron N, Holler E (1992) Vibrational spectroscopy of fullerenes (C60 and C70). Temperature dependant studies. J Phys Chem 96:4262–4266. https://doi.org/10.1021/j100190a029

[50] Roy D, Chhowalla M, Wang H, Sano N, Alexandrou I, Clyne TW, Amaratunga GAJ (2003) Characterisation of carbon nano-onions using Raman spectroscopy. Chem Phys Lett 373:52–56. https://doi.org/10.1016/S0009-2614(03)00523-2

[51] Tan P, Dimovski S, Gogotsi Y (2004) Raman scattering of non–planar graphite: arched edges, polyhedral crystals, whiskers and cones. Philos Trans R Soc A 362:2289–2310. https://doi.org/10.1098/rsta.2004.1442

[52] Krishnan A, Dujardin E, Treacy MMJ, Hugdahl J, Lynum S, Ebbesen TW (1997) Graphitic cones and the nucleation of curved carbon surfaces. Nature 388:451–454. https://doi.org/10.1038/41284

[53] Zhao X, Ando Y, Qin LC, Kataura H, Maniwa Y, Saito R (2002) Radial breathing modes of multiwalled carbon nanotubes. Chem Phys Lett 361:169–174. https://doi.org/10.1016/S0009-2614(02)00955-7

[54] Singh DK, Iyer PK, Giri PK (2012) Distinguishing defect induced intermediate frequency modes from combination modes in the Raman spectrum of single walled carbon nanotubes. J Appl Phys 111:064304–064314. https://doi.org/10.1063/1.3692070

[55] Ergun S, Tiensuu V (1959) Tetrahedral structures in amorphous carbons. Acta Crystallogr 12:1050–1051. https://doi.org/10.1107/S0365110X59002936

[56] Tessonnier JP, Rosenthal D, Hansen TW, Hess C, Schuster ME, Blume R, Girgsdies F, Pfänder N, Timpe O, Su DS et al (2009) Analysis of the structure and chemical properties of some commercial carbon nanostructures. Carbon 47:1779–1798. https://doi.org/10.1016/j.carbon.2009.02.032

[57] Berger SD, McKenzie DR, Martin PJ (1988) EELS analysis of vacuum arc-deposited diamond-like films. Philos Mag Lett 57:285–290. https://doi.org/10.1080/09500838808214715

[58] Urbonaite S, Wachtmeister S, Mirguet C, Coronel E, Zou WY, Csillag S, Svensson G (2007) EELS studies of carbide derived carbons. Carbon 45:2047–2053. https://doi.org/10.1016/j.carbon.2007.05.0222048

[59] Fink J, Müller-Heinzerling T, Pflüger J, Scheerer B, Dischler B, Koidl P, Bubenze A, Sah RE (1984) Investigation of hydrocarbon-plasma-generated carbon films by electron-energy-loss spectroscopy. Phys Rev B 30:4713–4718. https://doi.org/10.1103/PhysRevB.30.4713

[60] Papworth AJ, Kiely CJ, Burden AP, Silva SRP, Amaratunga GAJ (2000) Electron-energy-loss spectroscopy characterization of the sp^2 bonding fraction within carbon thin films. Phys Rev B 62:12628–12631. https://doi.org/10.1103/PhysRevB.62.12628

[61] Jurkiewicz K, Duber S, Fischer HE, Burian A (2017) Modelling of glass-like carbon structure and its experimental verification by neutron and X-ray diffraction. J Appl Crystallogr 50:36–48. https://doi.org/10.1107/S1600576716017660

[62] Daniels H, Brydson R, Rand B, Brown A (2007) Investigating carbonization and graphitization using electron energy loss spectroscopy (EELS) in the transmission electron microscope (TEM). Philos Mag 87:4073–4092. https://doi.org/10.1080/14786430701394041

[63] Nyberg M, Luo Y, Triguero L, Pettersson LG, Ågren H (1999) Core-hole effects in X-ray-absorption spectra of fullerenes. Phys Rev B 60:7956–7960. https://doi.org/10.1103/physrevb.60.7956

[64] Iwashita N, Swain MV, Field JS, Ohta N, Bitoh S (2001) Elasto-plastic deformation of glass-like carbons heat-treated at different temperatures. Carbon 39:1525–1532. https://doi.org/10.1016/S0008-6223(00)00272-4

[65] Kawamura K, Jenkins GM (1972) Mechanical properties of glassy carbon fibres derived from phenolic resin. J Mater Sci 7:1099–1112. https://doi.org/10.1007/BF00550191

[66] Rodrigues MG, Da Cruz NC, Rangel EC, Zimmerman RL, Ila D, Poker DB, Hensley DK (2005) Effects of ion beam on nanoindentation characteristics of glassy polymeric carbon surface. Surf Coat Technol 196:251–256. https://doi.org/10.1016/j.surfcoat.2004.08.094

[67] Stein IY, Constable AJ, Morales-Medina N, Sackier CV, Devoe ME, Vincent HM, Wardle BL (2017) Structure-mechanical property relations of non-graphitizing pyrolytic carbon synthesized at low temperatures. Carbon 117:411–420. https://doi.org/10.1016/j.carbon.2017.03.001

[68] Yu MF, Lourie O, Dyer MJ, Moloni K, Kelly TF, Ruoff RS (2000) Strength and breaking mechanism of multiwalled carbon nanotubes under tensile load. Science 287:637–640. https://doi.org/10.1126/science.287.5453.637

[69] Iwashita N, Field JS, Swain MV (2002) Indentation hysteresis of glassy carbon materials. Philos Mag A 82:1873–1881. https://doi.org/10.1080/01418610208235699

5. References

1. http://www.2spi.com.

2. http://www.als-japan.com.

3. http://www.htw-germany.com.

4. Yamada, S., & Sato, H. (1962). Some physical properties of glassy carbon. *Nature*, *193*, 261-262.

5. Harris, P. J. F. (2004). Fullerene-related structure of commercial glassy carbons. *Philosophical Magazine*, *84*(29), 3159-3167.

6. Driver, M. (Ed.). (2012). *Coatings for biomedical applications*. Elsevier.

7. Jenkins, G. M., & Kawamura, K. (1971). Structure of glassy carbon. *Nature*, *231*, 175-176.

8. Jenkins, G. M., & Kawamura, K. (1976). *Polymeric carbons--carbon fibre, glass and char*. Cambridge University Press.

9. Harris, P. J., & Tsang, S. C. (1997). High-resolution electron microscopy studies of non-graphitizing carbons. *Philosophical Magazine A*, *76*(3), 667-677.

10. Harris, P. J. F. (1997). Structure of non-graphitising carbons. *International Materials Reviews*, *42*(5), 206-218.

11. Harris, P. J. (2013). Fullerene-like models for microporous carbon. *Journal of Materials Science*, *48*(2), 565-577.

12. Harris, P. J., Liu, Z., & Suenaga, K. (2008). Imaging the atomic structure of activated carbon. *Journal of Physics: Condensed Matter*, *20*(36), 362201.

13. Ban, L. L., Crawford, D., & Marsh, H. (1975). Lattice-resolution electron microscopy in structural studies of non-graphitizing carbons from polyvinylidene chloride (PVDC). *Journal of Applied Crystallography*, *8*(4), 415-420.

14. Pesin, L. A., & Baitinger, E. M. (2002). A new structural model of glass-like carbon. *Carbon*, *40*(3), 295-306.

15. Franklin, R. E. (1951, October). Crystallite growth in graphitizing and non-graphitizing carbons. In *Proceedings of the Royal Society of London A: Mathematical, Physical and Engineering Sciences* (Vol. 209, No. 1097, pp. 196-218). The Royal Society.

16. Petkov, V., DiFrancesco, R. G., Billinge, S. J. L., Acharya, M., & Foley, H. C. (1999). Local structure of nanoporous carbons. *Philosophical Magazine B*, *79*(10), 1519-1530.

17. O'Malley, B., Snook, I., & McCulloch, D. (1998). Reverse Monte Carlo analysis of the structure of glassy carbon using electron-microscopy data. *Physical Review B*, *57*(22), 14148.

18. Lentz, C. M., Samuel, B. A., Foley, H. C., & Haque, M. A. (2011). Synthesis and characterization of glassy carbon nanowires. *Journal of Nanomaterials*, *2011*, 9.

19. Li, X., & Gao, H. (2016). Mechanical metamaterials: Smaller and stronger. *Nature materials*, *15*(4), 373-374.

20. Kassegne, S., Vomero, M., Gavuglio, R., Hirabayashi, M., Özyilmaz, E., Nguyen, S., Rodriguez, J., Özyilmaz, E., van Niekerk, P., & Khosla, A. (2015). Electrical impedance, electrochemistry, mechanical stiffness, and hardness tunability in glassy carbon MEMS µECoGelectrodes. *Microelectronic Engineering*, *133*, 36-44.

21. Vomero, M., Castagnola, E., Ciarpella, F., Maggiolini, E., Goshi, N., Zucchini, E., Carli, S., Fadiga, L., Kassenge, S., & Ricci, D. (2017). Highly stable glassy carbon interfaces for long-term neural stimulation and low-noise recording of brain activity. *Scientific Reports*, *7,* 40332.

22. Harris, P. J. F., Burian, A., & Duber, S. (2000). High-resolution electron microscopy of a microporous carbon. *Philosophical Magazine Letters*, *80*(6), 381-386.

23. Jenkins, R. G., & Walker, P. L. (1976). Small angle X-ray scattering studies on carbons derived from polyfurfuryl alcohol and polyfurfuryl alcohol-ferrocene copolymers. *Carbon*, *14*(1), 7-11.

24. Rothwell, W. S. (1968). Small-angle X-ray scattering from glassy carbon. *Journal of Applied Physics*, *39*(3), 1840-1845.

25. Fukuyama, K., Nishizawa, T., & Nishikawa, K. (2001). Investigation of the pore structure in glass-like carbon prepared from furan resin. *Carbon*, *39*(13), 2017-2021.

26. Kroto, H. W., & McKay, K. (1988). The formation of quasi-icosahedral spiral shell carbon particles. *Nature*, *331*(6154), 328-331.

27. Krishnan, A., Dujardin, E., Treacy, M. M. J., Hugdahl, J., Lynum, S., & Ebbesen, T. W. (1997). Graphitic cones and the nucleation of curved carbon surfaces. *Nature*, *388*(6641), 451-454.

28. Khavryuchenko, V. D., & Khavryuchenko, O. V. (2013). Quantum chemical simulation of phenol-formaldehyde resin carbonization in the presence of phosphoric acid: computational evidence of Michaelis–Arbuzov-type reaction. *The Journal of Physical Chemistry C*, *117*(15), 7628-7635.

29. Dresselhaus, M. S., Dresselhaus, G., Saito, R., & Jorio, A. (2005). Raman spectroscopy of carbon nanotubes. *Physics reports*, *409*(2), 47-99.

30. Rao, A. M., Richter, E., Bandow, S., Chase, B., Eklund, P. C., Williams, K. A., Fang, S., Subbaswamy, K. R., Menon, M., Thess, A., Smalley, R. E., Dresselhaus, G., & Dresselhaus M. S. (1997). Diameter-selective Raman scattering from vibrational modes in carbon nanotubes.*Science*, *275*(5297), 187-191.

31. Dresselhaus, M. S., Dresselhaus, G., & Eklund, P. C. (1996). *Science of fullerenes and carbon nanotubes: their properties and applications*. Academic press.

32. Pimenta, M. A., Dresselhaus, G., Dresselhaus, M. S., Cancado, L. G., Jorio, A., & Saito, R. (2007). Studying disorder in graphite-based systems by Raman spectroscopy. *Physical chemistry chemical physics*, *9*(11), 1276-1290.

33. Sadezky, A., Muckenhuber, H., Grothe, H., Niessner, R., & Pöschl, U. (2005). Raman microspectroscopy of soot and related carbonaceous materials: spectral analysis and structural information. *Carbon*, *43*(8), 1731-1742.

34. Couzi, M., Bruneel, J. L., Talaga, D., & Bokobza, L. (2016). A multi wavelength Raman scattering study of defective graphitic carbon materials: The first order Raman spectra revisited. *Carbon*, *107*, 388-394.

35. Ergun, S., & Tiensuu, V. (1959). Tetrahedral structures in amorphous carbons. *Acta Crystallographica*, *12*(12), 1050-1051.

36. Tomita, S., Burian, A., Dore, J. C., LeBolloch, D., Fujii, M., & Hayashi, S. (2002). Diamond nanoparticles to carbon onions transformation: X-ray diffraction studies. *Carbon*, *40*(9), 1469-1474.

37. Hawelek, L., Brodka, A., Tomita, S., Dore, J. C., Honkimäki, V., & Burian, A. (2011). Transformation of nano-diamonds to carbon nano-onions studied by X-ray diffraction and molecular dynamics. *Diamond and Related Materials*, *20*(10), 1333-1339.

38. Oberlin, A. (1989). High-resolution TEM studies of carbonization and graphitization. *Chemistry and physics of carbon*, *22*, 1-143.

39. More, R. B., Haubold, A. D., & Bokros, J. C. (2004). Pyrolytic carbon for long-term medical implants. *Biomaterials Science: An Introduction to Materials in Medicine, 2nd Ed. New York: Elsevier*, 170-182.

40. Salkeld, S. L., Patron, L. P., Lien, J. C., Cook, S. D., & Jones, D. G. (2016). Biological and functional evaluation of a novel pyrolytic carbon implant for the treatment of focal osteochondral defects in the medial femoral condyle: assessment in a canine model. *Journal of orthopaedic surgery and research*, *11*(1), 155.

41. Ananth, H., Kundapur, V., Mohammed, H. S., Anand, M., Amarnath, G. S., & Mankar, S. (2015). A review on biomaterials in dental implantology. *International journal of biomedical science: IJBS*, *11*(3), 113.

42. Jenkins, G. M., & Grigson, C. J. (1979). The fabrication of artifacts out of glassy carbon and carbon-fiber-reinforced carbon for biomedical applications. *Journal of Biomedical Materials Research Part A*, *13*(3), 371-394.

43. Zhao, J. X., Bradt, R. C., & Walker, P. L. (1985). The fracture toughness of glassy carbons at elevated temperatures. *Carbon*, *23*(1), 15-18.

44. Pec, M. K., Reyes, R., Sánchez, E., Carballar, D., Delgado, A., Santamaría, J., Arruebo, M., & Evora, C. (2010). Reticulated vitreous carbon: a useful material for cell adhesion and tissue invasion. *Eur Cell Mater*, *20*, 282-94.

45. Warren, B. E. (1941). X-ray diffraction in random layer lattices. *Physical Review*, *59*(9), 693-698.

46. Hosemann, R., & Bagchi, S. N. (1962). Direct analysis of diffraction by matter. North-Holland. *Amsterdam*.

47. Hosemann, R., & Hindeleh, A. M. (1995). Structure of crystalline and paracrystalline condensed matter. *Journal of Macromolecular Science, Part B: Physics*, *34*(4), 327-356.

48. Stone, A. J., & Wales, D. J. (1986). Theoretical studies of icosahedral C 60 and some related species. *Chemical Physics Letters*, *128*(5), 501-503.

49. Brenner, D. W., Shenderova, O. A., Harrison, J. A., Stuart, S. J., Ni, B., & Sinnott, S. B. (2002). A second-generation reactive empirical bond order (REBO) potential energy expression for hydrocarbons. *Journal of Physics: Condensed Matter*, *14*(4), 783.

50. Girifalco, L. A., Hodak, M., & Lee, R. S. (2000). Carbon nanotubes, buckyballs, ropes, and a universal graphitic potential. *Physical Review B*, *62*(19), 13104.

51. Tuinstra, F., & Koenig, J. L. (1970). Raman spectrum of graphite. *The Journal of Chemical Physics*, *53*(3), 1126-1130.

52. Ferrari, A. C., & Robertson, J. (2000). Interpretation of Raman spectra of disordered and amorphous carbon. *Physical review B*, *61*(20), 14095.

53. Fujimori, T., Radovic, L. R., Silva-Tapia, A. B., Endo, M., & Kaneko, K. (2012). Structural importance of Stone–Thrower–Wales defects in rolled and flat graphenes from surface-enhanced Raman scattering. *Carbon*, *50*(9), 3274-3279.

54. Wu, G., & Dong, J. (2006). Raman characteristic peaks induced by the topological defects of carbon nanotube intramolecular junctions. *Physical Review B*, *73*(24), 245414.

55. Dresselhaus, M. S., Pimenta, M. A., Eklund, P. C., & Dresselhaus, G. (2000). Raman scattering in fullerenes and related carbon-based materials. In *Raman Scattering in Materials Science*, 314-364. Springer Berlin Heidelberg.

56. Chase, B., Herron, N., & Holler, E. (1992). Vibrational spectroscopy of fullerenes (C60 and C70). Temperature dependant studies. *The Journal of Physical Chemistry*, *96*(11), 4262-4266.

57. Roy, D., Chhowalla, M., Wang, H., Sano, N., Alexandrou, I., Clyne, T. W., & Amaratunga, G. A. J. (2003). Characterisation of carbon nano-onions using Raman spectroscopy. *Chemical Physics Letters*, *373*(1), 52-56.

58. Tan, P., Dimovski, S., & Gogotsi, Y. (2004). Raman scattering of non–planar graphite: arched edges, polyhedral crystals, whiskers and cones. *Philosophical Transactions of the Royal Society of London A: Mathematical, Physical and Engineering Sciences*, *362*(1824), 2289-2310.

59. Zhao, X., Ando, Y., Qin, L. C., Kataura, H., Maniwa, Y., & Saito, R. (2002). Radial breathing modes of multiwalled carbon nanotubes. *Chemical Physics Letters*, *361*(1), 169-174.

60. Singh, D. K., Iyer, P. K., & Giri, P. K. (2012). Distinguishing defect induced intermediate frequency modes from combination modes in the Raman spectrum of single walled carbon nanotubes. *Journal of Applied Physics*, *111*(6), 064304.

61. Tessonnier, J. P., Rosenthal, D., Hansen, T. W., Hess, C., Schuster, M. E., Blume, R., et al. (2009). Analysis of the structure and chemical properties of some commercial carbon nanostructures. *Carbon*, *47*(7), 1779-1798.

62. Berger, S. D., McKenzie, D. R., & Martin, P. J. (1988). EELS analysis of vacuum arc-deposited diamond-like films. *Philosophical Magazine Letters*, *57*(6), 285-290.

63. Zhang, Z. L., Brydson, R., Aslam, Z., Reddy, S., Brown, A., Westwood, A., et al. (2011). Investigating the structure of non-graphitising carbons using electron energy loss spectroscopy in the transmission electron microscope. *Carbon*, *49*(15), 5049-5063.

64. Yu, M. F., Lourie, O., Dyer, M. J., Moloni, K., Kelly, T. F., & Ruoff, R. S. (2000). Strength and breaking mechanism of multiwalled carbon nanotubes under tensile load. *Science*, *287*(5453), 637-640.

65. Duda, P., Jurkiewicz, K., Kaptacz, S., & Szymańska, J. (2014). Charakterystyki tribologiczne materiałów węglowych przeznaczonych na płatki zastawek serca. *Tribologia*, (3), 9-18.

66. Duda, P., Jurkiewicz, K., Kaptacz, S., & Salwa, P. (2016). Tribological characteristics of carbon materials subjected to annealing intended for use in heart valves. *Tribologia: tarcie, zużycie, smarowanie*, (3), 49-60.

6. *Appendix – author's scientific activity*

List of publications

1. Jurkiewicz, K., Pawlyta, M., Zygadlo, D., Chrobak, D., Duber, S., Wrzalik, R., Ratuszna, A. & Burian, A. Evolution of glassy carbon under heat treatment: correlation structure-mechanical properties.
Journal of Materials Science, DOI: 10.1007/s10853-017-1753-7.

2. Rams-Baron, M., Wojnarowska, Z., Knapik-Kowalczuk, J., Jurkiewicz, K., Burian, A., Wojtyniak, M., Pioteck, J., Jaworska, M., Rodríguez-Tinoco, C., & Paluch, M. (2017). The dielectric signature of glass density.
Applied Physics Letters, *111*(12), 121902.

3. Chmiel, K., Knapik-Kowalczuk, J., Jurkiewicz, K., Sawicki, W., Jachowicz, R., & Paluch, M. (2017). A new method to identify physically stable concentration of Amorphous Solid Disspersions (I): case of Flutamide+ Kollidon VA64.
Molecular Pharmaceutics. 14(10). 3370-3380.

4. Szklarz, G., Adrjanowicz, K., Knapik-Kowalczuk, J., Jurkiewicz, K., & Paluch, M. (2017). Crystallization of supercooled fenofibrate studied at ambient and elevated pressures.
Physical Chemistry Chemical Physics, *19*(15), 9879-9888.

5. Dobrzańska-Danikiewicz, A. D., Wolany, W., Łukowiec, D., Jurkiewicz, K., & Niedziałkowski, P. (2017). Characteristics of multiwalled carbon nanotubes-rhenium nanocomposites with varied rhenium mass fractions.
Nanomaterials and Nanotechnology, *7*, 1-8.

6. Grzybowska, K., Chmiel, K., Knapik-Kowalczuk, J., Grzybowski, A., Jurkiewicz, K., & Paluch, M. (2017). Molecular factors governing the liquid and glassy states recrystallization of celecoxib in binary mixtures with excipients of different molecular weights.
Molecular Pharmaceutics, *14*(4), 1154-1168.

7. Madejczyk, O., Kaminska, E., Tarnacka, M., Dulski, M., Jurkiewicz, K., Kaminski, K., & Paluch, M. (2017). Studying the crystallization of various polymorphic forms of nifedipine from binary mixtures with the use of different experimental techniques.
Molecular Pharmaceutics, 14(6), 2116–2125.

8. Knapik-Kowalczuk, J., Wojnarowska, Z., Rams-Baron, M., Jurkiewicz, K., Cielecka-Piontek, J., Ngai, K. L., & Paluch, M. (2017). Atorvastatin as a promising crystallization inhibitor of amorphous probucol: dielectric studies at ambient and elevated pressure.
Molecular Pharmaceutics, *14*(8), 2670-2680.

9. Madejczyk, O., Kaminski, K., Kaminska, E., Jurkiewicz, K., Tarnacka, M., Burian, A., & Paluch, M. (2017). Interplay between the static ordering and dynamical heterogeneities determining the dynamics of rotation and ordinary liquid phases in 1, 6-anhydro-β-D-glucose.
Scientific Reports, *7*, 42103.

10. Hawelek, L., Schiavon, M., Szade, J., Wlodarczyk, P., Jurkiewicz, K., Fischer, H. E., Kolano-Burian, A., & Burian, A. (2017). The atomic scale structure of dahlia-like single wall carbon nanohorns produced by direct vaporization of graphite.
Diamond and Related Materials, *72*, 26-31.

11. Kaminska, E., Madejczyk, O., Tarnacka, M., Jurkiewicz, K., Kaminski, K., & Paluch, M. (2017). Studying of crystal growth and overall crystallization of naproxen from binary mixtures.
European Journal of Pharmaceutics and Biopharmaceutics, *113*, 75-87.

12. Jurkiewicz, K., Duber, S., Fischer, H. E., & Burian, A. (2017). Modelling of glass-like carbon structure and its experimental verification by neutron and X-ray diffraction.
Journal of Applied Crystallography, *50*(1), 36-48.

13. Hawelek, L., Wlodarczyk, P., Hudecki, A., Lis, M., Zackiewicz, P., Jurkiewicz, K., Szade, J., Kubacki, J., Balin, K., Fischer, H.E., Kolano-Burian, A., & Burian, A. (2016). The atomic scale structure of glass-like carbon obtained from fullerene extract via spark plasma sintering.
Carbon, *110*, 172-179.

14. Duda, P., Jurkiewicz, K., Kaptacz, S., & Salwa, P. (2016). Tribological characteristics of carbon materials subjected to annealing intended for use in heart valves.
Tribologia: tarcie, zużycie, smarowanie, (3), 49-60.

15. Knapik, J., Wojnarowska, Z., Grzybowska, K., Jurkiewicz, K., Stankiewicz, A., & Paluch, M. (2016). Stabilization of the amorphous ezetimibe drug by confining its dimension.
Molecular pharmaceutics, *13*(4), 1308-1316.

16. Kaminska, E., Tarnacka, M., Jurkiewicz, K., Kaminski, K., & Paluch, M. (2016). High pressure dielectric studies on the structural and orientational glass.
The Journal of chemical physics, *144*(5), 054503.

17. Jurkiewicz, K., Duber, S., & Burian, A. (2016). Paracrystalline structure of glass-like carbons.
International Journal of Applied Glass Science, *7*(3), 355-363.

18. Knapik, J., Wojnarowska, Z., Grzybowska, K., Jurkiewicz, K., Tajber, L., & Paluch, M. (2015). Molecular dynamics and physical stability of coamorphous ezetimib and indapamide mixtures.
Molecular pharmaceutics, *12*(10), 3610-3619.

19. Kaminska, E., Tarnacka, M., Wlodarczyk, P., Jurkiewicz, K., Kolodziejczyk, K., Dulski, M., Haznar-Garbacz, D., Hawelek, L., Kaminski, K., Wlodarczyk, A., & Paluch, M. (2015). Studying the impact of modified saccharides on the molecular dynamics and crystallization tendencies of model API nifedipine.
Molecular pharmaceutics, *12*(8), 3007-3019.

20. Rams-Baron, M., Wojnarowska, Z., Grzybowska, K., Dulski, M., Knapik, J., Jurkiewicz, K., Smolka, W., Sawicki, W., Ratuszna, A., & Paluch, M. (2015). Toward a better understanding of the physical stability of amorphous anti-inflammatory agents: the roles of molecular mobility and molecular interaction patterns. *Molecular pharmaceutics*, *12*(10), 3628-3638.

21. <u>Jurkiewicz, K.</u>, Hawełek, Ł., Balin, K., Szade, J., Braghiroli, F. L., Fierro, V., Celzard, A., & Burian, A. (2015). Conversion of natural tannin to hydrothermal and graphene-like carbons studied by wide-angle X-ray scattering.
The Journal of Physical Chemistry A, *119*(32), 8692-8701.

22. Duda, P., <u>Jurkiewicz, K.</u>, Kaptacz, S., & Szymańska, J. (2014). Charakterystyki tribologiczne materiałów węglowych przeznaczonych na płatki zastawek serca.
Tribologia, (3), 9-18.

List of oral presentations

1. "Correlations the atomic structure-mechanical properties for glass-like carbons"
CARBON2017, Melbourne, Australia, 07.2017

2. "On the structure-properties correlations in glass-like carbons"
X Konferencja Naukowo-Techniczna: Materiały węglowe i kompozyty polimerowe, Ustroń, Poland, 04.2017

3. "Dlaczego szkliste węgle są twarde? Korelacje struktura-właściwości mechaniczne"
Katowicko-Krakowskie seminarium "Fizyka Fazy Skondensowanej", Kraków, Poland, 04.2017

4. "Wyznaczanie struktury atomowej materiałów niekrystalicznych na podstawie materiałów węglowych"
Katowicko-Krakowskie seminarium "Fizyka Fazy Skondensowanej", Chorzów, Poland, 06.2016

5. "Atomic structure of nanomaterials and its effect on properties"
Internano Poland, Katowice, Poland, 06.2016

6. "Complex modeling of glass-like carbon structure"
ADD Analysis of Diffraction Data in Real Space, Grenoble, France, 03.2016

7. "Modeling studies of carbon nanostructures and its experimental verification using diffraction method"
CESEP 2015 Conference, Poznań, Poland, 10.2015

8. "Badania strukturalne materiałów węglowych metodą dyfrakcji promieni X oraz neutronów"
Spotkanie Polskiego Towarzystwa Węglowego, Chorzów, Poland, 03.2014

9. "Wide-angle X-ray scattering studies of ghlassy carbon produced for medical implants"
9th Torunian Carbon Symposium, Toruń, Poland, 09.2014

10. "Badania struktury węgla szklistego metodami dyfrakcji promieni X, rozpraszania Ramana i dynamiki molekularnej"
Katowicko-Krakowskie seminarium "Fizyka Fazy Skondensowanej", Kraków, Poland, 11.2013

List of poster presentations

1. "Complex structural characterization of glassy carbons and correlations structure – mechanical properties"
   DCMS International summer school Materials 4.0, Drezno, Germany, 09.2017

2. "Complex structural characterization of glassy carbons"
   XIVth International Conference on Molecular Spectroscopy, Białka Tatrzańska, Poland, 09.2017

3. "The role of topological defects on the structure and properties of glass-like carbon"
   CARBON2015, Drezno, Germany, 07.2015

Grants

1. Grant Preludium, from National Science Center, nr 2015/19/N/ST3/01037, "Atomic structure - porosity - mechanical properties correlations of glass-like carbon for potential applicactions in medicine" (leader)